ΕΘΝΙΚΟ ΜΕΤΣΟΒΙΟ ΠΟΛΥΤΕΧΝΕΙΟ

ΣΧΟΛΗ ΕΦΑΡΜΟΣΜΕΝΩΝ
ΜΑΘΗΜΑΤΙΚΩΝ ΚΑΙ
ΦΥΣΙΚΩΝ ΕΠΙΣΤΗΜΩΝ

ΤΟΜΕΑΣ ΦΥΣΙΚΗΣ

ΕΘΝΙΚΟ ΚΕΝΤΡΟ
ΕΡΕΥΝΑΣ ΦΥΣΙΚΩΝ
ΕΠΙΣΤΗΜΩΝ
"ΔΗΜΟΚΡΙΤΟΣ"

ΙΝΣΤΙΤΟΥΤΟ ΠΥΡΗΝΙΚΗΣ ΚΑΙ
ΣΩΜΑΤΙΔΙΑΚΗΣ ΦΥΣΙΚΗΣ

ΔΙΑΤΜΗΜΑΤΙΚΟ ΠΡΟΓΡΑΜΜΑ ΜΕΤΑΠΤΥΧΙΑΚΩΝ ΣΠΟΥΔΩΝ
"ΦΥΣΙΚΗ ΚΑΙ ΤΕΧΝΟΛΟΓΙΚΕΣ ΕΦΑΡΜΟΓΕΣ"

The LAMS Analysis Framework for Measuring Optical Properties of Sea-Water

Ανάλυση των Δεδομένων του Συστήματος LAMS για τη Μέτρηση των Οπτικών Ιδιοτήτων του Θαλασσινού Νερού

Μεταπτυχιακή Διπλωματική Εργασία

Γεώργιος Ζαρπάπης

Επιβλέπουσα:

Αικατερίνη Τζαμαριουδάκη
Διευθύντρια Ερευνών Α΄ - Ε.Κ.Ε.Φ.Ε. "ΔΗΜΟΚΡΙΤΟΣ"

Αθήνα

Ιούνιος 2022

Acknowledgments

English

This thesis was prepared at the Institute of Nuclear and Particle Physics of NCSR "Demokritos" within the Interdepartmental Program of Postgraduate Studies "Physical and Technological Applications", in which participate the National Technical University of Athens and the NCSR "Demokritos". I could not have undertaken this journey without my supervisor Dr. Tzamarioudaki Aikaterini, Director of Research A' at the Institute of Nuclear and Particle Physics at NCSR "Demokritos", who supported, guided and tolerated me through it all.

I would also like to express my deepest appreciation to Dr. Markou Christos, Director of Research A' and Director of the Institute of Nuclear and Particle Physics at NCSR "Demokritos", again towards my supervisor Dr. Tzamarioudaki Aikaterini and towards Dr Kostas Pikounis, PhD candidates Anna Sinopoulou and Dimitris Stavropoulos who inspired me and I consider my mentors.

Finally, I want to express my utmost gratitude to the people who stood by my side unconditionally, always. Those who never lost their faith in me, helping me at times to restore my own faith in me. Those who assured me that all will be well after every risk I took. My parents and friends who were the positive force in my life.

Ελληνικά

Η παρούσα διπλωματική εργασία εκπονήθηκε στο Ινστιτούτο Πυρηνικής και Σωματιδιακής Φυσικής του ΕΚΕΦΕ «Δημόκριτος» στο πλαίσιο του Διατμηματικού Προγράμματος Μεταπτυχιακών Σπουδών «Φυσικές και Τεχνολογικές Εφαρμογές», στο οποίο συμμετέχουν το Εθνικό Μετσόβιο Πολυτεχνείο και το ΕΚΕΦΕ «Δημόκριτος». Δεν θα μπορούσα να κάνω αυτό το ταξίδι χωρίς την επιβλέπουσα Δρ. Τζαμαριουδάκη Αικατερίνη, Διευθύντρια Ερευνών Α΄ στο Ινστιτούτο Πυρηνικής και Σωματιδιακής Φυσικής του ΕΚΕΦΕ «Δημόκριτος», που με στήριξε, καθοδήγησε και με ανέχτηκε όλη αυτή την περίοδο.

Θα ήθελα επίσης να εκφράσω τη βαθύτατη εκτίμηση μου στον Δρ. Μάρκου Χρήστο, Διευθυντή Ερευνών Α΄ και Διευθυντή του Ινστιτούτου Πυρηνικής και Σωματιδιακής Φυσικής στο ΕΚΕΦΕ «Δημόκριτος», και πάλι προς την επιβλέπουσα μου Δρ. Τζαμαριουδάκη Αικατερίνη και προς τον Δρ Κώστα Πικούνη, τους υποψήφιους διδάκτορες Άννα Σινοπούλου και Δημήτρη Σταυρόπουλο που με ενέπνευσαν και θεωρώ μέντορες μου.

Τέλος, θέλω να εκφράσω την απόλυτη ευγνωμοσύνη μου στους ανθρώπους που στάθηκαν δίπλα μου άνευ όρων, πάντα. Αυτοί που δεν έχασαν ποτέ την πίστη τους σε μένα, βοηθώντας με μερικές φορές να αποκαταστήσω τη δική μου πίστη μου σε μένα. Αυτοί που με διαβεβαίωσαν ότι όλα θα πάνε καλά μετά από κάθε ρίσκο που έπαιρνα. Τους γονείς και φίλους μου που ήταν η θετική δύναμη στη ζωή μου.

Abstract

This thesis is focused on the software development of a framework for automising the analysis of the Long Arm Marine Spectrophotometer (LAMS) data. This analysis software has also been widely used during the testing phase of the upgraded LAMS device. The pattern recognition methods for identifying pulses and cycles in the data are described, the analysis of the data collected with the original LAMS device during the 2009 sea campaigns using the newly developed framework are presented. Finally, some examples of tests and the corresponding results are discussed.

The first and second chapters include a theoretical introduction for the physics goals of the KM3NeT experiment.

The third chapter presents information about KM3NeT, its goal and technical means of operation. For the fourth chapter, the original and improved designs of the LAMS system are described.

In the fifth chapter my personal contribution is presented: the features of the framework I developed are described together with the analysis of the original LAMS data. Finally, the tests carried out to validate the electronics and the problems identified and solved, are described. My personal contribution in this project is clearly stated and the necessary future steps are discussed.

Περίληψη

Αυτή η διατριβή επικεντρώνεται στην ανάπτυξη λογισμικού ενός πλαισίου για την αυτοματοποίηση της ανάλυσης των δεδομένων του Long Arm Marine Spectrophotometer (LAMS). Αυτό το λογισμικό ανάλυσης έχει επίσης χρησιμοποιηθεί ευρέως κατά τη φάση δοκιμής της αναβαθμισμένης συσκευής LAMS. Περιγράφονται οι μέθοδοι αναγνώρισης προτύπων για την αναγνώριση παλμών και κύκλων στα δεδομένα, παρουσιάζεται η ανάλυση των δεδομένων που συλλέχθηκαν με την αρχική συσκευή LAMS κατά τις θαλάσσιες εκστρατείες του 2009 χρησιμοποιώντας το πρόσφατα αναπτυγμένο πλαίσιο. Τέλος, συζητούνται μερικά παραδείγματα δοκιμών και τα αντίστοιχα αποτελέσματα.

Το πρώτο και το δεύτερο κεφάλαιο περιλαμβάνουν μια θεωρητική εισαγωγή για τους στόχους της φυσικής του πειράματος KM3NeT.

Στο τρίτο κεφάλαιο παρουσιάζονται πληροφορίες για το KM3NeT, τον στόχο και τα τεχνικά μέσα λειτουργίας του. Για το τέταρτο κεφάλαιο, περιγράφονται τα πρωτότυπα και βελτιωμένα σχέδια του συστήματος LAMS.

Στο πέμπτο κεφάλαιο παρουσιάζεται η προσωπική μου συμβολή: περιγράφονται τα χαρακτηριστικά του πλαισίου που ανέπτυξα μαζί με την ανάλυση των αρχικών δεδομένων LAMS. Τέλος, περιγράφονται οι δοκιμές που πραγματοποιήθηκαν για την επικύρωση των ηλεκτρονικών και τα προβλήματα που εντοπίστηκαν και επιλύθηκαν. Η προσωπική μου συμβολή σε αυτό το έργο δηλώνεται ξεκάθαρα και συζητούνται τα απαραίτητα μελλοντικά βήματα.

Contents

List of Figures

List of Tables

Περιγραφή

Καθιερωμένο Πρότυπο

Το Καθιερωμένο Πρότυπο είναι μια θεωρία της σωματιδιακής φυσικής που περιγράφει την τρέχουσα κατανόησή μας για τα θεμελιώδη συστατικά του σύμπαντος (στοιχειώδη σωματίδια) και τις αλληλεπιδράσεις τους (δυνάμεις).

Τα φερμιόνια και τα μποζόνια είναι δύο τύποι στοιχειωδών σωματιδίων που μπορούν να διακριθούν από τις τιμές σπιν τους, οι οποίες είναι τιμές μισού περιττού ακέραιου αριθμού για τα φερμιόνια και ακέραιες τιμές για τα μποζόνια. Γενικά, τα φερμιόνια συνδέονται με την ύλη ενώ τα μποζόνια είναι φορείς αλληλεπιδράσεων.

Τα φερμιόνια χωρίζονται σε κουάρκ και λεπτόνια, καθώς και σε τρεις γενιές με βάση τη μάζα και τη σταθερότητά τους: Τα ελαφρύτερα και πιο σταθερά σωματίδια βρίσκονται στην πρώτη γενιά, ενώ τα βαρύτερα και πιο ασταθή σωματίδια είναι στην τρίτη γενιά, με τη δεύτερη γενιά στο ενδιάμεσο. Επειδή όλη η σταθερή ύλη στον κόσμο αποτελείται από σωματίδια πρώτης γενιάς, οποιαδήποτε βαρύτερα σωματίδια διασπώνται αμέσως σε πιο σταθερά.

Υπάρχουν 6 κουάρκ: (*u*)p, (*d*)own, (*c*)harm, (*s*)trange, (*t*)op και (*b*)ottom. Κάθε κουάρκ έχει ένα αντικουάρκ, το οποίο είναι έχει την ίδια μάζα αλλά αντίθετο ηλεκτρικό φορτίο. Όταν τα κουάρκ (και αντικουάρκ) ενώνονται, σχηματίζουν αδρόνια, τα οποία είναι σύνθετα σωματίδια. Τα αδρόνια ταξινομούνται σε βαρυόνια (qqq), αντιβαρυόνια ($\overline{q}\overline{q}\overline{q}$) ή μεσόνια ($q\overline{q}$) ανάλογα με τη σύστασή τους σε κουάρκ. Τα βαρυόνια με περιεχόμενο κουάρκ (uud) και (udd) είναι πρωτόνια και νετρόνια, αντίστοιχα.

Τα λεπτόνια, από την άλλη πλευρά, μπορούν να υπάρχουν μόνο ως μεμονωμένα σωματίδια και δεν μπορούν να σχηματίσουν σύνθετα σωματίδια. Το ηλεκτρόνιο (e), το μιόνιο (μ) και το ταυ (τ) είναι ηλεκτρικά φορτισμένα (-1) λεπτόνια, ταξινομημένα ανάλογα με την αύξηση της μάζας. Σε καθένα από αυτά αντιστοιχεί ένα νετρίνο: το νετρίνο ηλεκτρονίων (ν_e), το νετρίνο μιονίου (ν_μ) και το νετρίνο ταυ (ν_τ). Τα νετρίνα έχουν πολύ μικρή μάζα και είναι ηλεκτρικά ουδέτερα. Τα αντιλεπτόνια είναι σωματίδια με αντίθετο ηλεκτρικό φορτίο (όπου αυτό είναι δυνατό) και αντίθετο αριθμό λεπτονίων. Ο αριθμός λεπτονίων είναι ένας διατηρημένος κβαντικός αριθμός που έχει τιμή είτε +1 είτε -1 και κάνει διάκριση μεταξύ λεπτονίων και αντιλεπτονίων.

Ένα από τα μποζόνια είναι πολύ γνωστό σωματίδιο: το φωτόνιο γ, το οποίο είναι ο φορέας της ηλεκτρομαγνητικής αλληλεπίδρασης. Το Καθιερωμένο Μοντέλο ενσωματώνει επίσης δύο επιπλέον αλληλεπιδράσεις: την ισχυρή αλληλεπίδραση (επίσης γνωστή ως κβαντική χρωμοδυναμική ή QCD) και την ασθενή αλληλεπίδραση.

Οι ισχυρές και οι ασθενείς δυνάμεις, σε αντίθεση με την ηλεκτρομαγνητική και τη βαρυτηική, υπάρχουν μόνο σε πολύ μικρές αποστάσεις και δεν έχουν αντιστοιχία στην κλασική φυσική. Το γλουόνιο g είναι ο φορέας δύναμης της ισχυρής δύναμης και είναι υπεύθυνο για τη συγκράτηση των ατομικών πυρήνων. Η ραδιενεργή διάσπαση ασταθών υλικών όπως το ουράνιο προκαλείται από την ασθενή δύναμη. Οι φορείς της ασθενούς αλληλεπίδρασης είναι τα μποζόνια W^+, W^- και Z. Η βαρυτική δύναμη θεωρείται επίσης ότι μεταφέρεται από ένα μποζόνιο, ονομαστικά το βαρυτόνιο, αλλά δεν έχει ανακαλυφθεί ακόμη.

Το μποζόνιο Higgs παρέχει τον μηχανισμό με τον οποίο όλα τα άλλα σωματίδια αποκτούν μάζα. Χωρίς αυτό, τα σωματίδια θα ήταν χωρίς μάζα και θα διαδίδονταν με την ταχύτητα του φωτός. Στην Κβαντική Θεωρία Πεδίου, όταν πρόκειται για θεμελιώδη φερμιόνια και μποζόνια, τα πεδία τους έχουν μηδενική προσδοκώμενη τιμή στο κενό. Το ίδιο δεν ισχύει για το πεδίο Higgs. Η αλληλεπίδραση των αρχικά χωρίς μάζα σωματιδίων με αυτό το μη μηδενικό πεδίο Higgs τους δίνει τις μάζες τους.

Εισαγωγή

Ο Pauli πρότεινε την υπόθεση των νετρίνων το 1930. Όλα ξεκίνησαν με μια επιστολή που έγραψε ο Pauli στις 4 Δεκεμβρίου 1930, προς τους συμμετέχοντες σε ένα συνέδριο πυρηνικής φυσικής στο Tubingen της Γερμανίας, στο οποίο πρότεινε την ύπαρξη ενός νέου ουδέτερου ασθενούς αλληλεπίδρασης σωματίδιο με σπιν $\frac{1}{2}$ και το ονόμασαν ¨νετρόνιο¨ ως ¨verzweifelten Ausweg¨ (απελπισμένη διέξοδο) για να εξηγήσει δύο εξαιρετικά προβλήματα στη σύγχρονη πυρηνική φυσική που δημιούργησαν μεγάλες δυσκολίες σε σχέση με τις θεωρητικές ερμηνείες των επιστημόνων.

Αυτά τα δύο ζητήματα συνδέθηκαν με το παζλ της εξοικονόμησης ενέργειας σε β-διασπάσεις πυρήνων, που ανακαλύφθηκε από τον Θ. ϔαδωιςκ το 1914, καθώς και με ανωμαλίες στην κατανόηση της σχέσης spin-statistics στην περίπτωση των $^1 4N$ και $^6 Li$ πυρήνες στο πλαίσιο του μοντέλου πυρηνικής δομής, στο οποίο τα ηλεκτρόνια και τα πρωτόνια θεωρούνταν πυρηνικά συστατικά. Όταν ο Chadwick ανακάλυψε το 1932 το νετρόνιο όπως το ξέρουμε σήμερα, ο E. Fermi μετονόμασε το σωματίδιο του Pauli σε νετρίνο. Το νετρίνο αναφέρθηκε αρχικά στα Πρακτικά της Διάσκεψης Solvay τον Οκτώβριο του 1933. Την ίδια χρονιά, οι Fermi και Perrin κατέληξαν ανεξάρτητα στο ίδιο συμπέρασμα ότι τα νετρίνα θα μπορούσαν να είναι χωρίς μάζα.

Το 1934 ο Fermi διατύπωσε μια θεωρία β-διάσπασης, τώρα γνωστή ως θεωρία Fermi, σε αναλογία με την κβαντική ηλεκτροδυναμική (QED). Προκειμένου να εξηγήσουν την παρατηρούμενη μεταβολή μιας μονάδας του πυρηνικού σπιν σε μερικές διασπάσεις β, οι G. Gamow και E. Teller το 1936 επέκτειναν τη θεωρία εισάγοντας αξονικά διανυσματικά

ρεύματα με τέτοιο τρόπο ώστε η ισοτιμία ήταν ακόμα διατηρημένη αφού η παραβίαση της ισοτιμίας εκείνη την εποχή ήταν αδιανόητη.

Η αξιοσημείωτη επιτυχία της θεωρίας Fermi άφησε λίγους να αμφισβητήσουν την ύπαρξη του νετρίνου, ωστόσο, κανένα δεν είχε ακόμη παρατηρηθεί στις αλληλεπιδράσεις, εν μέρει λόγω της προβλεπόμενης ισχύος των αλληλεπιδράσεων από τους H. Bethe και R. Peierls, οι οποίοι ισχυρίστηκαν το 1934 ότι θα μπορούσε να να μην παρατηρηθεί ποτέ. Προτρέπονται, ιδιαίτερα από τον B. Pontecorvo στις αρχές της δεκαετίας του 1950, οι F. Reines και ο C.L. Cowan αναζήτησε έναν τρόπο μέτρησης της αντίστροφης διάσπασης β, στον οποίο ένα αντινετρίνο μπορεί να παράξει ένα ποζιτρόνιο. Αφού εξέτασαν διάφορες μεθόδους, συμπεριλαμβανομένης μιας πυρηνικής έκρηξης, κατέληξαν στη χρήση της μεγάλης ροής αντινετρίνων από έναν πυρηνικό αντιδραστήρα και 10 τόνων εξοπλισμού, συμπεριλαμβανομένων 1400 λίτρων υγρών σπινθηριστών. Αυτό το πείραμα ήταν το πρώτο πείραμα αντιδραστήρα-νετρίνο. Τον Ιούνιο του 1956, ο Reines και ο Cowan έστειλαν ένα τηλεγράφημα ενημερώνοντας τον Pauli για την ανακάλυψη. Ο Reines (ο Cowan απεβίωσε) τιμήθηκε με το βραβείο Νόμπελ 40 χρόνια αργότερα.

Τα νετρίνα αμφισβητούν τις προσδοκίες μας σχετικά με την εγκυρότητα ορισμένων αρχών συμμετρίας και νόμων διατήρησης στη σωματιδιακή φυσική. Η μελέτη των νετρίνων και η αλληλεπίδρασή τους με την ύλη έχει συνεισφέρει πολλές σημαντικές στη σημερινή μας γνώση της φυσικής, γεγονός που τονίζεται από το γεγονός ότι έχουν απονεμηθεί δέκα βραβεία Νόμπελ για ανακαλύψεις φυσικής σε θέματα είτε απευθείας στον τομέα της φυσικής των νετρίνων είτε στον τομέα της φυσικής. θέματα στα οποία ο ρόλος της φυσικής των νετρίνων ήταν πολύ κρίσιμος.

Αλληλεπιδράσεις νετρίνων

Οι αλληλεπιδράσεις των νετρίνων περιγράφονται, με εντυπωσιακή ακρίβεια, από το Καθιερωμένο Πρότυπο. Μέχρι στιγμής δεν έχουν βρεθεί αποκλίσεις από τις τυπικές αλληλεπιδράσεις νετρίνων σε πειραματικά δεδομένα.

Οι τυπικές αλληλεπιδράσεις νετρίνων περιγράφονται από το λεπτονικό φορτισμένο ρεύμα ως:

$$j^{\rho}_{W,L} = 2 \sum_{a=e,\mu,\tau} \overline{\nu_{aL}} \cdot \gamma^{\rho} \cdot l_{aL} = \sum_{a=e,\mu,\tau} \overline{\nu_a} \cdot \gamma^{\rho} \cdot (1-\gamma^5) \cdot l_a$$

και το τμήμα νετρίνων του λεπτονικού ουδέτερου ρεύματος είναι:

$$j^{\rho}_{Z,L} = \sum_{a=e,\mu,\tau} \overline{\nu_{aL}} \cdot \gamma^{\rho} \cdot \nu_{aL} = \frac{1}{2} \sum_{a=e,\mu,\tau} \overline{\nu_a} \cdot \gamma^{\rho} \cdot (1-\gamma^5) \cdot \nu_a$$

Ταλαντώσεις

Μέχρι τα τέλη της δεκαετίας του 1990, σχετικά λίγα ήταν γνωστά για τα νετρίνα πέρα από το ότι υπάρχουν τρεις ξεχωριστές γεύσεις και ότι είναι εξαιρετικά ελαφριά (και πιθανώς χωρίς μάζα). Ωστόσο, ακόμη και εκείνη την εποχή πολλά πειράματα είχαν αναφέρει πιθανές ανωμαλίες στους παρατηρούμενους ρυθμούς αλληλεπίδρασης ατμοσφαιρικών και ηλιακών νετρίνων. Αυτή η εικόνα άλλαξε με τη δημοσίευση των ηλιακών και ατμοσφαιρικών δεδομένων νετρίνων από τον ανιχνευτή Super Kamiokande, ο οποίος παρείχε συναρπαστικά πειραματικά στοιχεία για το φαινόμενο των ταλαντώσεων γεύσης νετρίνων σε πολύ μεγάλες αποστάσεις. Η μετέπειτα μελέτη των ταλαντώσεων νετρίνων ήταν ένα από τα σημαντικότερα σημεία της σωματιδιακής φυσικής τα τελευταία χρόνια.

Οι ιδιοκαταστάσεις μάζας είναι οι στατικές καταστάσεις του Hamiltonian ελεύθερου σωματιδίου και ικανοποιούν

$$\widehat{H}\psi = \imath\frac{\partial\psi}{\partial t} = E\psi \tag{0.1}$$

Η χρονική εξέλιξη μιας ιδιοκατάστασης μάζας παίρνει τη μορφή

$$\psi(\mathbf{x},t) = \phi(\mathbf{x})e^{-\imath Et}$$

Οι ιδιοκαταστάσεις μάζας νετρίνων (τα θεμελιώδη σωματίδια) χαρακτηρίζονται ως ν_1, ν_2 και ν_3. Δεν υπάρχει λόγος να πιστεύουμε ότι οι ιδιοκαταστάσεις μάζας πρέπει να αντιστοιχούν στις ασθενείς ιδιοκαταστάσεις, ν_e, ν_μ και ν_τ, οι οποίες παράγονται μαζί με την αντίστοιχη γεύση φορτισμένου λεπτονίου σε μία ασθενή αλληλεπίδραση. Οποιαδήποτε από τις τρεις ιδιοκαταστάσεις μάζας μπορεί να παραχθεί σε συνδυασμό με το ηλεκτρόνιο στην αρχική ασθενή αλληλεπίδραση. Εφόσον δεν είναι δυνατό να γνωρίζουμε ποια ιδιοκατάσταση μάζας παρήχθη, το σύστημα πρέπει να περιγραφεί με μια συνεκτική γραμμική υπέρθεση καταστάσεων ν_1, ν_2 και ν_3. Στην κβαντομηχανική, η βάση των ασθενών ιδιοκαταστάσεων μπορεί να συσχετιστεί με τη βάση των ιδιοκαταστάσεων μάζας μέσω ενός ενιαίου πίνακα U,

$$\begin{bmatrix}\nu_e\\ \nu_\mu\\ \nu_\tau\end{bmatrix} = \begin{bmatrix}U_{e1} & U_{e2} & U_{e3}\\ U_{\mu1} & U_{\mu2} & U_{\mu3}\\ U_{\tau1} & U_{\tau2} & U_{\tau3}\end{bmatrix}\begin{bmatrix}\nu_1\\ \nu_2\\ \nu_3\end{bmatrix}$$

Ως εκ τούτου, το νετρίνο ηλεκτρονίων, το οποίο είναι η κβαντική κατάσταση που παράγεται μαζί με ένα ποζιτρόνιο σε μια ασθενή αλληλεπίδραση φορτισμένου-ρεύματος, είναι ο γραμμικός συνδυασμός των ιδιοκαταστάσεων μάζας που ορίζονται από τους

σχετικούς ασθενούς αλληλεπίδρασης φορτισμένου ρεύματος συζεύξεις των ν_1, nu_2 και ν_3 στην κορυφή $W^+ \to e^+ + \nu_e$

$$|\psi\rangle = U^*_{e1}|\nu_1\rangle + U^*_{e2}|\nu_2\rangle + U^*_{e3}|\nu_3\rangle$$

Η κατάσταση του νετρίνου στη συνέχεια διαδίδεται ως μια συνεκτική γραμμική υπέρθεση των τριών ιδιοκαταστάσεων μάζας έως ότου αλληλεπιδράσει και η κυματοσυνάρτηση καταρρέει σε μια ασθενή ιδιοκατάσταση, παράγοντας ένα παρατηρήσιμο φορτισμένο λεπτόνιο συγκεκριμένης γεύσης. Εάν οι μάζες των ν_1, ν_2 και ν_3 δεν είναι ίδιες, προκύπτουν διαφορές φάσης μεταξύ των διαφορετικών συνιστωσών της κυματοσυνάρτησης και εμφανίζεται το φαινόμενο των ταλαντώσεων νετρίνων. Με αυτόν τον τρόπο, ένα νετρίνο που παράγεται μαζί με μια γεύση φορτισμένου λεπτονίου μπορεί να αλληλεπιδράσει για να παράγει ένα φορτισμένο λεπτόνιο διαφορετικής γεύσης.

Τα πρώτα πειραματικά αποτελέσματα σχετικά με τις ταλαντώσεις των νετρίνων ελήφθησαν από μελέτες των ηλιακών νετρίνων και των νετρίνων που παράγονται σε καταρράκτες που προκαλούνται από κοσμικές ακτίνες στην ατμόσφαιρα. Πιο πρόσφατα αποτελέσματα έχουν ληφθεί από πειράματα δέσμης ταλαντώσεων νετρίνων μακράς γραμμής βάσης και από τη μελέτη ηλεκτρονικών αντινετρίνων από αντιδραστήρες πυρηνικής σχάσης. Υπάρχουν δύο πιθανές υπογραφές για τις ταλαντώσεις νετρίνων. Πρώτον, οι ταλαντώσεις νετρίνων μπορεί να έχουν ως αποτέλεσμα την εμφάνιση ¨λάθος¨ φορτισμένων λεπτονίων με γεύση, για παράδειγμα την παρατήρηση e^- και/ή μ^- από μια αρχικά καθαρή δέσμη ν_μ. Εναλλακτικά, οι ταλαντώσεις νετρίνων μπορούν να παρατηρηθούν ως η εξαφάνιση του «σωστού» φορτισμένου λεπτονίου με γεύση, όπου παράγονται λιγότερα από τα αναμενόμενα μ^- από μια αρχικά καθαρή δέσμη ν_μ.

Αστρονομία Νετρίνων

Η ενεργός διατομή αλληλεπίδρασης νετρίνων είναι πολύ μικρή και είναι ο λόγος για τον οποίο η αστρονομία νετρίνων είναι ένας πολύ πρόσφατος κλάδος. Για παράδειγμα, τα νετρίνα που παράγονται σε πυρηνικούς αντιδραστήρες με ενέργεια $\sim 1MeV$ έχουν ενεργό διατομή $\sim 10^{-44}cm^2$. Αυτό σημαίνει ότι από τα νετρίνα 10^{11} που θα ταξιδέψουν στη διάμετρο της Γης, μόνο ένα θα αλληλεπιδράσει. Αυτή η μικρή διατομή προσφέρει μια εξαιρετική ευκαιρία ανίχνευσης νετρίνων που προέρχονται από βαθιά μέσα στον πυρήνα των αστροφυσικών αντικειμένων, αποκαλύπτοντας άμεσα τις φυσικές διεργασίες που λειτουργούν εκεί. Σε αντίθεση με άλλους αγγελιοφόρους του Σύμπαντος όπως οι ακτίνες γ, τα πρωτόνια, τα ηλεκτρόνια και οι βαρύτεροι πυρήνες, τα νετρίνα που φτάνουν στη Γη δεν έχουν εκτραπεί ή απορροφηθεί ποτέ από την

παραγωγή τους, πράγμα που σημαίνει ότι δεν χάνουν ενέργεια και μπορούν να εντοπιστούν οι πηγές τους, ανακατασκευάζοντας τα ίχνη τους.

Η ιδέα ενός τηλεσκοπίου νετρίνων υψηλής ενέργειας που βασίζεται στην ανίχνευση δευτερογενών σωματιδίων που παράγονται από αλληλεπιδράσεις νετρίνων διατυπώθηκε για πρώτη φορά τη δεκαετία του 1960 από τον Markov. Η θεμελιώδης ποσότητα που πρέπει να γνωρίζουμε όταν προσπαθούμε να ανιχνεύσουμε νετρίνα είναι η ενεργός διατομή, η οποία είναι ένα μέτρο της αποτελεσματικής περιοχής στην οποία ένα νετρίνο αλληλεπιδρά με άλλη ύλη. Τα φαινόμενα της διάσπασης βήτα και αντίστροφης βήτα υποδηλώνουν ότι οι κατάλληλοι «στόχοι» πρέπει να είναι τα πρωτόνια και τα νετρόνια, αν και η σκέδαση ηλεκτρονίων μπορεί επίσης να είναι σχετική. Μπορούν να εντοπιστούν μόνο δύο τύποι αλληλεπιδράσεων. Ο πρώτος τύπος είναι η αλληλεπίδραση κατά την οποία ένα νετρίνο προκαλεί μια αντίδραση και αλλάζει κάποιο χημικό στοιχείο. Ένα παράδειγμα θα ήταν:

$$\nu_e + {}^{37}Cl \rightarrow e^- + {}^{37}Ar$$

Το νετρόνιο που συνδέεται με τον πυρήνα του χλωρίου μετατρέπεται σε πρωτόνιο, μέσω της ασθενούς αλληλεπίδρασης. Το άτομο που προκύπτει μετά την αντίδραση (${}^{37}Ar$) είναι χημικά διαφορετικό και η μέτρησή του μπορεί να αποκαλύψει τον αριθμό των νετρίνων που αλληλεπίδρασαν. Ο άλλος τύπος αλληλεπίδρασης θα ήταν:

$$\nu_e + e^- \rightarrow \nu_e + e^-$$

Σε αυτή την περίπτωση, είναι το φορτισμένο σωματίδιο (ηλεκτρόνιο) που μπορεί να ανιχνευθεί. Το σχήμα (1.6) δείχνει τη διατομή αυτής της αλληλεπίδρασης ως συνάρτηση της ενέργειας, που επικαλύπτεται με πηγές νετρίνων και πειράματα.

Η βασική αρχή ενός τηλεσκοπίου νετρίνων είναι μια διάταξη ανιχνευτών φωτός σε νερό ή πάγο, που προσφέρει μεγάλο όγκο ελεύθερου στόχου για αλληλεπιδράσεις νετρίνων ενώ ταυτόχρονα παρέχει θωράκιση έναντι των δευτερογενών κοσμικών ακτίνων. Τα σχετικιστικά φορτισμένα σωματίδια που παράγονται από αλληλεπιδράσεις νετρίνων εκπέμπουν ακτινοβολία Cherenkov στο διαφανές μέσο. Ένας ανιχνευτής πρέπει να μετρήσει με μεγάλη ακρίβεια τον αριθμό και τον χρόνο άφιξης αυτών των φωτονίων, από τον οποίο μπορούν να συναχθούν ορισμένες από τις ιδιότητες του νετρίνου (γεύση, κατεύθυνση, ενέργεια).

Υπάρχουν πολλές διαφορετικές διαδικασίες που παράγουν νετρίνα και μπορεί να είναι είτε φυσικά είτε ανθρωπογενή. Η φύση μας παρέχει ηλιακά νετρίνα που εκπέμπονται από τον ήλιο, ατμοσφαιρικά νετρίνα που παράγονται από την αλληλεπίδραση κοσμικών ακτίνων στην ατμόσφαιρα, κοσμολογικά νετρίνα από διάφορα βίαια γεγονότα στο διάστημα, γεωλογικά νετρίνα από πυρηνικές διασπάσεις στον πυρήνα της γης καθώς και νετρίνα από διασπάσεις βήτα. Τα τεχνητά νετρίνα παράγονται από πυρηνικούς αντιδραστήρες ή από ειδικά σχεδιασμένες δέσμες σε

επιταχυντές ή από πηγές υψηλής ραδιενέργειας.

Ακτινοβολία Cherenkov

Όταν ένα φορτισμένο σωματίδιο ταξιδεύει μέσα από ένα διαφανές μέσο με ταχύτητα μεγαλύτερη από την ταχύτητα του φωτός σε αυτό το μέσο, παράγονται φωτόνια (σωματίδια φωτός). Το μέσο μπορεί να είναι αέριο, υγρό ή στερεό. Αυτά τα φωτόνια εκτείνονται σε ένα εύρος μηκών κύματος από την υπεριώδη ακτινοβολία μέχρι το ορατό τμήμα του φάσματος της ηλεκτρομαγνητικής ακτινοβολίας. Η εκπομπή φωτονίων είναι αποτέλεσμα μιας συνεκτικής διαταραχής των παρακείμενων μορίων της ύλης που προκαλείται από το ταξιδεύον φορτισμένο σωματίδιο, το οποίο πρέπει να διαθέτει ένα ορισμένο κατώφλι ενέργειας. Αυτά τα φωτόνια αναφέρονται ως ακτινοβολία Cherenkov προς τιμήν του Ρώσου φυσικού Pavel A. Cherenkov για την ανακάλυψή του και τη βασική του έρευνα για τη μέτρηση των ιδιοτήτων της ακτινοβολίας και του φαινομένου, που τώρα αναφέρεται ως φαινόμενο Cherenkov.

Το φαινόμενο Cherenkov και η ακτινοβολία που παράγεται από ένα φορτισμένο σωματίδιο που ταξιδεύει σε ένα διαφανές μέσο με ταχύτητα που υπερβαίνει την ταχύτητα του φωτός σε αυτό το μέσο είχαν προβλεφθεί θεωρητικά ήδη από το 1888 από τον Oliver Heaviside, αλλά ξεχάστηκαν για πολύ μέχρι που η ακτινοβολία ανακαλύφθηκε τελικά από τον Cherenkov και ερμηνεύεται από τους Frank και Tamm (1937). Ο Govorkov (2005) εξέτασε την ιστορική σημασία της πρόβλεψης του Heaisιδε, δηλαδή ότι ο Heaviside προέβλεψε για πρώτη φορά θεωρητικά ότι ένα σημειακό φορτίο (ηλεκτρόνιο) θα παρήγαγε ένα μέτωπο κωνικού κύματος κάθε φορά που θα ταξίδευε με ταχύτητα μεγαλύτερη από την ταχύτητα του φωτός σε ένα μέσο. Η πρόβλεψη του Heaisιδε ήταν πριν από τη θεωρία της σχετικότητας του Αϊνστάιν, η οποία υποστηρίζει ότι η ύλη δεν μπορεί να ταξιδέψει ταχύτερα από το φως στο κενό, αλλά ότι η ύλη μπορεί να ταξιδέψει ταχύτερα από το φως σε ένα μέσο. Την εποχή του Heaviside, ακόμη και ο χώρος δεν θεωρούνταν κενό, αλλά ότι αποτελούνταν από έναν «αιθέρα», και επομένως, σύμφωνα με τον Heaisιδε, το κωνικό μέτωπο κύματος θα παρήχθη στον «αιθέρα» καθώς και σε οποιοδήποτε άλλο μέσο παρεχόταν. το ηλεκτρόνιο ή το σημειακό φορτίο ταξιδεύει με ταχύτητα μεγαλύτερη από αυτή του φωτός. Φυσικά, τα ηλεκτρόνια καθώς και άλλα φορτισμένα σωματίδια με επαρκή ενέργεια μπορούν πράγματι να ταξιδέψουν ταχύτερα από το φως σε μέσα όπου το φως ταξιδεύει με ταχύτητες μικρότερες από την ταχύτητά του στο κενό.

Η ακτινοβολία Cherenkov αποτελείται από ένα συνεχές φάσμα μηκών κύματος που εκτείνεται από την περιοχή κοντά στην υπεριώδη ακτινοβολία έως το ορατό τμήμα του φάσματος που κορυφώνεται στα 420 νμ περίπου. Μόνο μια αμελητέα ποσότητα εκπομπών φωτονίων βρίσκεται στις περιοχές υπερύθρων ή μικροκυμάτων. Η εκπομπή φωτονίων Cherenkov είναι το αποτέλεσμα τοπικής πόλωσης κατά μήκος της διαδρομής

του φορτισμένου σωματιδίου με την εκπομπή ηλεκτρομαγνητικής ακτινοβολίας όταν τα πολωμένα μόρια επιστρέψουν στην αρχική τους κατάσταση. Αυτό έχει περιγραφεί ως το ηλεκτρομαγνητικό κύμα «σοκ» που είναι ανάλογο με το ακουστικό κρουστικό κύμα ή ηχητική έκρηξη που δημιουργείται από υπερηχητικά αεροσκάφη.

Η συνθήκη κατωφλίου για την παραγωγή ακτινοβολίας Cherenkov σε διαφανές μέσο δίνεται από

$$\beta n = 1$$

όπου β είναι η σχετική ταχύτητα φάσης του σωματιδίου, δηλαδή η ταχύτητα του σωματιδίου διαιρεμένη με την ταχύτητα του φωτός στο κενό και n τον δείκτη διάθλασης του μέσου (δηλ. αναλογία της ταχύτητας του φωτός στο κενό προς την ταχύτητά του στο μέσο). Μόνο φορτισμένα σωματίδια με

$$\beta > \frac{1}{n}$$

παράγουν φωτόνια Cherenkov σε διαφανή μέσα. Μια σημαντική ιδιότητα της ακτινοβολίας Cherenkov είναι η ασυμμετρία της, δηλαδή η κατευθυντική εκπομπή των φωτονίων Cherenkov. Η ακτινοβολία Cherenkov δεν εκπέμπεται προς όλες τις κατευθύνσεις. Όταν ο Cherenkov (1936) ανακάλυψε τις ασύμμετρες ιδιότητες αυτής της ακτινοβολίας, ήξερε ότι είχε ανακαλύψει έναν τύπο ακτινοβολίας ακόμη άγνωστο. Οι Frank και Tamm (1937) εξήγησαν τη χωρική ασυμμετρία της ακτινοβολίας ως αποτέλεσμα του φορτισμένου σωματιδίου που ταξιδεύει σε ένα μέσο με ταχύτητα που υπερβαίνει την ταχύτητα του φωτός στο μέσο. Οι Frank και Tamm θεώρησαν ότι όταν η ταχύτητα φάσης του φορτισμένου σωματιδίου β υπερβαίνει το αντίστροφο του δείκτη διάθλασης ν του μέσου, δηλαδή $\beta > \frac{1}{n}$, τα φωτόνια Cherenkov εκπέμπονται ως κώνος υπό γωνία θ προς την κατεύθυνση του φορτισμένου σωματιδίου. Σύμφωνα με τη θεωρία των Frank και Tamm, η γωνία θ εκπομπής φωτονίων θα καθοριζόταν από τη σχέση

$$cos\theta = \frac{1}{\beta n}$$

η γωνία θ ορίζεται από την εξίσωση

$$cos\theta = \frac{\text{απόσταση διαδρομής μετώπου ακτινοβολίας στο μέσο}}{\text{απόσταση διαδρομής φορτισμένου σωματιδίου στο μέσο}}$$

ή

$$cos\theta = \frac{(\text{ταχύτητα φωτός στο μέσο}) \cdot \Delta t}{(\text{ταχύτητα σωματιδίου στο μέσο}) \cdot \Delta t} = \frac{(\frac{c}{n}) \cdot \Delta t}{\beta \cdot c \cdot \Delta t}$$

Καθώς η ενέργεια Ε του σωματιδίου αυξάνεται σε σχετικιστικές ταχύτητες, η τιμή του β πλησιάζει το 1

$$cos\theta = \frac{1}{n}$$

Εάν το νερό είναι το μέσο ($n = 1,33$):

$$cos\theta = \frac{1}{1,33} = 0,752\ , \qquad cos^{-1}(0,752) = 41,2^{\circ}$$

Διάδοση του φωτός σε μέσο

Η απορρόφηση είναι η μετατροπή της φωτεινής ενέργειας σε θερμική ενέργεια, ενώ η σκέδαση είναι η ανακατεύθυνση της φωτεινής ενέργειας με την παρουσία σκεδαστών. Η σκέδαση μπορεί επίσης να αντιμετωπιστεί ως απλή κατοπτρική ανάκλαση, διάθλαση και περίθλαση μέσα και γύρω από τα σωματίδια, ή ακόμα και με απορρόφηση και εκ νέου ακτινοβολία της ηλεκτρομαγνητικής ενέργειας.

Η μείωση του φωτός καθώς ταξιδεύει μέσα από ένα μέσο τόσο για απορρόφηση όσο και για σκέδαση μπορεί να περιγραφεί ως από τον νόμο Βεερ-Λαμβερτ:

$$I = I_0 \cdot e^{-ax}$$

$$I = I_0 \cdot e^{-bx}$$

όπου I_0 είναι η αρχική ένταση του φωτός, I είναι η ένταση του φωτός μετά τη διέλευση από το μέσο, x είναι το μήκος της διαδρομής μέσα στο μέσο και a, b είναι οι συντελεστές απορρόφησης και σκέδασης αντίστοιχα.

Η εξασθένηση του φωτός σε ένα μέσο είναι το συνδυασμένο αποτέλεσμα τόσο της απορρόφησης όσο και της σκέδασης, που εκφράζεται επίσης με την ίδια εξίσωση:

$$I = I_0 \cdot e^{-cx}$$

όπου

$$c = a + b$$

Οι εντάσεις μετρώνται σε $\frac{W}{m^2}$ και το γινόμενο cx πρέπει να είναι χωρίς μονάδα (αν $x \to m$, τότε $c \to m^{-1}$). Ο νόμος Βεερ-Λαμβερτ εφαρμόζεται μόνο σε ευθυγραμμισμένες δέσμες φωτός, όπως φαίνεται στο σχήμα (2.4).

Για μια ευθυγραμμισμένη δέσμη φωτός που ταξιδεύει σε κενό χώρο (χωρίς εμπόδια ή ηλεκτρομαγνητικά πεδία), η ένταση σε οποιαδήποτε απόσταση από την πηγή θα παραμείνει σταθερή καθώς τα ίχνη των φωτονίων δεν θα αλλάξουν λόγω της σκέδασης. Ενώ σε ένα μέσο, υπάρχουν δύο τύποι μονοπατιών που το φως μπορεί να ταξιδέψει από μία πηγή σε έναν δέκτη. Το συνολικό φως είναι το άθροισμα της μόνοδρομης και της σκεδασμένης ακτινοβολίας, όπως φαίνεται στο σχήμα (2.5).

Σημειακές ή σφαιρικές πηγές φωτός (ή πηγές που δεν ευνοούν μια συγκεκριμένη κατεύθυνση) ακτινοβολούν σε σφαιρικά μέτωπα, ακολουθώντας τον νόμου του Αντίστροφου Τετραγώνου. Η μετρούμενη ένταση σε ένα μέσο, σε συγκεκριμένη απόσταση μακριά από την πηγή, θα είναι ο συνδιασμός των νόμων Beer-Lambert και Αντίστροφου Τετραγώνου:

$$I = \frac{S}{4\pi R^2} \cdot e^{-\beta R}$$

όπου R είναι η απόσταση μέτρησης από τη σφαιρική πηγή σε m. Η ένταση I εξακολουθεί να μετράται σε $\frac{W}{m^2}$, αλλά η αρχική ένταση I_0 αντικαταστάθηκε με την ισχύ S, η οποία μετράται σε W. Ήταν επίσης απαραίτητο να μετονομαστεί ο συντελεστής εξασθένησης c σε συντελεστή μετάδοσης β, όπως κάνει η περισσότερη βιβλιογραφία, για να διαφοροποιηθεί η εξασθένηση του ευθυγραμμισμένου φωτός σε μη ευθυγραμμισμένο, σφαιρικά διασκορπισμένο φως.

Ο συντελεστής μετάδοσης β εξαρτάται από το μήκος κύματος του φωτός και τις φυσικές ιδιότητες του μέσου, ως επέκταση της εξάρτησης της απορρόφησης και της σκέδασης σε αυτές τις παραμέτρους. Σε αυτή τη διατριβή, το μέσο ενδιαφέροντος είναι το θαλασσινό νερό και οι σφαιρικές πηγές φωτός θα είναι ΛΕΔ που εκπέμπουν σε συγκεκριμένα μήκη κύματος. Ο συντελεστής μετάδοσης β μπορεί επίσης να αναφέρεται ως μήκος μετάδοσης, που ορίζεται από τη μαθηματική έκφραση:

$$R_\beta = \frac{1}{\beta}$$

Το σχετικό σφάλμα στη μέτρηση του β δίνεται από

$$\frac{\Delta\beta}{\beta} = \frac{1}{\beta \cdot R}\frac{\Delta I}{I}$$

Σε καθαρά νερά ο συντελεστής μετάδοσης έχει μικρές τιμές (και το μήκος μετάδοσης

L_β έχει μεγάλες τιμές), επομένως μια ακριβής μέτρηση του β απαιτεί είτε ένα όργανο ικανό να μετρήσει την ένταση του φωτός με εξαιρετική ακρίβεια (έτσι ώστε $\frac{\Delta I}{I}$ μπορεί να είναι πολύ μικρό) ή ένα όργανο με μεγάλη οπτική διαδρομή (έτσι ώστε το P να είναι επαρκώς μεγάλο).

Σε πολλές περιπτώσεις, η σκέδαση είναι τόσο μικρή που η απορρόφηση είναι η κύρια αιτία μετάδοσης φωτός. Οι ιδιότητες απορρόφησης του νερού μπορούν εύκολα να προσδιοριστούν. Τόσο το μακρινό κόκκινο όσο και το μακρινό ιώδες άκρο του ορατού φάσματος εξασθενούν πολύ έντονα από την απορρόφηση, ενώ υπάρχει μια κορυφή στο μπλε-πράσινο τμήμα, στα 470 νανόμετρα περίπου. Η σκέδαση είναι κατά κύριο λόγο μια συνάρτηση των αιωρούμενων υλικών στο νερό, η ποσότητα και ο τύπος της διασποράς ποικίλλει ανάλογα με την ποσότητα και τον τύπο των αιωρούμενων. Θα ήταν αναμενόμενο, για παράδειγμα, ότι τα αποτελέσματα σκέδασης για μικρά σωματίδια αργίλου και εκείνα για πλαγκτόν παρόμοιου μεγέθους θα ήταν διαφορετικά, όπως θα ήταν αυτά για μικρά και μεγάλα σωματίδια του ίδιου υλικού. Όχι μόνο η σκέδαση ποικίλλει τόσο σε μέγεθος όσο και σε κατεύθυνση με την ποσότητα των σωματιδίων σε εναιώρημα, αλλά ποικίλλει ανάλογα με το μέγεθος των σωματιδίων σε σχέση με το μήκος κύματος του προσπίπτοντος φωτός και τον δείκτη διάθλασης του υλικού σκέδασης.

Neutrinos

1.1 The Standard Model

The Standard Model is a particle physics theory that describes our current understanding of our universe's fundamental constituents (elementary particles) and their interactions (forces).

Fermions and bosons are two types of elementary particles that can be distinguished by their spin values, which are half-odd-integer values for fermions and integer values for bosons. Generally, fermions are associated with matter while bosons are force-carrier particles.

Fermions are separated into quarks and leptons, as well as three generations based on their mass and stability: The lightest and most stable particles are in the first generation, while the heaviest and most unstable particles are in the third generation, with the second generation in the middle. Because all stable matter in the cosmos is made up of first-generation particles, any heavier particles immediately decay into more stable ones.

There are 6 quarks: (*u*)p, (*d*)own, (*c*)harm, (*s*)trange, (*t*)op and (*b*)ottom. Each quark has an antiquark, which is a quark with the same mass but the opposite charge. When quarks (and antiquarks) come together, they form hadrons, which are composite particles. These hadrons are classified as baryons (qqq), antibaryons ($\overline{qqq}$), or mesons ($q\bar{q}$) depending on their quark composition. Baryons with quark content (uud) and (udd) are protons and neutrons, respectively.

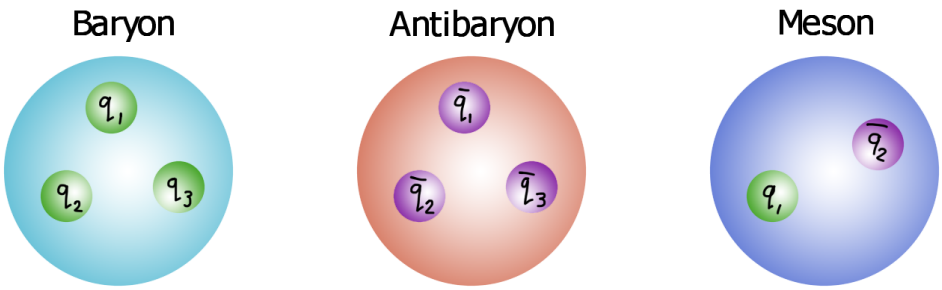

Figure 1.1: All types of hadrons: Baryons are composed of 3 quarks, antibaryons of 3 antiquarks and mesons contain 1 quark and 1 antiquark

Leptons, on the other hand, can only exist as single particles and cannot form composite particles. The electron (e), muon (μ), and tau (τ) are electrically charged (-1) leptons, sorted by increasing mass. A neutrino is assigned to each of them: the electron neutrino (ν_e), muon neutrino (ν_μ), and tau neutrino (ν_τ). Neutrinos have very little mass and are electrically neutral. Antileptons are particles with opposite electric charge (wherever that's possible) and opposite lepton number. The lepton number is a conserved quantum number which has a value of either +1 or -1 and distinguishes between leptons and anti-leptons.

One of the bosons is a very well-known particle: the photon γ, which is the force carrier of electromagnetism. The Standard Model also incorporates two extra forces: the strong force (also known as quantum chromodynamics or QCD) and the weak force. The strong and weak forces, unlike electromagnetic and gravity, exist only over very small distances and have no equivalents in classical physics. The gluon g is the strong force's force carrier, and it is responsible for holding atomic nuclei together. The radioactive decay of unstable materials like uranium is mediated by the weak force. The force carriers of the weak force are the W^+, W^- and Z bosons. The gravitational force is also theorized to be carried by a boson, namely the graviton, but it has not been discovered yet.

The Higgs boson provides the mechanism by which all other particles acquire mass. Without it, the particles would be massless and would propagate at the speed of light. In Quantum Field Theory, when it comes to fundamental fermions and bosons, their fields have zero expectation value in the vacuum. The Higgs field however does not. The interaction of the initially massless particles with this non-zero Higgs field gives them their masses. [1]

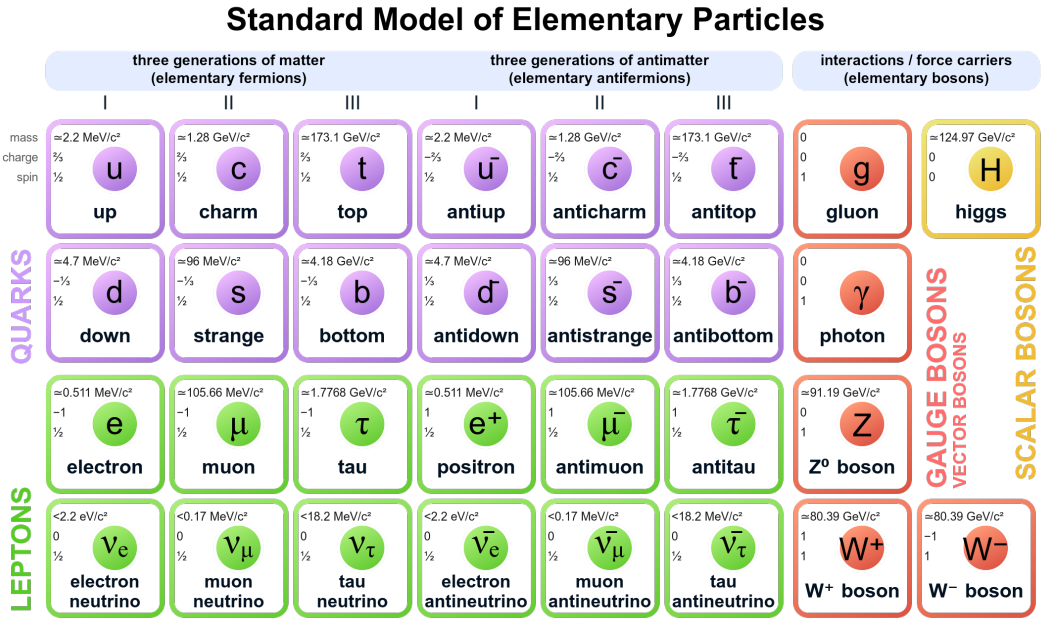

Figure 1.2: The Standard Model in a picture

1.2 History

Pauli proposed the neutrino hypothesis in 1930. It all began with a letter written by Pauli on December 4, 1930, to the participants of a nuclear physics conference in Tubingen, Germany, in which he proposed the existence of a new neutral weakly interacting particle with spin $\frac{1}{2}$ and dubbed it "neutron" as a "verzweifelten Ausweg" (desperate remedy) to explain two outstanding problems in contemporary nuclear physics that posed major difficulties with respect to the scientists' theoretical interpretations. [2]

These two issues were linked to the puzzle of energy conservation in β-decays of nuclei, discovered by J. Chadwick in 1914, as well as anomalies in understanding the spin-statistics relation in the case of ${}^{1}4N$ and ${}^{6}Li$ nuclei in the context of the nuclear structure model, in which electrons and protons were considered nuclear constituents. When Chadwick discovered in 1932 the neutron as we know it today, E. Fermi renamed the Pauli particle as neutrino. The neutrino was originally mentioned in the Proceedings of the Solvay Conference in October 1933. In the same year, Fermi and Perrin independently came to the same conclusion that neutrinos could be massless. [3]

In 1934 Fermi formulated a theory of β-decay, now known as Fermi theory, in analogy with quantum electrodynamics (QED). In order to explain the observed change of one unit of the nuclear spin in some β-decays, G. Gamow and E. Teller in 1936 extended the theory by introducing axial-vector currents in such a way that parity was still conserved since parity violation at that time was unthinkable.

The remarkable success of the Fermi theory left few in doubt of the neutrino's existence, however, none had yet been observed in interactions, partly because of the predicted strength of interactions by H. Bethe and R. Peierls, who claimed in 1934 that it might never be observed. Urged, in particular by B. Pontecorvo in the early 1950s, F. Reines and C.L. Cowan searched for a way to measure inverse β-decay, in which an antineutrino can produce a positron. After considering several methods, including a nuclear explosion, they settled on using the large flux of antineutrinos from a nuclear reactor and 10 tons of equipment, including 1400 liters of liquid scintillators. This experiment was the first reactor-neutrino experiment. In June of 1956, Reines and Cowan sent a telegram informing Pauli of the discovery. Reines (Cowan passed away) was awarded the Nobel prize 40 years later.

Neutrinos challenge our expectations regarding the validity of certain symmetry principles and conservation laws in particle physics. The study of neutrinos and their interaction with matter has made many important contributions to our present knowledge of physics, which is highlighted by the fact that ten Nobel Prizes have been awarded for physics discoveries in topics either directly in the field of neutrino physics or in the topics in which the role of neutrino physics has been very crucial.

1.3 Interactions

Neutrino interactions are described, with an impressive accuracy, by the Standard Model. So far no deviations from the standard neutrino interactions have been found in experimental data. [4] [2]

The standard neutrino interactions are described by the leptonic charged current as:

$$j^{\rho}_{W,L} = 2 \sum_{a=e,\mu,\tau} \overline{\nu_{aL}} \cdot \gamma^{\rho} \cdot l_{aL} = \sum_{a=e,\mu,\tau} \overline{\nu_a} \cdot \gamma^{\rho} \cdot (1-\gamma^5) \cdot l_a \tag{1.1}$$

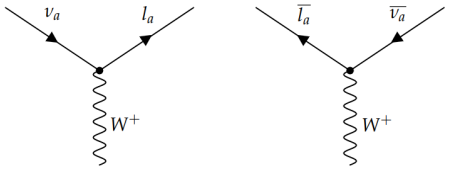

Figure 1.3: The Feynman diagrams for neutrino positive charge current interactions

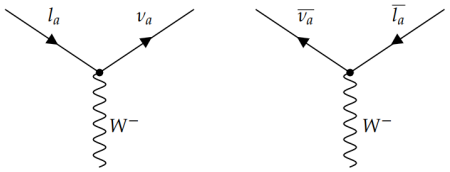

Figure 1.4: The Feynman diagrams for neutrino negative charge current interactions

and the neutrino part of the leptonic neutral current is:

$$j^{\rho}_{Z,L} = \sum_{a=e,\mu,\tau} \overline{\nu_{aL}} \cdot \gamma^{\rho} \cdot \nu_{aL} = \frac{1}{2} \sum_{a=e,\mu,\tau} \overline{\nu_a} \cdot \gamma^{\rho} \cdot (1-\gamma^5) \cdot \nu_a \tag{1.2}$$

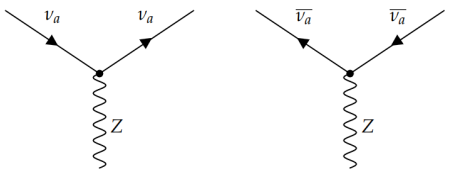

Figure 1.5: The Feynman diagrams for neutrino neutral charge current interactions

1.4 Oscillations

Until the late 1990s, relatively little was known about neutrinos beyond that there are three distinct flavours and that they are extremely light (and possibly massless). However, even at that time several experiments had reported possible anomalies in the observed interaction rates of atmospheric and solar neutrinos. This picture changed with the publication of the solar and atmospheric neutrino data from the Super-Kamiokande detector, which provided compelling experimental evidence for the phenomenon of neutrino flavour oscillations over very large distances. The subsequent study of neutrino oscillations has been one of the highlights of particle physics in recent years. [5]

The mass eigenstates are the stationary states of the freeparticle Hamiltonian and satisfy

$$\widehat{H}\psi = \imath\frac{\partial\psi}{\partial t} = E\psi \tag{1.3}$$

The time evolution of a mass eigenstate takes the form of

$$\psi(\mathbf{x}, t) = \phi(\mathbf{x})e^{-\imath Et} \tag{1.4}$$

The neutrino mass eigenstates (the fundamental particles) are labeled ν_1, ν_2 and ν_3. There is no reason to believe that the mass eigenstates should correspond to the weak eigenstates, ν_e, ν_μ and ν_τ, which are produced along with the respective flavor of charged lepton in a weak interaction. Any one of the three mass eigenstates can be produced in conjunction with the electron in the initial weak interaction. Since it is not possible to know which mass eigenstate was produced, the system has to be described by a coherent linear superposition of ν_1, ν_2 and ν_3 states. In quantum mechanics, the basis of weak eigenstates can be related to the basis of mass eigenstates by a unitary matrix U,

$$\begin{bmatrix}\nu_e\\ \nu_\mu\\ \nu_\tau\end{bmatrix} = \begin{bmatrix}U_{e1} & U_{e2} & U_{e3}\\ U_{\mu1} & U_{\mu2} & U_{\mu3}\\ U_{\tau1} & U_{\tau2} & U_{\tau3}\end{bmatrix}\begin{bmatrix}\nu_1\\ \nu_2\\ \nu_3\end{bmatrix} \tag{1.5}$$

Hence the electron neutrino, which is the quantum state produced along with a positron in a charged-current weak interaction, is the linear combination of the mass eigenstates defined by the relative charged-current weak interaction couplings of the ν_1, ν_2 and ν_3 at the $W^+ \rightarrow e^+ + \nu_e$ vertex

$$|\psi\rangle = U_{e1}^*|\nu_1\rangle + U_{e2}^*|\nu_2\rangle + U_{e3}^*|\nu_3\rangle \tag{1.6}$$

The neutrino state subsequently propagates as a coherent linear superposition of the three mass eigenstates until it interacts and the wavefunction collapses into a weak eigenstate, producing an observable charged lepton of a particular flavor. If the masses of the ν_1, ν_2 and ν_3 are not the same, phase differences arise between the different components of the wavefunction and the phenomenon of neutrino oscillations occurs. In this way, a neutrino produced along with one flavor of charged lepton can interact to produce a charged lepton of a different flavor.

Early experimental results on neutrino oscillations were obtained from studies of solar neutrinos and the neutrinos produced in cosmic-ray-induced cascades in the atmosphere. More recent results have been obtained from long-baseline neutrino oscillation beam experiments and from the study of electron anti-neutrinos from nuclear fission reactors. There are two possible signatures for neutrino oscillations. Firstly neutrino oscillations can result in the appearance of ”wrong” flavor charged leptons, for example the observation of e^- and/or μ^- from an initially pure beam of ν_μ. Alternatively, neutrino oscillations can be observed as the disappearance of the ”right” flavor charged lepton, where fewer than expected μ^- are produced from an initially pure ν_μ beam.

1.5 Neutrino Astronomy

The neutrino interaction cross-section is very small and is the reason why neutrino astronomy is a very recent discipline. For example, neutrinos produced in nuclear reactors with $\sim 1MeV$ energy have a cross-section of $\sim 10^{-44}cm^2$. This means that out of 10^{11} neutrinos that will travel through the Earth's diameter, only one will interact. This small cross-section offers an excellent opportunity to detect neutrinos that originate from deep inside the core of astrophysical objects, revealing directly the physical processes in operation there. Unlike other messengers of the Universe like γ-rays, protons, electrons and heavier nuclei, neutrinos that reach the Earth have never been deflected or absorbed since their production, meaning they do not lose energy and can be traced back to their sources by reconstructing their tracks. [6] [7]

The idea of a telescope for high-energy neutrinos based on the detection of secondary particles produced by neutrino interactions was first formulated in the 1960s by Markov. The fundamental quantity we need to know when trying to detect neutrinos is the cross-section, which is a measure of the effective area over which a neutrino interacts with other matter. The phenomena of beta and inverse beta decay suggest that appropriate "targets" should be protons and neutrons, although electron scattering may also be relevant. Only two types of interactions can be detected. The first type is the interaction in which a neutrino provokes a reaction and changes some chemical element. An example would be:

$$\nu_e + {}^{37}Cl \rightarrow e^- + {}^{37}Ar \tag{1.7}$$

The neutron bound to the chlorine nucleus is converted into a proton, through the weak interaction. The resulting atom after the reaction (^{37}Ar) is chemically different and counting it can reveal the number of neutrinos that interacted. The other type of interaction would be:

$$\nu_e + e^- \rightarrow \nu_e + e^- \tag{1.8}$$

In this case, it is the charged particle (electron) that can be detected. Figure (1.6) shows the cross-section of this interaction as a function of energy, overlaid with neutrino sources and experiments.

The basic principle of a neutrino telescope is a matrix of light detectors in water or ice, which offers large volume of free target for neutrino interactions while providing at the same time a shielding against secondary cosmic rays. The relativistic charged particles produced by neutrino interactions emit Cherenkov radiation (will be explained in section 2.1) in the transparent medium. A detector must measure with high precision the number and arrival time of these photons, from which some of the properties of the neutrino (flavor, direction, energy) can be inferred.

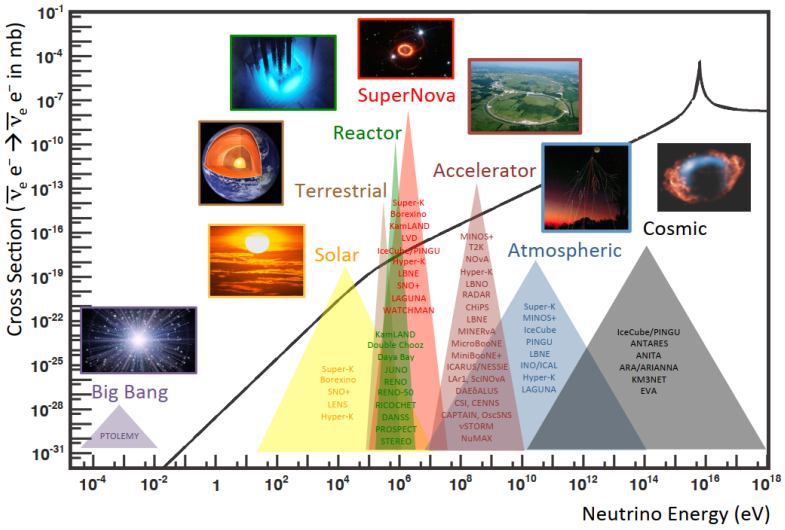

Figure 1.6: Scattering cross-section of $\nu_e + e^- \to \nu_e + e^-$ as a function of energy, showing typical energy regimes accessible by different neutrino sources and experiments. [8]

There are several different processes that produce neutrinos and they can be either natural or man-made. Nature provides us with solar neutrinos emitted by the sun, atmospheric neutrinos produced by the interaction of cosmic rays in the atmosphere, cosmological neutrinos produced by a variety of deep space violent events, geological neutrinos produced by nuclear decays in the earth core as well as neutrinos produced in beta decay. Man-made neutrinos are produced by nuclear reactors or by specially designed beams at accelerators or by highly radioactive sources. [9]

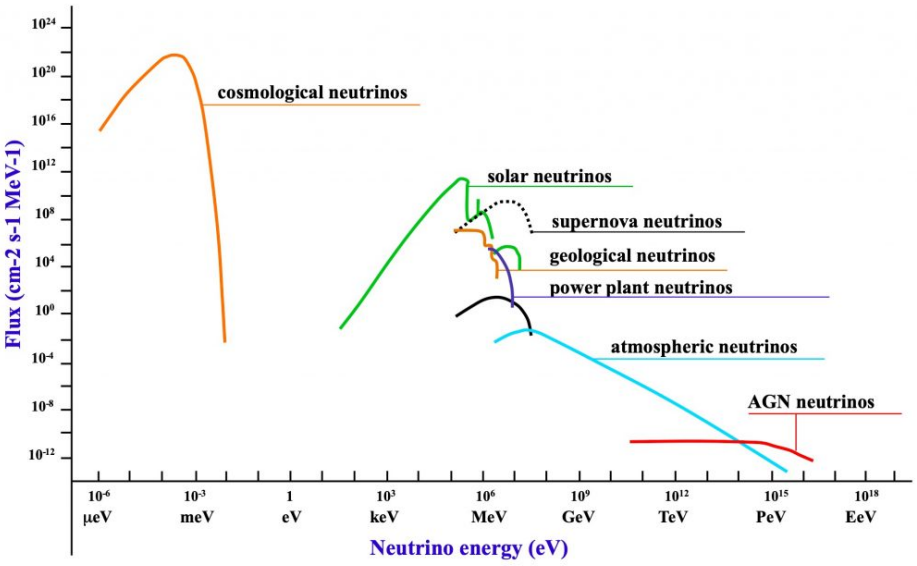

Figure 1.7: Variations of neutrino energies depending on the source

1.5.1 Atmospheric Neutrinos

Atmospheric neutrinos are typically produced in the interaction of primary cosmic ray particles with the earth's atmosphere. Cosmic rays are high energy particles, mainly protons and alpha particles, also categorized as primary cosmic rays. The observed energy and isotropy of the cosmic rays suggest that they come from outside the solar system, but within our galaxy, apart from a small component coming from solar flares. There is also a small fraction of cosmic rays that have other galactic and extra galactic sources. The exact source of cosmic rays is not yet known but may possibly be black holes, neutron stars, pulsars, quasars, or even the Big Bang. The composition of the primary cosmic rays are protons (90.6%), alpha particles (9%), and a small fraction of CNO nuclei (0.4%) above $\sim$ 100 MeV/nucleus, and 95.2% protons, 4.5% alpha particles, and 0.3% of CNO nuclei above $\sim$ 2 GeV/nucleus.The differential energy spectrum follows a power law of the form:

$$N(E)\,dE \propto E^{\gamma}\,dE \tag{1.9}$$

with features known as "knee" and "ankle" at $10^{15}eV$ and $10^{18}eV$, respectively. Hence, the spectrum steepens to $\gamma \simeq 3$ at the knee. At the 'ankle', there is a flattening of spectrum, again resulting in $\gamma \simeq 2.7$. This can be seen in the figure below.

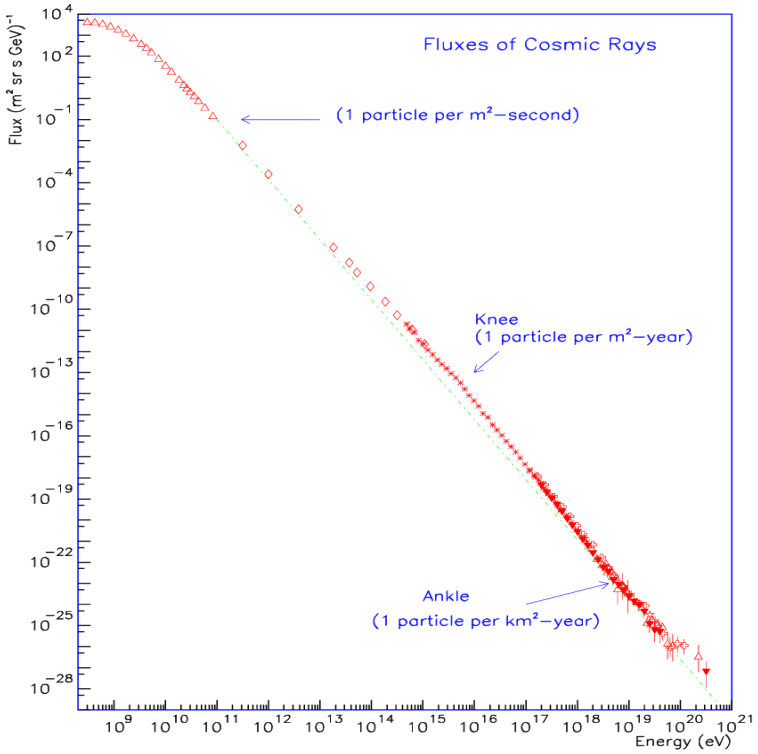

Figure 1.8: Fluxes of cosmic rays as a function of energy [10]

When these primary cosmic rays interact with the earth's atmosphere, they produce secondary cosmic rays, consisting mainly of pions and kaons: [2]

$$\pi^+ \rightarrow \mu^+ + \nu_\mu \tag{1.10}$$

$$\pi^- \rightarrow \mu^- + \overline{\nu}_\mu \tag{1.11}$$

$$K^+ \rightarrow \mu^+ + \nu_\mu \tag{1.12}$$

$$K^- \rightarrow \mu^- + \overline{\nu}_\mu \tag{1.13}$$

$$K_s^0 \rightarrow \pi^+ + \pi^- \tag{1.14}$$

$$K_l^0 \rightarrow \pi^+ + \pi^- + \pi^0 \tag{1.15}$$

The muons which decay before hitting the ground generate electrons, electron neutrinos, and muon neutrinos through the processes

$$\mu^+ \rightarrow e^+ + \nu_e + \overline{\nu}_\mu \tag{1.16}$$

$$\mu^- \rightarrow e^- + \overline{\nu}_e + \nu_\mu \tag{1.17}$$

The sources of neutrinos of energies up to around 100 GeV are mainly pion decays, while the higher energy neutrinos are produced from kaon decays, as the mean free path for the pions becomes sufficiently large at higher energies and they are able to reach the earth before decaying into muons and neutrinos. The most abundant charged particles at sea level are muons, which are produced high in the atmosphere ($\sim 15km$) and come to ground, after ionization losses. The number of μ^+ is more than the number of μ^-, because there are more π^+, K^+ than π^-, K^-, as there are more protons than neutrons present in the primary cosmic ray components.

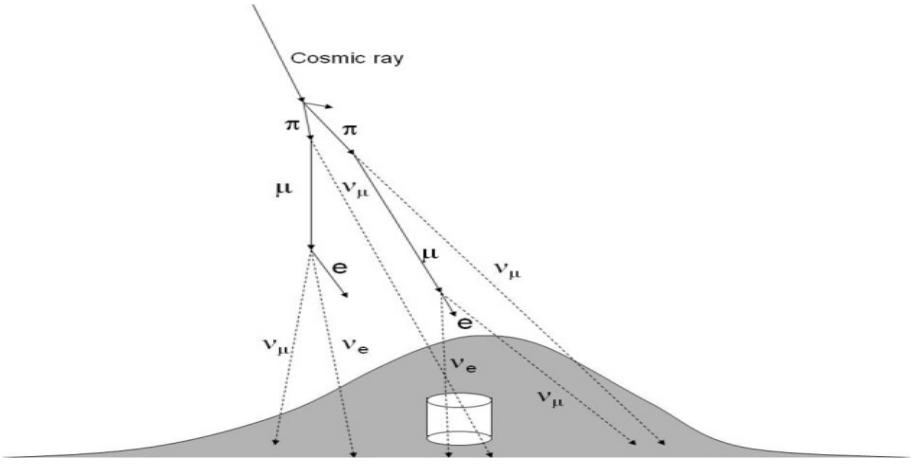

Figure 1.9: Schematic of cosmic rays interacting with the atmosphere and the reactions

1.5.2 Cosmic Neutrinos

Relic neutrinos are one of the most abundant components of the universe. They are also known as the cosmic neutrino background (CNB). These neutrinos are the relics of the Big Bang, originating from the decoupling of matter through weak interactions when the universe was about one second old and the primordial plasma had a temperature of about 1 MeV ($\sim 10^{10}K$). Thus, apart from the 3 K black body electromagnetic radiation known as cosmic microwave background radiation (CMBR), the universe is filled with a sea of relic neutrinos. The average relic electron neutrino number density is around $\langle n \rangle \approx 56cm^{-3}$, while that of CMBR is $\langle n_\gamma \rangle \approx 450cm^{-3}$. These relic neutrinos have played a crucial role in primordial nucleosynthesis, structure formation, and the evolution of the universe as a whole. They may also provide clues about the mechanism of baryogenesis. [2]

Cosmic neutrinos are very important probes to learn the fundamental physics beyond the TeV scale. The energy scale which can be achieved with cosmic sources at the surface of the earth, is well beyond the energy available from solar neutrinos, atmospheric neutrinos, supernova neutrinos, reactor antineutrinos, or even with the present accelerators.

At the EeV scale, cosmogenic neutrinos are produced due to the interaction of ultra high energy (UHE) cosmic rays with the cosmic microwave background radiations through the Greisen–Zatsepin–Kuzmin (GZK) effect. When an ultra high energy proton, produced in some far away astrophysical object like a black hole accreting matter, scatters off a photon present as CMBR, it produces very high energy pions, that is

$$p + \gamma \rightarrow n + \pi^+ \tag{1.18}$$

The threshold energy required by the proton in the rest frame of the cosmic background radiation is obtained by the following considerations. The temperature of the CMBR is approximately 2.7 K, which corresponds to $235\mu eV = 2.35 \cdot 10^{-13} GeV$. [2]

High-energy neutrino fluxes from cosmologically distant sources are generally expected in association with the production of cosmic rays, whose energy spectrum extends to 1020 eV and is likely dominated above $\sim$ 3 eV by protons, neutrons, and nuclei of extragalactic origin. Source candidates include galactic sources like supernova remnants and extragalactic sources like active galactic nuclei and gamma ray bursts. [3]

1.5.3 Active Galactic Nuclei

Active galaxies are distinguished from normal galaxies by the amount of radio emission that they produce. The centers of these galaxies contain small, dense and luminous components known as active galactic nuclei (AGN). AGNs emit strongly over the whole electromagnetic spectrum, including the radio, X-ray, and γ-ray regions where most galaxies hardly radiate at all. With luminosities exceeding $10^{12} L_{\odot}$, many are bright enough to be seen most of the way across the observable Universe. The emitting region however, may be no bigger than the solar system. Their power source is probably the energy released by gas falling into a supermassive accreting black hole in their center. Such systems can be extremely efficient in converting gravitational energy into radiation. The enormous energy output of AGNs may have an important feedback effect on the formation and evolution of galaxies. It is estimated that in the local universe, about 1 out of 50 galaxies contains a fast-accreting supermassive black hole, and about 1 in 3 contains a slowly accreting supermassive black hole. Observations of neutrinos associated with the AGN known as TXS 0506+056 indicated of neutrino production in AGNs and thus neutrino astronomy was born. The neutrinos' energy range is between 100 GeV and a few TeV. [11] [12] [13] [14] [15]

We can identify three major classes of active galaxies: Seyfert galaxies, quasars, and radio galaxies. Seyfert galaxies can be thought of as low-luminosity compared to quasars but are otherwise similar to each other. Radio galaxies are different in that their nuclear emission often is not prominent in wavelengths other than radio.

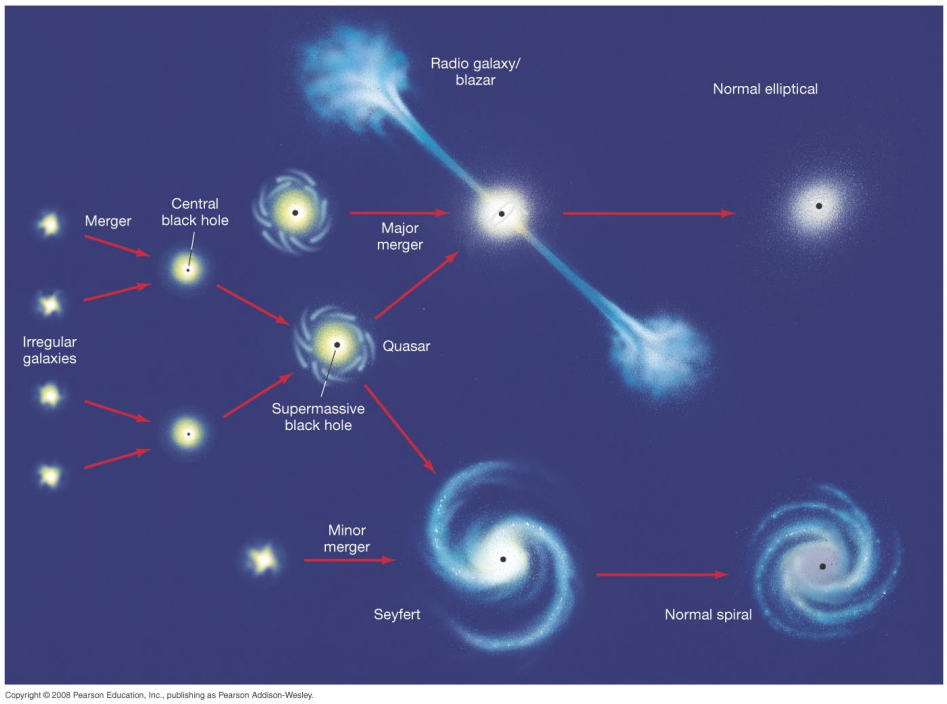

Figure 1.10: A possible evolutionary sequence for active galaxies [16]

1.5.4 Gamma Ray Bursts

Gamma Ray Bursts (GRBs) were discovered in the 1960s by both the United States and the former Soviet Union, when they launched military satellites to monitor adherence to the nuclear test-ban treaty. These satellites were γ-ray detectors, as the signature of a nuclear detonation is a brief but intense pulse of γ-rays. On July 1967, a γ-ray signal was detected by those satellites but did not match the profile of a nuclear weapon explosion, as neither the intense initial flash nor the gradual fading were characteristic of an explosion. In 1973 the observations became public and identified a cosmic source as the origin of the γ-rays. [6]

The next milestone in the history of GRBs was the launch of the BATSE experiment on the CGRO satellite. BATSE found conclusive proof that GRBs occur isotropically in the sky and categorized GRBs in two families: short-duration ($\sim 0.3s$) and long-duration ($\sim 30s$) GRBs, which have different spectra. Thanks to the BATSE data it has also been possible to measure the typical fluence (the flux integrated over time) of GRBs. The emission spectra of the GRBs show a peculiar nonthermal behavior, peaking at around a few hundred keV and extending up to several GeV.

Each family of GRBs is associated with a different progenitor. Observations show that host galaxies of long GRBs are active star forming galaxies. In several cases it has been proven that long GRBs happen in correlation with supernovae, linking them unambiguously with the death of a massive star. Core-collapse supernovae are the explosive deaths of massive stars that occur when their iron cores collapse to neutron stars or black holes. In the case of short GRBs, it was found that they are distributed uniformly among galaxies that contain a considerable quantity of old stars. In these galaxies there is no evidence of significant star formation, and such an old population is compatible with the presence of neutron star binary systems. The estimated total kinetic energy emitted by short GRBs exceeds that of long GRBs by many orders of magnitude. The current hypothesis attributes the origin of short GRBs to the merging of two compact objects. Possible candidates for such a process are mergers of neutron star binaries or neutron star-black hole binaries, which lose angular momentum and undergo a merger.

It is important to notice that although the two families of GRBs are known to have different progenitors, the acceleration mechanism that gives rise to the γ-rays themselves (and probably to the production of neutrinos) is most likely independent of the progenitor of the event. The fireball model is the most widely used theoretical framework to describe the physics of the GRBs. Based on the release of the large amounts of energy (10^3 erg on timescales of tens of seconds or less) the observed emission of γ-rays and the afterglow must arise from an emission region moving at relativistic velocities. The energy release in such short times in such compact regions produces a luminosity which exceeds the Eddington luminosity, above which radiation pressure overwhelms gravity.

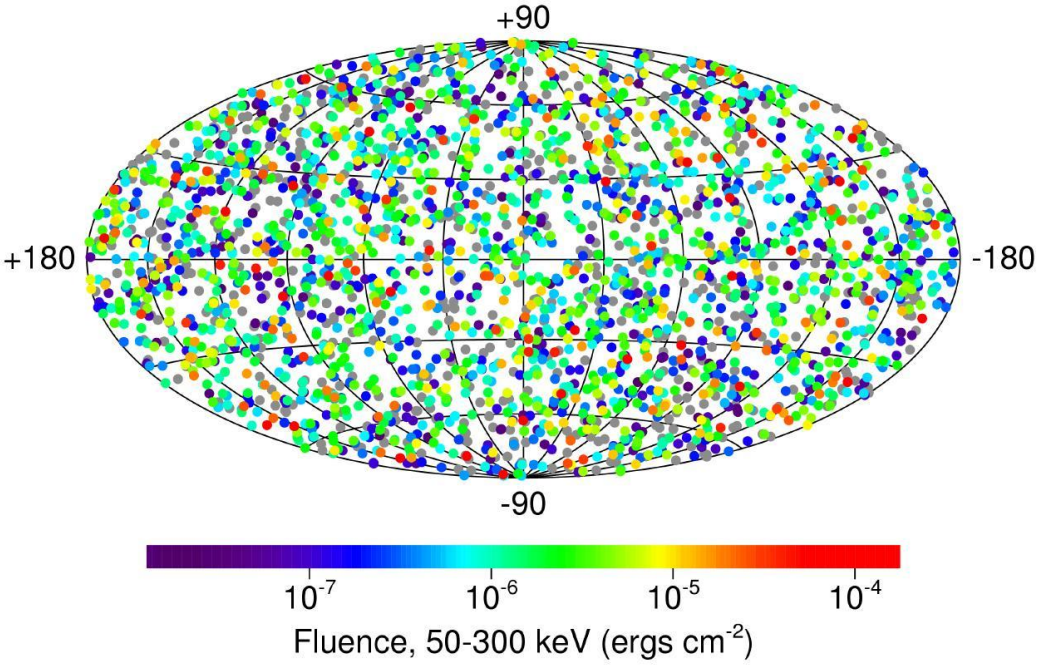

Figure 1.11: Sky distribution of the GRBs detected by BATSE GRBs. Long duration, bright bursts are shown in red, while shorter, weak bursts appear in purple

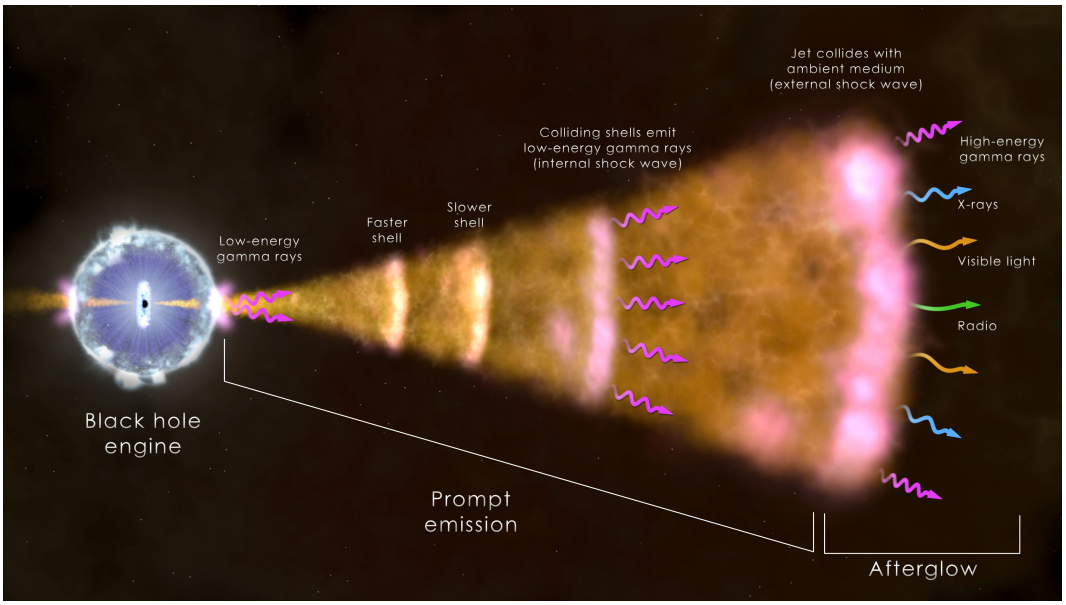

Figure 1.12: Gamma Ray Bursts - Fireball Model as illustrated by NASA

1.5.5 Supernovae

The term nova was introduced by the Danish astronomer Tycho Brahe in his printed work *De Nova Stella* ("On the New Star"), which signified "new" in Latin. The term described unresolved celestial objects whose flux increased abruptly in a short period of time, which gave the impression that new stars appeared in the sky. The modern definition of nova states that it is a type of cataclysmic variable, in which a normal star dumps gas onto a white dwarf. Thus, a nova is actually a close binary system in which a star and a white dwarf orbit their mutual center of mass. [17] [11]

Novae are energetic events and the brightest nova outburst can produce as much light in a week as the Sun does in 10,000 years. Supernovae are at least 7 magnitudes brighter than the brightest novae. The term "super-nova" was proposed by Fritz Zwicky and Walter Baade in 1934, when they suggested that outbursts of light much brighter than ordinary novae would be produced when the core of a massive star collapsed to form a neutron star. Supernovae can be classified according to their spectra, to "type I" and "type II":

- Type I supernovae do not show hydrogen absorption lines, such as the Balmer lines, in their spectra.
- Type II supernovae do show hydrogen absorption lines.

The distinction of spectra is also a distinction of the events that take place. Type Ia supernovae accumulate matter from a nearby neighbor until a runaway nuclear reaction ignites. Type II supernovae are stars that run out of nuclear fuel and collapse under their own gravity. Type 1b are similar to type II supernovae, with the difference of having lost completely their hydrogen rich outer layers first and then undergo core collapse. The physics of type Ib and II are basically the same, with the exception of showing hydrogen absorption lines. Through these events, the supernovae emit energy as kinetic energy, light and neutrinos. The energy distribution of these emissions is shown in Table (1.1)

	Energy Distribution	
Emission	Type Ia	Types Ib, II
Kinetic Energy	99%	1%
Neutrinos	0%	99%
Light	1%	0.01%

Table 1.1: Energy distribution of the emissions of different types of supernovae

From Table (1.1) it is apparent that core-collapse supernovae emit most of their energy as neutrinos. When the core of the star becomes constituted primarily of iron, further compression of the core does not ignite nuclear fusion and the star is unable to thermodynamically support its outer envelope. As the surrounding matter falls inward under gravity, the temperature of the core rises and iron dissociates into α particles and nucleons. Electron capture on protons becomes heavily favored and electron neutrinos are produced as the core gets neutronized (a process known as neutronization). When the core reaches densities above $10^3 \frac{g}{cm^3}$, neutrinos become trapped (in so-called neutrinospheres). The collapse continues until 3-4 times nuclear density is reached, after which the inner core rebounds, sending a shock-wave across the outer core and into the mantle. This shock-wave loses energy as it heats the matter it traverses and incites further electron capture on the free protons left in the wake of the shock. During the few milliseconds in which the shock-wave travels from the inner core to the neutrinosphere, electron neutrinos are released in a pulse.

Physics Principles for Under-Water Measurements

2.1 Cherenkov Radiation

Particles of light (photons) are produced when a charged particle travels through a transparent medium at a speed greater than the speed of light in that medium. The medium may be a gas, liquid, or solid. These photons extend over a spectrum of wavelengths from the UV into the visible part of the electromagnetic radiation spectrum. The photon emission is a result of a coherent disturbance of adjacent molecules in matter caused by the traveling charged particle, which must possess a certain threshold energy. These photons are referred to as Cherenkov radiation in honor of the Russian physicist Pavel A. Cherenkov for his discovery and his basic research to measure the properties of the radiation and the phenomenon, now referred to as the Cherenkov effect.[18]

The Cherenkov effect and the radiation produced by a charged particle traveling in a transparent medium at a velocity exceeding the speed of light in that medium were predicted theoretically as early as 1888 by Oliver Heaviside, but long forgotten until the radiation was discovered finally by Cherenkov and interpreted by Frank and Tamm (1937). Govorkov (2005) reviewed the historical significance of Heaviside's prediction, namely, that Heaviside first predicted theoretically that a point charge (electron) would produce a conical wave front whenever it were to travel at a speed greater than the speed of light in a medium. Heaviside's prediction was before Einstein's theory of relativity, which holds that matter cannot travel faster than light in a vacuum but that matter can travel faster than light in a medium. At the time of Heaviside, even space was not considered to be a vacuum but to consist of an "ether", and therefore, according to Heaviside, the conical wave front would be produced in the "ether" as well as any other medium provided the electron or point charge travels at a speed exceeding that of light. Of course, electrons as well as other charged particles with sufficient energy can indeed travel faster than light in media where light travels at speeds less than its speed in a vacuum.

Cherenkov radiation consists of a continuous spectrum of wavelengths extending from the near UV region to the visible part of the spectrum peaking at approximately 420 nm. Only a negligible amount of photon emissions is found in the infrared or microwave regions. Cherenkov photon emission is the result of local polarization along the path of travel of the charged particle with the emission of electromagnetic radiation when the polarized molecules return to their original states. This has been described as the electromagnetic "shock" wave that is analogous to the acoustical shock wave or sonic boom created by supersonic aircraft.

The threshold condition for the production of Cherenkov radiation in a transparent medium is given by

$$\beta n = 1 \tag{2.1}$$

where β is the relative phase velocity of the particle, that is, the velocity of the particle divided by the speed of light in a vacuum and n the refractive index of the medium (i.e., the ratio of the velocity of light in a vacuum to its velocity in the medium). Only charged particles with

$$\beta > \frac{1}{n} \tag{2.2}$$

produce Cherenkov photons in transparent media. An important property of Cherenkov radiation is its asymmetry, that is, the directional emission of the Cherenkov photons. Cherenkov radiation is not emitted in all directions. When Cherenkov (1936) discovered the asymmetric properties of this radiation, he knew he had discovered a type of radiation yet unknown. Frank and Tamm (1937) explained the spatial asymmetry of the radiation as a result of the charged particle traveling in a medium at a velocity exceeding the velocity of light in the medium. Frank and Tamm theorized that when the phase velocity of the charged particle β exceeded the reciprocal of the index of refraction n of the medium, that is $\beta > \frac{1}{n}$, Cherenkov photons are emitted as a cone at an angle θ to the direction of the charged particle. According to the theory of Frank and Tamm, the angle θ of photon emission would be defined by the relationship

$$cos\theta = \frac{1}{\beta n} \tag{2.3}$$

the angle θ is defined by the equation

$$cos\theta = \frac{\text{distance of travel of radiation front in the medium}}{\text{distance of travel of charged particle in the medium}}$$

or

$$cos\theta = \frac{(\text{speed of light in the medium}) \cdot \Delta t}{(\text{speed of particle in the medium}) \cdot \Delta t} = \frac{(\frac{c}{n}) \cdot \Delta t}{\beta \cdot c \cdot \Delta t}$$

As the particle energy E increases to relativistic speeds, the value of β approaches 1

$$cos\theta = \frac{1}{n} \tag{2.4}$$

If water is the medium ($n = 1.33$):

$$cos\theta = \frac{1}{1.33} = 0.752\,, \qquad cos^{-1}(0.752) = 41.2^{\circ} \tag{2.5}$$

2.2 Physical Properties of Sea-water

Many of the process that occur in the sea, have a dependence on the properties of sea-water. The presence of salts, dissolved substances and undissolved suspended particles, either organic or inorganic greatly influence the characteristics of the water and phenomena such as light absorption and scattering. The propagation of light, the tracks and times of photons emitted in Cherenkov radiation as well as "noise" illumination by other processes in water, depend on parameters such as salinity, temperature, pressure and depth. [19]

It is common knowledge that sea-water is salty. However, it proved unexpectedly difficult to agree on a practical and useful definition for salinity. In 1901, salinity was defined as "*the total weight in grams of solid matter dissolved in 1 kg of sea-water*". This definition was dropped since it was extremely difficult to measure salinity directly but measurements of the most prominent components did follow by Carl Forch, Martin Knudsen, and S. P. L. Sorensen (presented in Table 1). [20]

More definitions followed that were progressively more practical, the measurements of which were also translated to the original definition. It was determined that the average salinity of ocean water is about 35 grams of salts per kilogram of sea-water or 35 PSUs (practical salinity units). Fully enclosed or partially enclosed bodies of water can have lower or higher values of salinity. For example, salinity in the Mediterranean Sea has a value of $\sim$38 PSUs, a little higher than average ocean water but much lower compared to the Dead Sea with a value of $\sim$250 PSUs. [21]

Component	$\frac{\text{Component}}{\text{Sea-Water}} \left[\frac{g}{kg}\right]$	% of all Dissolved Material
Clorine	19.353	55.0 %
Sodium	10.760	30.6 %
Sulphate	2.712	7.7 %
Magnesium	1.294	3.7 %
Calcium	0.413	1.6 %
Potassium	0.387	1.1 %
Bicarbonate	0.142	0.4 %

Table 2.1: Concentration of the main dissolved constituents found in sea-water [21]

Salinity is affected by many parameters, such as time, temperature, changes in weather, proximity to land (and mineral composure of the land area), latitude. The salinity of the oceans is relatively constant. There are isolated areas where deviations may be occur at the surface, sometimes quite large, due to evaporation, precipitation, runoff, ice formation, ice

melting, and mixing with other water masses. In coastal regions where large amounts of runoff from rivers mingle with ocean waters, salinity is likely to be somewhat less than 35 PSUs, and in tropical regions where the evaporation rate is quite high salinity is likely to be somewhat greater. Ice formation tends to increase surface salinity and ice melting decreases it. Salinity also depends on depth, as shown in Figure 2.1

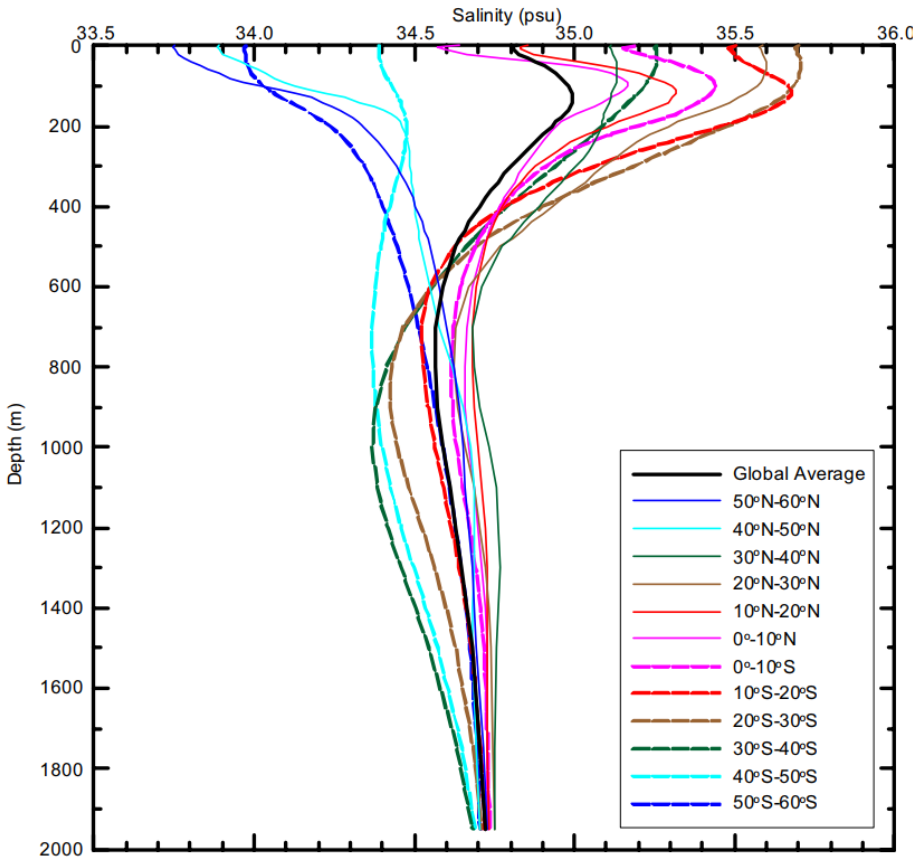

Figure 2.1: Layer-averaged climatological mean (2004–2014) of ocean salinity as a function of depth for different zonal bands. The thick black line is for the global mean [22]

The approximate limits of temperature in sea-water are between -2°C and +40°C (including coastal and estuarine areas). In the open ocean the maximum temperature of surface waters rarely rises above about 30°C. This limitation is caused mainly by the fact that over half of the solar heat energy absorbed in the upper layers of the water is used for evaporation rather than for temperature change.

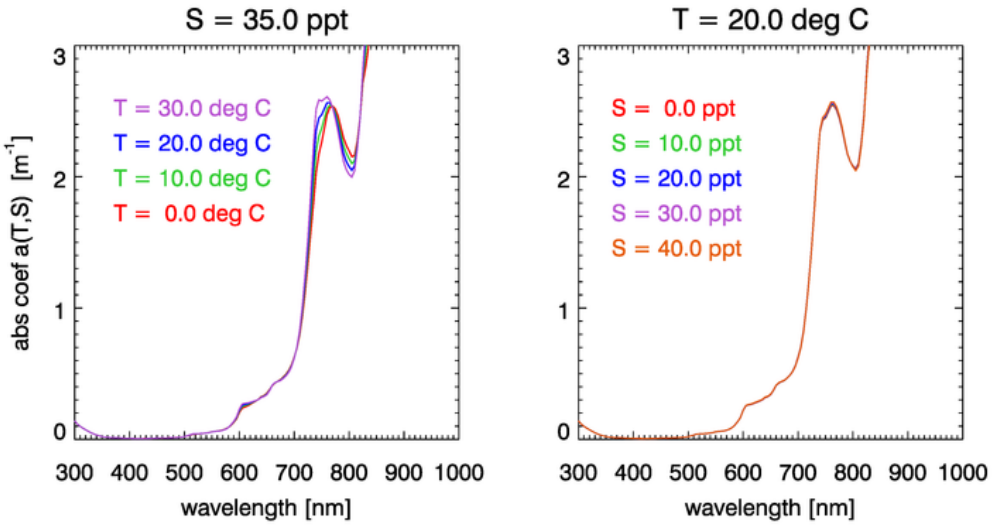

Figure 2.2: The absorption coefficient as a function of wavelength, for different temperatures (left) or salinities (right). Salinity does not affect absorption in the wavelength range of $300nm \rightarrow 1000nm$. Temperature seems to create slight variations in the range $700nm \rightarrow 800nm$ [23]

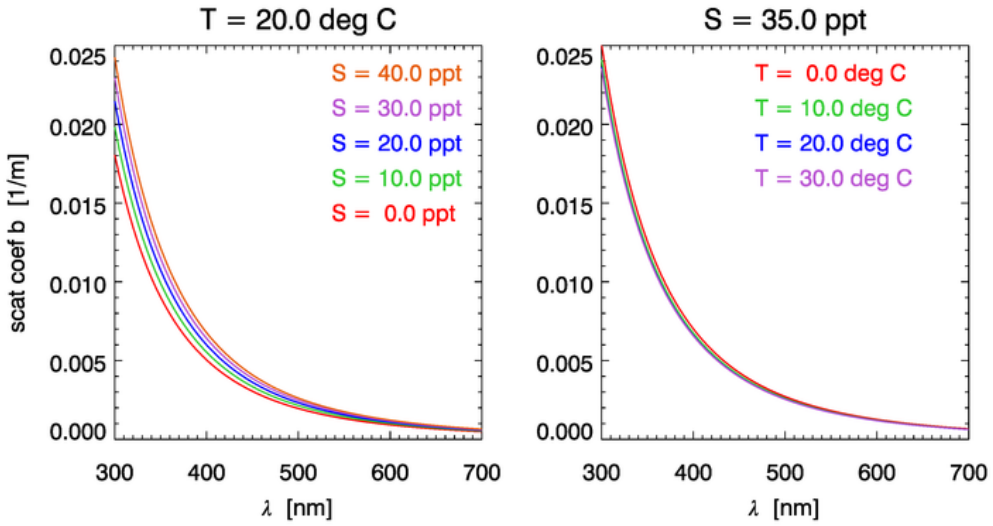

Figure 2.3: The scattering coefficient as a function of wavelength, for different temperatures (right) or salinities (left). Salinity affects scattering more in than temperature in the violet region of visible light. Increase in wavelength creates an independence on both variables [23]

2.3 Light Propagation in a Medium

Absorption is the conversion of light energy to heat energy, while scattering is the redirection of light energy by the presence of scatterers. Scattering may also be treated as simple specular reflectance, refraction and diffraction through and around the particles, or even by absorption and re-radiation of the electromagnetic energy.

The diminution of light as it travels through a medium for both absorption and scattering can be described as by the Beer-Lambert law:

$$I = I_0 \cdot e^{-ax} \tag{2.6}$$

$$I = I_0 \cdot e^{-bx} \tag{2.7}$$

where I_0 is initial intensity of light, I is intensity of light after passing through the medium, x is the path's length inside the medium and a, b are the coefficients of absorption and scattering respectively.

Attenuation of light in a medium is the combined result of both absorption and scattering, also expressed by the same equation:

$$I = I_0 \cdot e^{-cx} \tag{2.8}$$

where

$$c = a + b \tag{2.9}$$

Intensities are measured in $\frac{W}{m^2}$ and the product cx must be unitless (if $x \rightarrow m$, then $c \rightarrow m^{-1}$). The Beer-Lambert law only applies on collimated beams of light, as illustrated in Figure (2.4).

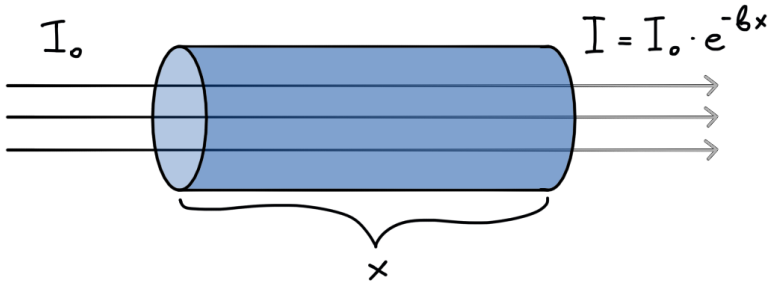

Figure 2.4: Light attenuation of a collimated beam of light traveling in a medium. β is the transmission coefficient

For a collimated beam of light that travels in empty space (no obstacles or e/m fields), intensity at any distance from the source will remain constant as the tracks of photons will not change due to scattering. While in a medium, there are two types of paths that light can travel from a source to a receiver. The total light is the sum of the non-scattered (mono-path) and the scattered (multi-path) irradiance, as illustrated in Figure (2.5)

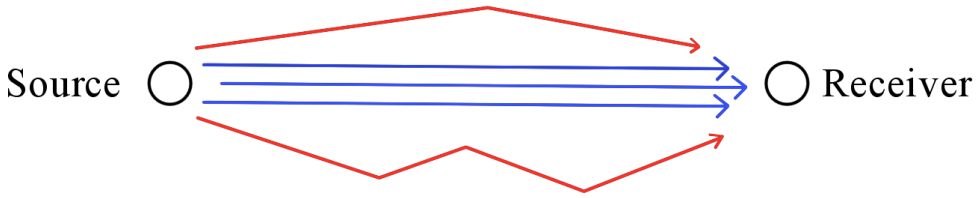

Figure 2.5: Blue-colored arrows represent the non-scattered tracks of light, red represent the scattered tracks, defining two types of paths for light irradiance

Point or spherical sources of light (or sources that do not favor a specific direction) radiate in sphere fronts, following the Inverse Square law. The measured intensity in a medium, at a specific distance away from the source, will be the combination of Beer-Lambert and Inverse Square laws:

$$I = \frac{S}{4\pi R^2} \cdot e^{-\beta R} \tag{2.10}$$

where R is the measurement distance from the spherical source in m. The intensity I is still measured in $\frac{W}{m^2}$, but the initial intensity I_0 was replaced with power S, which is measured in W. It was also necessary to rename the attenuation coefficient c to transmission coefficient β, as most bibliography does, to differentiate the attenuation of collimated light to uncollimated, spherically spread light.

The transmission coefficient β depends on the light's wavelength and the physical properties of the medium, as an extension of the dependence of absorption and scattering to these parameters. In this thesis, the medium of interest is sea-water and the spherical light sources will be LEDs that emit in specific wavelengths. The transmission coefficient β can also be referred to as transmission length, defined by the mathematical expression:

$$R_\beta = \frac{1}{\beta} \tag{2.11}$$

The relative error in the measurement of β is given by

$$\frac{\Delta\beta}{\beta} = \frac{1}{\beta \cdot R}\frac{\Delta I}{I} \tag{2.12}$$

In clear waters the transmission coefficient has small values (and the transmission length L_β has large values), therefore an accurate measurement of β requires either an instrument able to measure the light intensity with extreme accuracy (so that $\frac{\Delta I}{I}$ can be very small) or an instrument with a long optical path (so that R is adequately large). [24]

In many cases, scattering is so small that absorption is the primary cause of light transmission. The absorption properties of water can be easily specified. Both the far red and the far violet ends of the visible spectrum are attenuated very markedly by absorption, while there is a peak the blue-green portion, at about 470 nanometers. Scattering is primarily a function of the suspended materials in the water, the amount and type of scattering varies with the amount and type of suspensoids. It would be expected, for example, that scattering effects for small clay particles and those for similar sized plankton would be different, as would those for small and large particles of the same material. Not only does scattering vary both in magnitude and direction with the amount of particulate matter in suspension, but it varies with the size of the particles relative to the wavelength of impinging light and the index of refraction of the scattering material. [19]

2.4 Light Transmission

This section compares the three already mentioned laws for the transmission of light. The light transmission using the Beer-Lambert law, the Inverse Square law and the combination of both is shown in Figures (2.6) and (2.7).

As presented, between the Beer-Lambert and Inverse Square laws, the latter is the most effective, as the combined law follows closer to that, shown in Figures (2.6) and (2.7).

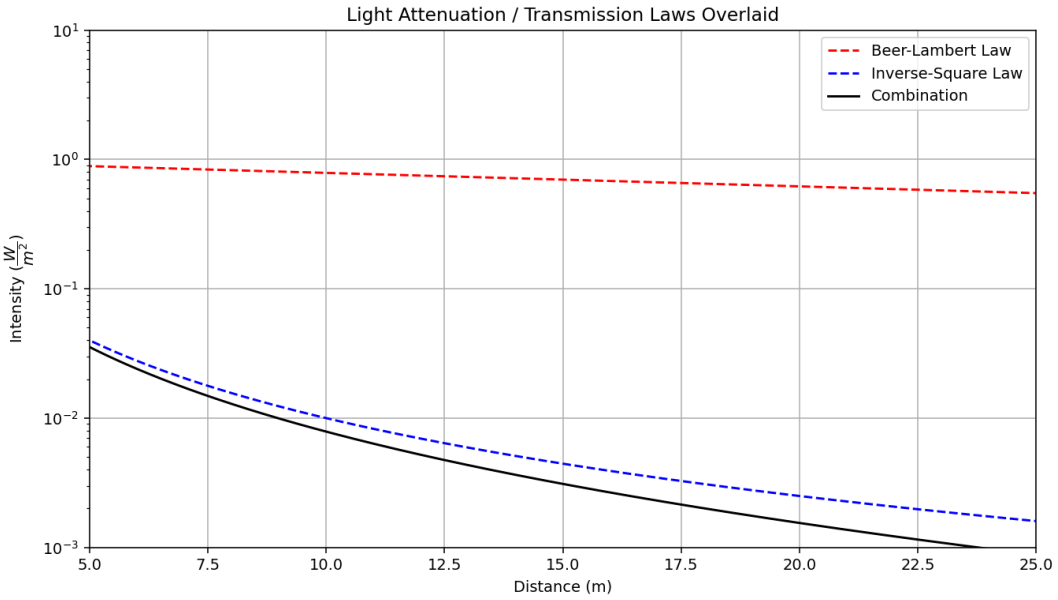

Figure 2.6: Theoretical calculation of light attenuation intensities of Beer-Lambert (red), Inverse Square (blue) and combined (black) as a function of distance. The attenuation / transmission coefficient was set equal to $0.024m^{-1} \simeq 42m$ in transmission length

Figure 2.7: Visual representation of light attenuation laws of Beer-Lambert (left), Inverse Square (center) and combined (right), as light being dispersed in a circle. The edges of the images are $25m$ away from their centers. Corners are $\sqrt{2} \cdot 25 \simeq 35.4m$ away. The attenuation / transmission coefficient was set equal to $0.024m^{-1} \simeq 42m$ in transmission length

The KM3NeT Neutrino Telescopes

3.1 Physics Goals of KM3NeT

The next-generation neutrino telescopes are housed in the KM3NeT research infrastructure. The telescopes will have detector volumes ranging from megatons to several cubic kilometers of clear seawater once they are built. KM3NeT, which is located in the Mediterranean's deepest oceans, will not only provide a new window into our Universe but will also aid in the study of the properties of elusive neutrino particles. The discovery and detection of high-energy neutrino sources in the Universe, as well as the determination of the neutrino mass hierarchy, are two primary scientific goals of KM3NeT.

IceCube's finding of a flow of very energetic cosmic neutrinos marks de facto the beginning of neutrino astronomy. Many issues arose about the origin of the observed cosmic neutrinos, including whether they came from within our galaxy or from beyond it, if they may be localized, and whether their sources are point-like or not. The energy dependence of the observed neutrino flux and the flavor composition are also giving rise to several theoretical scenarios.

Another goal of the KM3NeT is to investigate the characteristic properties of the neutrino particles. Daya Bay, Reno, and other experiments revealed a significant contribution of electron neutrinos to the third neutrino mass eigenstate, paving the way for the determination of the neutrino mass hierarchy, which is one of the remaining neutrino properties to be measured. The ORCA detector of KM3NeT was designed specifically for studying oscillations of low energy (few GeV) neutrinos produced by cosmic rays in the Earth's atmosphere.

3.2 The ARCA Detector [25]

The Astroparticle Research with Cosmics in the Abyss (ARCA) neutrino telescope at KM3NeT is dedicated to the hunt for very high-energy cosmic neutrinos. KM3NeT will look for neutrinos from distant astrophysical sources including supernovae, gamma-ray bursts, and colliding stars.

With the ARCA telescope's superior angular resolution, KM3NeT will investigate the cosmic neutrino flux, providing crucial information on its origin, energy spectrum, and flavor composition. The ARCA telescope will survey 87% of the sky from its location in the Mediterranean Sea, including most of the Galaxy and the Galactic Center, where other astroparticle detectors have observed some interesting unexplained phenomena. The low diffusion qualities of saltwater will allow precise measurement of neutrino direction, which is vital for the detection of emitting sources for which no hints are currently available.

At a depth of around 3500 meters, about 90 kilometers offshore Portopalo di Capo Passero, Sicily (Italy), the ARCA array of optical modules is progressively being developed and connected to the junction boxes in the seafloor network. The array's design is ideal for detecting high-energy neutrinos from cosmic sources. ARCA's target instrumented volume is one cubic kilometer, with the potential to expand. The array's optical modules are scattered across the seawater volume with an average horizontal distance of about 90 meters and a vertical distance of about 36 meters, with the lowest modules around 70 meters above the seabed. At the time of submission of this thesis, ARCA operates with 342 optical modules in 19 vertical detection units, while sea campaigns for the deployment of additional detection units are planned until the end of 2022.

When completed, the ARCA detector will achieve a median angular resolution of 0.1 degrees for muon tracks at 10 TeV and better than 2 degrees above 100 TeV for electromagnetic cascades by combining a nanosecond measurement of photon arrival times, 10 cm position accuracy ensured by an acoustic position calibration, photon flux estimation by counting the number of hit PMTs, and information on the direction of incoming photons.

3.3 The ORCA Detector [25]

ORCA stands for Oscillation Research with Cosmics in the Abyss. To main goal is to attain the angular and energy resolutions required for resolving the neutrino mass hierarchy. A multi-megaton scale array of KM3NeT light sensor modules with a granularity designed for researching atmospheric neutrino reactions with seawater will be employed. The ORCA detector aims at studying fundamental properties of neutrinos, by making use of the abundant neutrino fluxes created by cosmic ray interactions with the Earth's atmosphere.

The atmospheric flux of neutrinos has traditionally been seen as a background to the detection of a cosmic neutrino signal. However, it has recently been discovered that in the few-GeV energy range, this flux holds the key to resolving a fundamental question in particle physics: the relative ordering of neutrino masses, also known as the neutrino mass hierarchy – that is, whether the third neutrino mass eigenstate is heavier (normal hierarchy) or lighter (inverted hierarchy) than the first and second states. The influence of mass hierarchy on neutrino oscillations in matter leaves a mark on the atmospheric neutrino flux via the distinct neutrino flavors' characteristic appearance/disappearance patterns as a function of energy and passage through the Earth.

The ORCA detector array is being built about 40 kilometers off the coast of Toulon, France, at a depth of roughly 2500 meters. The ORCA setup is ideal for studying neutrino oscillations using neutrinos produced in the Earth's atmosphere by cosmic particles. Its array of optical modules will span around 7 megatons of seawater, with a horizontal spacing of about 20 meters and vertical spacing of roughly 9 meters. At the time of submission of this thesis, ORCA operates with 126 optical modules in 7 vertical detection units, while sea campaigns for the deployment of additional detection units are planned until the end of 2022. The goal for ORCA is to install more than 2070 optical modules across 115 detecting units.

3.4 Installation Sites [25]

KM3NeT is a collaboration of about 250 people from 55 institutes in 16 countries. There are three deep-sea sites identified for deployment:

- KM3NeT-Fr, off-shore Toulon (France)
- KM3NeT-It, off-shore Portopalo di Capo Passero (Italy)
- KM3NeT-Gr, off-shore Pylos (Greece)

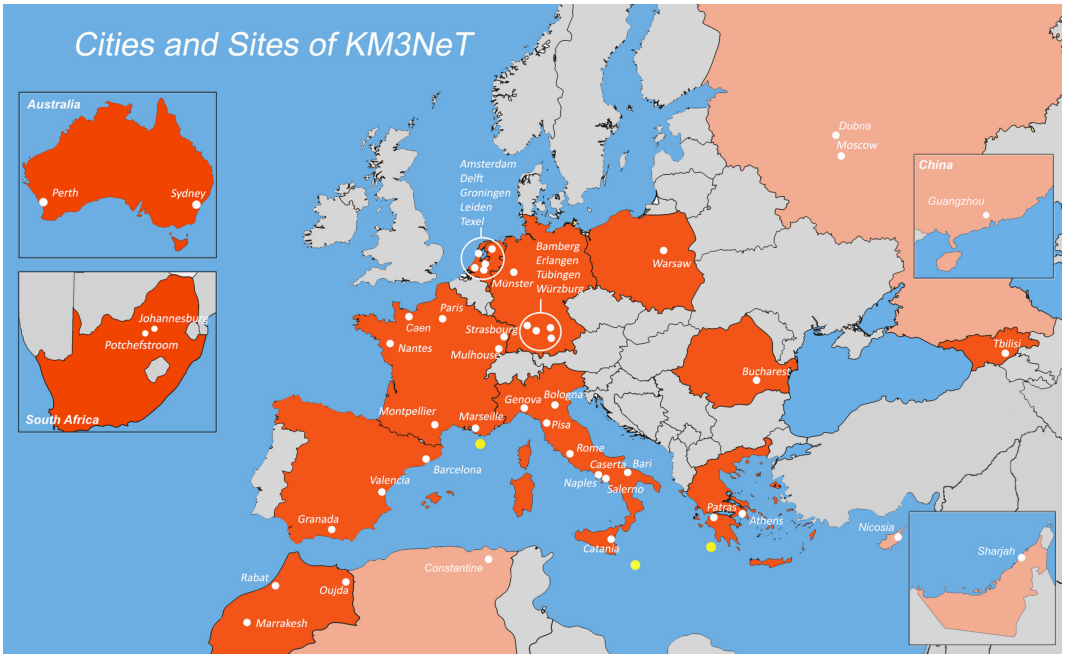

Figure 3.1: A map representation taken from the KM3NeT website. The intense color are countries that actively participate, while the faded color are observing countries. White dots specifically show the cities with institutes that participate. Yellow dots are the installation sites for the detectors

The KM3NeT-Fr deep sea installation site is located at $42°48' \ N \ 06°02' \ E$ about 40 km off-shore Toulon, France. It is located at a depth of about 2450 m and about 10 km west of the ANTARES neutrino telescope – the predecessor of KM3NeT. The shore station is located at the Institute Michel Pacha at La Seyne sur Mer. The ORCA neutrino detector is deployed at the KM3NeT-Fr installation site. The sensor modules will be arranged on vertical detection units with a height of about 150 m and in the dense configuration required for detection of neutrinos with energies as low as about a GeV, three orders of magnitude lower that the typical energy scale probed by the detector of the ARCA telescope for neutrino astroparticle physics.

The KM3NeT-It deep-sea installation site is located at 36°16′ *N* 16°06′ *E* about 100 km off-shore Portopalo di Capo Passero, Sicily, Italy, where the shore station is located. The site is the former NEMO site and is shared with the EMSO facility for Earth and sea science research. The shore station comprises the same facilities as that for KM3NeT-Fr.

KM3NeT-Gr is located off the coast of Pylos. At present, it is used for validation and qualification. Several locations at different depths between 3000 m and 4550 m are under investigation. The deepest site (4550 m) is located at 36°33′ *N* 21°30′ *E*. A suitable installation site is available to expand the KM3NeT Research Infrastructure for a next phase. This expansion is subject to future funding. A shore station is available which requires new facilities for power and computing.

The KM3NeT detectors will consist of blocks of 115 detection units. Detection blocks with two different granularity of light sensor modules will be installed: ARCA– and ORCA-types. For the ARCA-type blocks, the distance between DOMs along the string units is about 36 m and the distance between units is about 90 m. The height of these blocks is about 700 m. The instrumented volume of the two blocks about 1 km^3. An ORCA-type block of 115 units will be different in that the distance between DOMs along the unit will be 9 m and the distance between units will be 20 m. This arrangement instruments almost 4 cubic hectometer – almost 250 times smaller than the ARCA detector – optimised for the lower neutrino energies necessary for the measurement of the neutrino mass hierarchy.

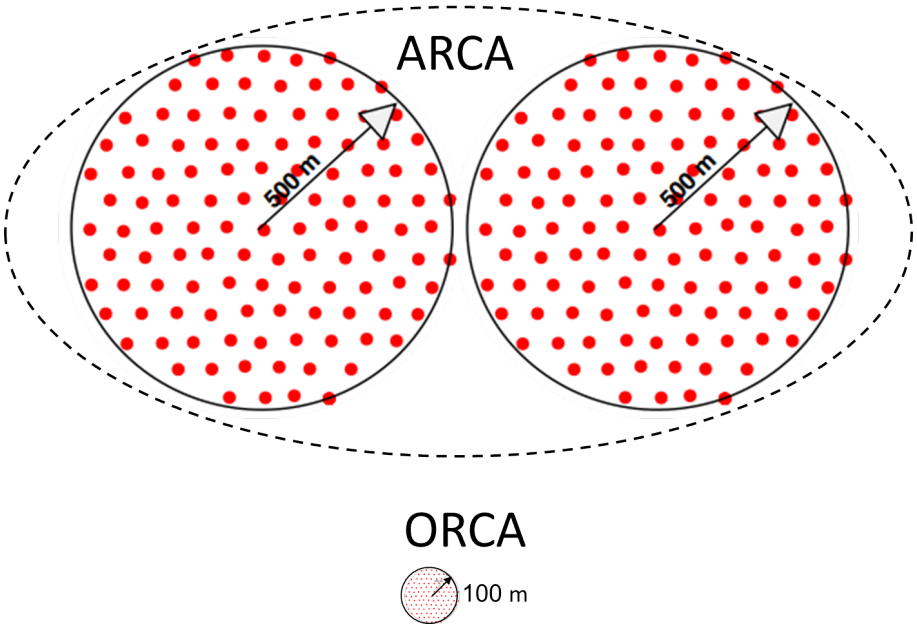

Figure 3.2: This is the visual representation of the detector configurations for ARCA and ORCA, placed adjacent for comparison. ARCA's volume is much more expanded than ORCA's, to increase the probability of high-energy neutrino detection. ORCA is optimized in size for measuring the neutrino mass hierarchy

3.5 Digital Optical Module (DOM) [25]

Each detector of the KM3NeT neutrino research infrastructure is a three dimensional array of sensor modules distributed over large volumes of the transparent water in the deep Mediterranean sea. The sensor modules are pressure resistant glass spheres housing photomultiplier tubes for light detection and several instruments to determine the geometrical position of the sensor modules and to calibrate the measured signals. The sensor module is also referred to as Digital Optical Module or DOM for short. The modules are arranged in vertical string-like detection units, DUs or strings for short.

The sensor modules register the time of arrival of the Cherenkov light generated in the sea water by charged particles created in neutrino induced interaction with the water inside or close to the detector; the modules also measure the brightness of the light and the geometrical position of the sensor at the time of arrival of the light. The measurements are transmitted to computers in a shore station via a network of optical fibers. In the shore station, intelligent software filters the data and reconstructs from the measurements the traces of the particles traversing the detector. The results are sent over the public internet to the KM3NeT data centers for further study.

A DOM consists of a glass spherical vessel with a wall thickness sufficient to withstand the enormous pressure of up to 350 times normal atmospheric pressure that exists at the bottom of the sea. In this glass vessel 31 photomultiplier tubes have been arranged to look in all directions for the faint light emitted by particles passing by.

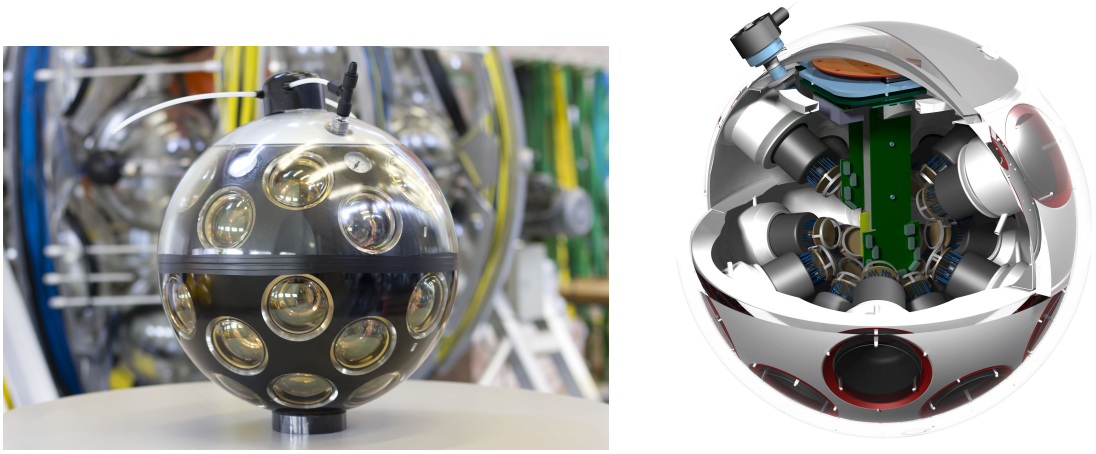

Figure 3.3: [Left] a DOM. [Right] A graphic showcasing the contents inside the DOM

The photomultiplier tubes need to be provided with a high voltage of around 1000V. This is provided by a custom made circuit on the back of the photomultiplier tube. This board has been miniaturized in order to fit in the limited space available in the innards of the glass sphere.

A small electrical pulse is created by the photomultiplier tube when a quantum of light hits it. This pulse is then amplified and transformed into a square wave pulse, by the time-over-threshold technique (the amount of light is transformed to an amount of charge which is in turn translated to the length of the square wave pulse), and sent to the central processing logic housed in a Field programmable gate Array (FPGA) where its arrival time and its pulse length is registered and stored for later transfer to shore. The DOM also contains other sensors used for calibration purposes. A compass makes it possible to know in what direction each of the photomultipliers is pointing. Accelerometers allow tilt, pitch and yaw of the module to be determined. A piezo-acoustic sensor allows for the determination of the position of the DOM in 3D using a sonar technique. All these measurements are important as the DOMs move under the influence of sea currents.

A collection of 18 DOMs connected by an electro-optical cable and arranged along a vertical structure with two ropes is called a Detection Unit or DU (or string) for short. For deployment and storage, the string-like detection unit is coiled around a large, i.e. 2 m diameter, spherical frame, the so-called launcher vehicle, LOM for short, in which the sensor modules slot into dedicated cavities. The anchor at the bottom of the detection unit is the interface with the seabed infrastructure. A surface vessel, with dynamic positioning capability, is used to deploy the LOM with the detection unit at its designated position on the seabed with an accuracy of 1 m. A remotely operated vehicle (ROV) is used to deploy and connect the interlink cables from the base of a string to the junction box or a previously deployed string in the daisy chain. Once the connection to the detection unit has been verified onshore, an acoustic signal from the boat triggers the unfurling of the unit. During this process, the launcher vehicle starts to rise to the surface while slowly rotating and releasing the sensor modules. The empty launcher vehicle floats to the surface and is recovered by the surface vessel. The use of compact strings allows for transportation of many units onboard and thus multiple deployments during a single cruise.

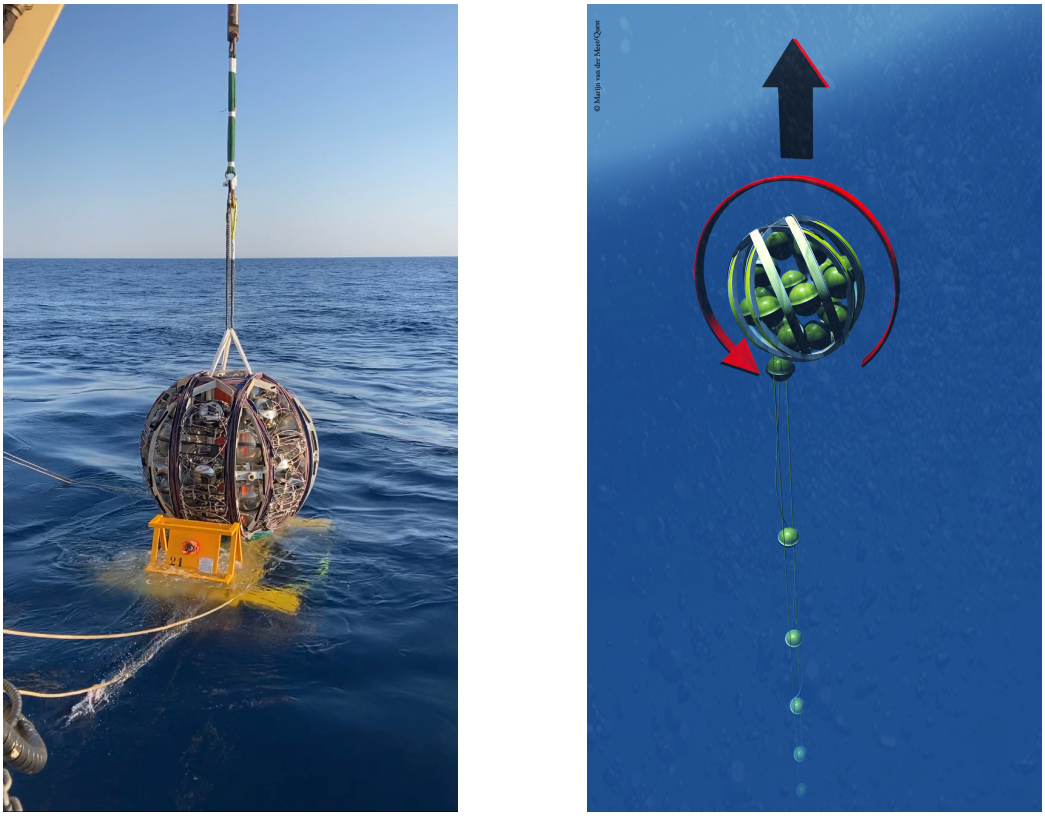

Figure 3.4: (Left) The LOM moments before its deployment commences. (Right) The LOM during deployment, unrolling in orderly fashion [26]

Figure 3.5: Empty LOMs of the deployed DUs that have been returned on shore. These LOMs are to be used again for deploying DUs during the next sea operation. [26]

LAMS

4.1 Long Arm Marine Spectrophotometer (LAMS)

The study of high energy neutrinos of astrophysical origin requires the use of very large target masses, in order to observe a reasonable number of neutrino interactions given the small interaction cross-section for neutrino-nucleon scattering. The observation, mainly via the production of muons, relies on the detection of the Cherenkov radiation produced and thus requires an optically transparent target material. Such large amounts of target material can be most easily obtained by using naturally abundant and transparent media, such as water or ice.

The spacing between optical modules will scale with some characteristic water transparency length α, in other words the effective volume of a detector, will depend on the water transparency. The exact scaling of such detector properties has been determined by detailed Monte-Carlo simulation studies.

The Cherenkov neutrino detector's sensitive volume as well as energy and angular resolution strongly depends on the optical parameters of the sea water. Therefore, interpretation of experimental data taken with a neutrino telescope requires a reasonably precise knowledge of these parameters. The sites, KM3NeT-It (near Capo Passero) and KM3NeT-Gr (near Pylos), are known to be oligotrophic (reduced biological activity) and the waters show extreme transparency. Correct measurement of the optical parameters is essential. Commercially available instruments are not fitted for measurements in very clear water because they require a complicated calibration process, which is not easily available on board. Moreover, the small length of optical base of commercial instruments (usually no more than 1 m) dictates increased accuracy of light intensity measurement. In order to measure light intensities over a long and variable light path, the Long Arm Marine Spectrophotometer (LAMS) was constructed. [24]

4.2 Original and Improved Design

The LAMS is an instrument that measures the light transmission length in deep sea for eight different wavelengths from the near UV to green visible region, where the transmission length is maximum. The operation principle is based on measuring the light intensity from a point source (LED sources of different wavelengths ranging from 375nm to 520nm) at a set of fixed length optical paths. By comparing the measurements one can eliminate the geometrical factor $\frac{1}{R^2}$ and thus determine the transmission coefficient. The original LAMS, shown in Figure 3.1, was used to measure the transmission length in the deep sea during the sea campaigns of 2008 and 2009. The measurements were taken at various distances between source and detector, namely at 10.00m, 15.10m, 17.17m, and 22.27m. The light emitter and the receiver were mounted on a mechanical support frame consisting of four titanium girders, each 5m long, and a stainless steel, 2m long girder, attached to each other to form a long linear structure. [27]

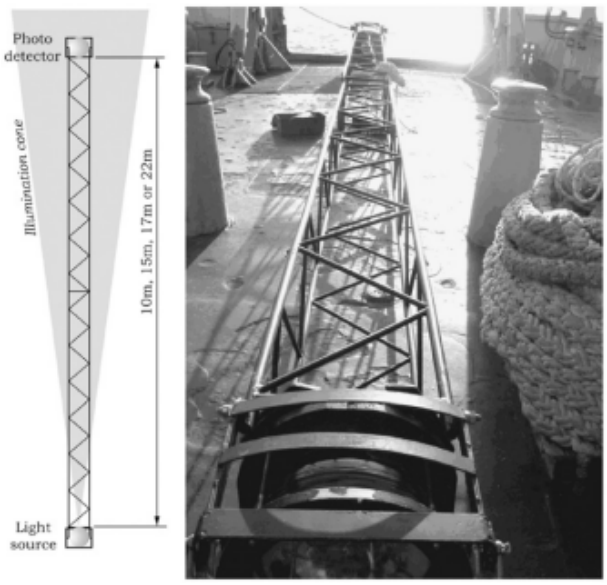

Figure 4.1: [Left] Block-diagram of the structure. [Right] LAMS on the deck of the R/V AEGAEO [28]

In order to achieve the optical paths of different length required for the different measurements, parts of the frame were added or removed appropriately on board before each deployment and measurement. Although this method proved to be successful, in order to perform measurements at all three different distances needed for an accurate determination of the transmission length, three consecutive deployments were necessary. Since the time needed to deploy the instrument to the desired depth is approximately 2 hours and taking into account that another 2 hours are needed to retrieve it, in order to take one hour of useful measurements at the desired depths, a total time of over 6 hours for each

deployment was necessary; hence a typical set of complete measurements could last well over 18 hours. This resulted in a great and unnecessary increase of the time required for the measurements, which could however not be avoided with the original design. As a consequence, the complexity of the system was also increased, as more batteries were needed in order to make it possible to perform successive measurements at different sites (Opening the LAMS to replace the batteries is a process that is advisable to be done in a clean room and not on board). More important was the increase of the cost of the whole operation, as a long deployment requires the rental of an expensive ship for a longer time.

Keeping the same idea of measuring the transmission length, we have constructed a new version of the LAMS device, by simplifying the process so that in a single deployment, simultaneous measurements can be performed at all three different distances between emitter and receiver. In this way, the total measurement time can be reduced to just a few (~ 6) hours, the time being dominated by the time required to deploy and recover the system at the intended water depth. The light emitter and the support structure (without the 2m long steel arm) of the original LAMS device are utilized, while three autonomous receiver units have been redesigned. In order to perform the three light intensity measurements simultaneously, the light sensor modules need to be smaller in size compared to the original LAMS, and to be mounted on the inside of the metal support at distances of 10m, 16m and 20m away from the light source. Custom made cylindrical steel casings have been constructed to house the new receivers. The new pressure steel casings are placed diagonally inside the frame at 10m, 16m and 20m mounted securely at the corners of the square cross section titanium frame, all facing the light emitter (scheme in figure 3.2).

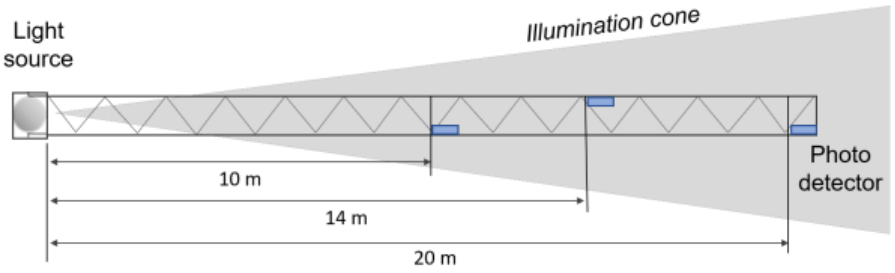

Figure 4.2: Rough schematic showing the placement of light receivers and light source [27]

The new receiver, like the old system, has two 18mm x 18mm photodiodes (PDs). The photodiodes (P/N: S3204-08) by Hamamatsu are new. The boards driving the PDs have a data taking rate of 100Hz and data are stored in an SDHC card up to 16GB. This data storage is more than sufficient as the file output from a single deployment is expected to be in the order of 50-100MB thus allowing the recording of multiple measurements. The new system will also record data from an external pressure sensor rated for a maximum pressure of 600 bar by BD Sensors (P/N: DMK331) in order to register the depth of the system during deployment. Finally, for monitoring purposes there is also a thermometer on the data taking electronics, to

ensure that the PD response is not affected by temperature.

Since the design and operation of the old version of LAMS was successful, it was decided that the changes of the redesigned system are limited to those necessary, that is the replacement of obsolete components, or to small changes that would greatly improve the efficiency of the measurement. The light source was one of the components that remained. It was constructed using eight groups of LEDs, which emit over a significant spectral region and are mounted on a circuit board and arranged in an almost circular pattern (Figure 3.3). The LEDs are driven from a regulated 5 V source. A different number of LEDs was used for each wavelength in order to provide the light intensity needed. The wavelength for the peak of the light intensity distribution, the full width at half maximum (FWHM) of the spectrum and the number of LEDs used for each one of the eight wavelength groups, are found in Table 1. Each LED group is activated sequentially and is controlled by a microcontroller with a crystal oscillator clock to count time. During a measurement cycle the LEDs of a particular wavelength are turned on for 10 s, are then switched off and after 2 s the LEDs of the next wavelength are turned on. The overall measurement cycle has a period of 108 s including a 14s no-light gap which is inserted between the light cycles.

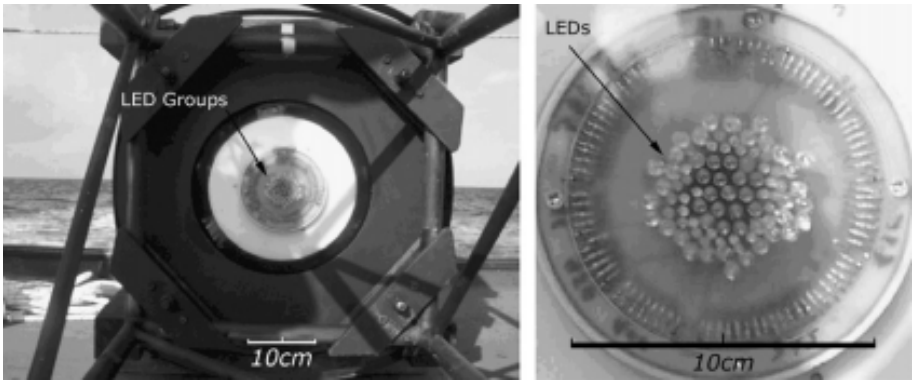

Figure 4.3: The light source of the LAMs. [Left] The cluster of LEDs inside the glass sphere and the mechanical support. [Right] a close-up of the cluster of LEDs [28]

The Analysis Framework of the LAMS Measurements

5.1 Estimation of the Transmission Coefficient β

The transmission coefficient β can be estimated from equation (2.10) by measuring the light intensity I_i at different distances R_i from the light source. So, if I is measured at two different distances R_1 and R_2, for the same wavelength:

$$I_1 = \frac{S}{4\pi R_1^2} \cdot e^{-\beta R_1}$$

$$I_2 = \frac{S}{4\pi R_2^2} \cdot e^{-\beta R_2}$$

the ratio of these intensities is:

$$\frac{I_1}{I_2} \cdot \frac{R_1^2}{R_2^2} = e^{\beta(R_2 - R_1)}$$

$$ln(\frac{I_1}{I_2} \cdot \frac{R_1^2}{R_2^2}) = \beta(R_2 - R_1)$$

which can be solved for β

$$\beta = \frac{ln(I_1) - ln(I_2) + 2ln(R_1) - 2ln(R_2)}{R_2 - R_1} \tag{4.1}$$

So, for the same wavelength, β depends on the measured intensities and the corresponding distance from the light source

$$\beta = \beta(I_1, I_2, R_1, R_2)$$

The error σ_β is calculated as:

$$\sigma_\beta = \sqrt{\left(\frac{\partial\beta}{\partial I_1}\sigma_{I_1}\right)^2 + \left(\frac{\partial\beta}{\partial I_2}\sigma_{I_2}\right)^2 + \left(\frac{\partial\beta}{\partial R_1}\sigma_{R_1}\right)^2 + \left(\frac{\partial\beta}{\partial R_2}\sigma_{R_2}\right)^2} \tag{4.2}$$

and the derivatives will be

$$\frac{\partial \beta}{\partial I_1} = \frac{1}{I_1 \cdot (R_2 - R_1)} \tag{4.3}$$

$$\frac{\partial \beta}{\partial I_2} = \frac{-1}{I_2 \cdot (R_2 - R_1)} \tag{4.4}$$

$$\frac{\partial \beta}{\partial R_1} = \frac{2}{R_1 \cdot (R_2 - R_1)} + \frac{2ln(R1)}{(R_2 - R_1)^2} \tag{4.5}$$

$$\frac{\partial \beta}{\partial R_2} = \frac{-2}{R_2 \cdot (R_2 - R_1)} + \frac{2ln(R2)}{(R_2 - R_1)^2} \tag{4.6}$$

As the sensors are mounted in the cylindrical steel casings the position of which is fixed on the frame, the error on the distance is minimized and the final equation for the error σ_β becomes:

$$\sigma_\beta = \sqrt{\left(\frac{\sigma_{I_1}}{I_1 \cdot (R_2 - R_1)}\right)^2 + \left(\frac{-\sigma_{I_2}}{I_2 \cdot (R_2 - R_1)}\right)^2} \tag{4.7}$$

$$\sigma_\beta = \frac{\sqrt{\left(\frac{\sigma_{I_1}}{I_1 \cdot}\right)^2 + \left(\frac{\sigma_{I_2}}{I_2}\right)^2}}{|R_2 - R_1|} \tag{4.8}$$

In the original LAMS, β and its error σ_β were derived from fitting the data to the equation (2.10).

5.2 The Pattern Recognition Algorithm

For the original LAMS, during the process of submersion of the frame, depth and time were recorded in a log-book. The data were exported as .txt files and contained the intensities of the photo-diodes (PDs) and a counter, each entry in a line. Therefore, the cycles and pulses of the data would be determined by hard coding the times in the program, along with their respective depths.

For the new LAMS, the .txt files contain different information and a new method was developed to automatically determine the cycles and pulses in the data. Firstly, the electronic boards export the intensities for the pairs of PDs, pressure and temperature, all contained in one line per sample, in hexadecimal. The sample rate is 100Hz, meaning 100 line entries in the .txt file per second. It is no longer necessary to track time or a counter. Instead, the intensities are scanned a few times, each time adding more information about a specific line entry. This process is split into 3 stages, so as to allow for more flexibility by allowing the programmer to intervene, if something looks out of place.

It must be mentioned that intensity values are not measured in physical units. The PDs are calibrated to output values in a range, according to the amount of light they are detecting. These values can be integers between 0 and 65535 (16^4). Values close to 0 indicate darkness, while values close to 65535 indicate light saturation.

There are in total 4 initial parameters that must be explicitly set:

1. Dark Current: (1000 by default) If an intensity value is below this threshold, the source is considered to not be emitting light. This threshold is needed because non-zero values are recorded when the source is not emitting, as a result of the current that exists in the electronic components at all times. If only one of the PDs records dark current, a special flag is raised for further inspection.

2. Light Saturation: (60000 by default) Values higher than this threshold indicate an extra source of light. This could be environmental illumination or other equipment, but is surely not due to LEDs. Line entries above this threshold are immediately marked as errors and are excluded from later analysis.

3. PDs Disagreement Tolerance: Should a PD disagree with its pair more than is tolerated, an alert flag is raised. It serves a debugging purpose and is in no other way affecting the process. If tolerance is 0.00, any different value between the PDs is untolerated. If it is equal to 1.00, any difference will be accepted regardless. The condition for this is:

$$Intensity_{Higher} - Intensity_{Lower} > Intensity_{Higher} \cdot Tolerance$$

4. Stability: (400 by default) The standard deviation is calculated for 3 consecutive line entries. Should it be less than 400 for both PDs (on any wavelength), the line entry is considered to have stable data, in the sense that the shape they make is flat. If the shape is flat and non - dark current, this is a good indication of the line entry belonging to a pulse. The default value was determined empirically.

The goal is to determine for each data line entry in what part of the shape they belong. Only data that belong on the flat surface of a pulse are used for the arithmetic operation to calculate the attenuation length. For that reason, four distinct and exclusive categories have been devised for the data:

1. Pulse
2. Stem
3. Dark Current
4. Error

A data line entry can only be one of the above and is excluded from being anything else. Figure (5.1) presents graphically the parts of the shapes that are considered pulse, stem or dark current. If a line entry fails to be categorized into anything of the three above, it is considered error.

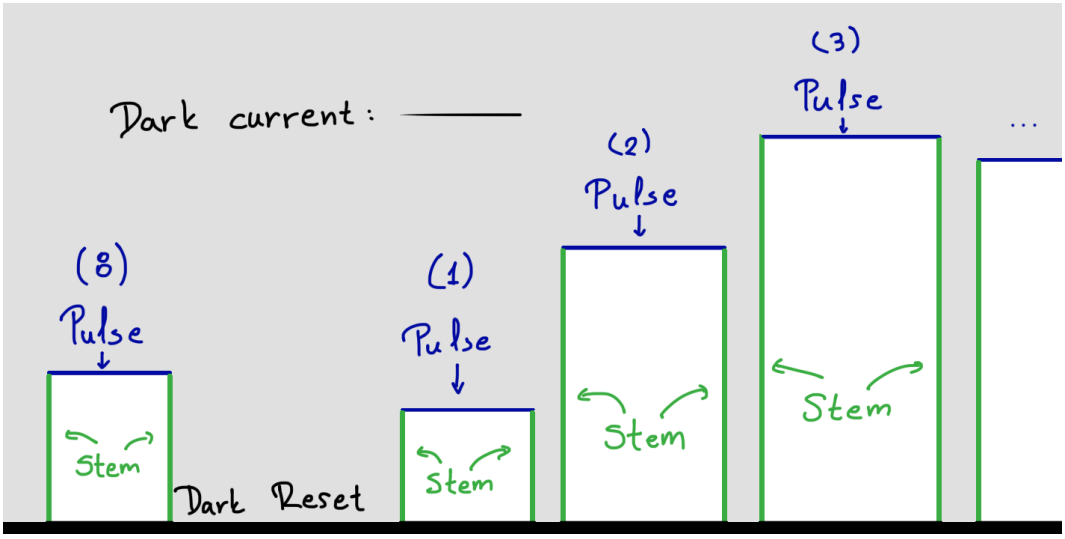

Figure 5.1: Graphic representation of the distinction between data. The prolonged dark current between the last pulse of one cycle and the first pulse of the second cycle is called dark reset in the code. Dark current is the black line at the bottom, stems are the green colored vertical lines and the blue horizontal lines are the pulses

The intensity of each wavelength on each cycle is calculated by taking the mean value of all the pulse values corresponding to that wavelength. The rest of the data do not contribute in any way in the arithmetic calculation of the attenuation length. Each pulse lasts for 10 seconds. The sampling rate of the boards is 100Hz. This means that for each pulse there are 1000 data line entries. The sample of data for each pulse is large enough to safely dismiss inconsistent data without affecting negatively that statistic.

The dark reset variable is responsible for separating the data into cycles. There is a simple means for finding this. Scan the data to calculate the number of dark current ranges. Find their average size in range (averageRange). If a dark current range is at least three times the size of this average range, it has to be a dark reset range. Recall that dark current lasts for 2 seconds while a dark reset lasts for 14 seconds. The average of the dark periods on a cycle would be 3.5 seconds. $3 \cdot 3.5s = 10.5s <$ dark reset duration of 12 seconds.

Knowing the positions of all dark resets in the data allows for separation into cycle candidates. All the above is the result of the first two stages. After the separation of data into cycles, a considerate amount of safeguards have been implemented, so as to confirm that the shape is as expected. The general condition for a cycle to be valid is the existence of exactly 8 pulses with relatively the same length. Stage 3 of the pattern recognition algorithm and the biggest stage overall is devoted to validating this condition and protecting against possible downfalls, such as a cycle being unacceptably small.

Cycles of data that pass stage 3 will be validated cycles and will be included in the analysis. Figure (5.2) presents a validated cycle with its separated pulses.

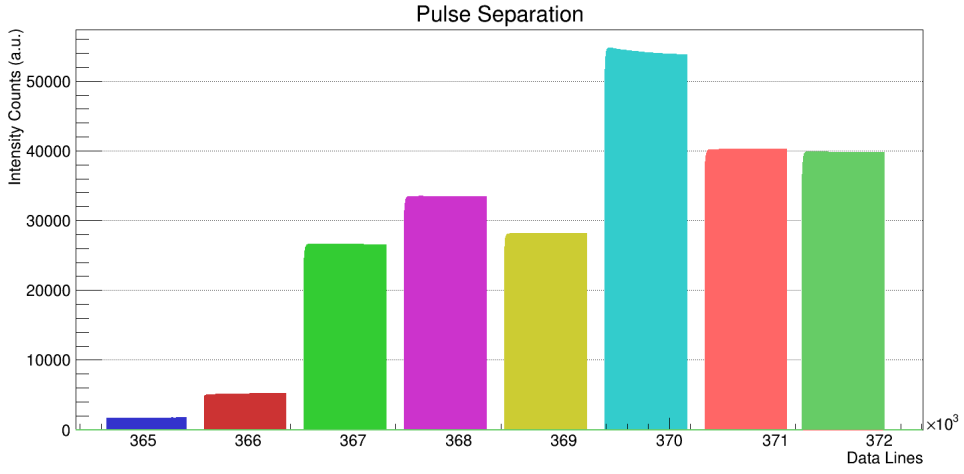

Figure 5.2: An example of a validated cycle of data. Different colors denote different wavelengths (pulses). The data in this figure have successfully passed all stages of the pattern recognition algorithm and will be included in the analysis

Cycles of data that fail in stage 3 will be excluded from further analysis but will also raise a special flag, that marks them as ”expected cycles”. Keeping track of expected cycles and checking them manually helps to expose unknown or catch already discovered problems, if they emerge again.

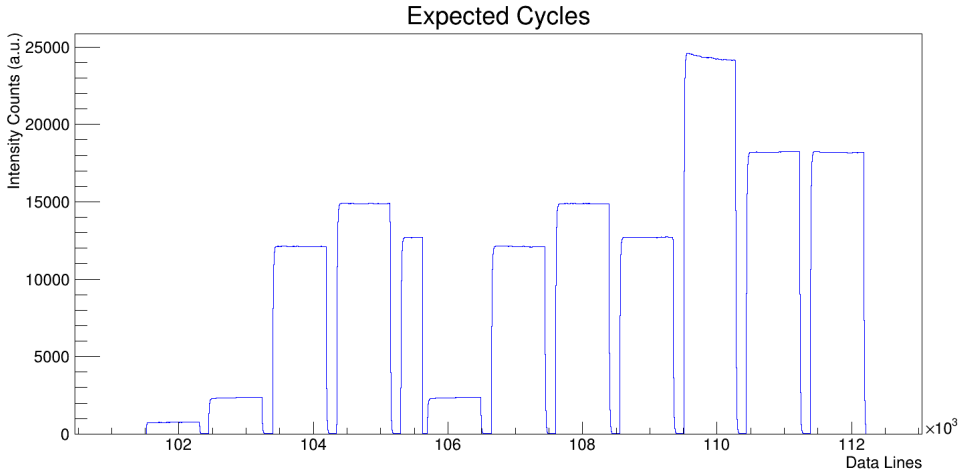

Figure 5.3: An abnormal cycle with 12 pulses. It was flagged as ”expected” due to respecting the general shape of a normal cycle but having too many pulses. This was caused by missing data in between two cycles, resulting to their merging

5.3 Re-Visiting the Original LAMS Data

The first task was to test the framework on the original LAMS data and validate their results. We could easily retrieve the data recorded from the 2008 and 2009 sea campaigns, but not the analysis. The unprocessed data are presented as histograms in the following figures, for each distance, on each location, where the intensity (in arbitrary units) is shown versus the time of the measurement (line entry in data file).

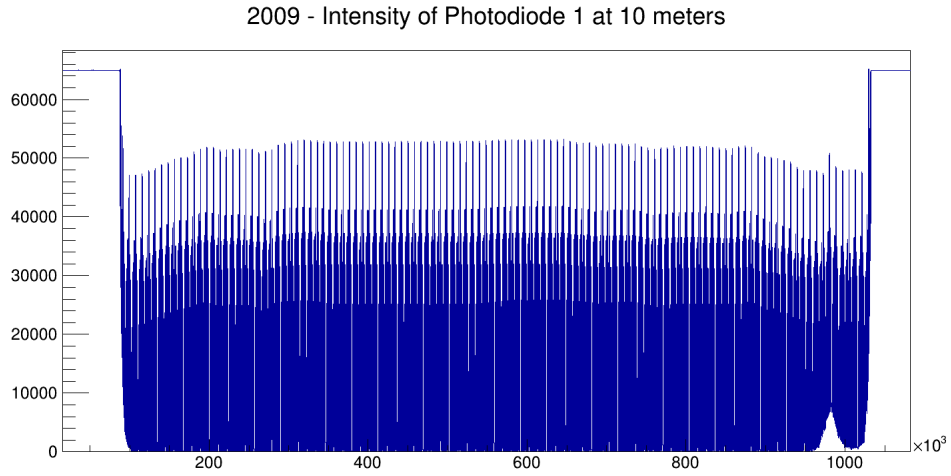

Figure 5.4: KM3NeT-It Site (Capo Passero): All data collected at a distance of 10m from the light source. Intensity (arbitrary units) versus time of measurement (line entry)

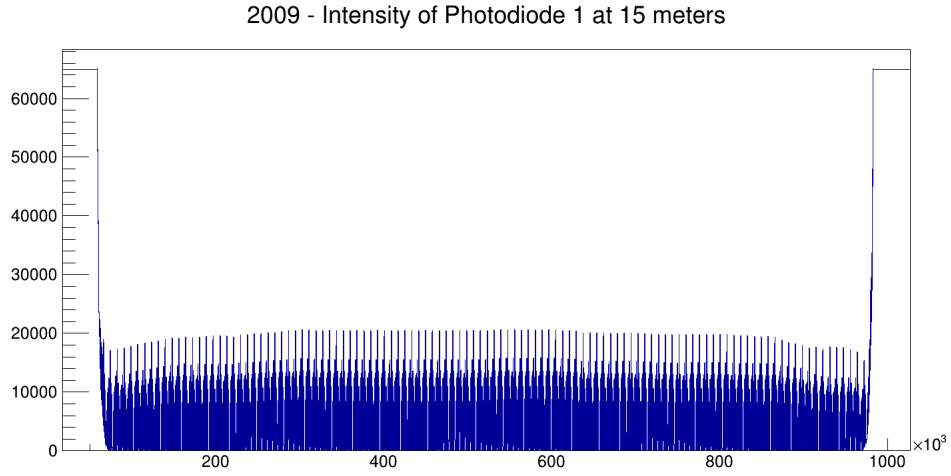

Figure 5.5: KM3NeT-It Site (Capo Passero): All data collected at a distance of 15m from the light source. Intensity (arbitrary units) versus time of measurement (line entry)

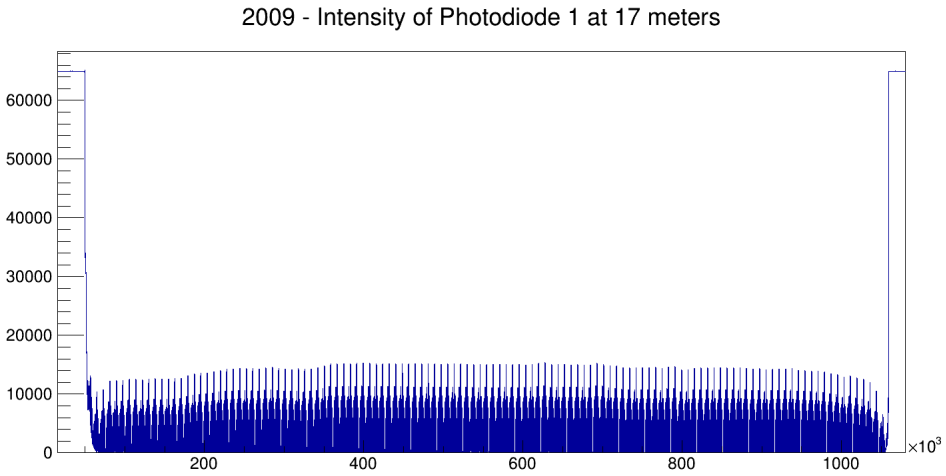

Figure 5.6: KM3NeT-It Site (Capo Passero): All data collected at a distance of 17m from the light source. Intensity (arbitrary units) versus time of measurement (line entry)

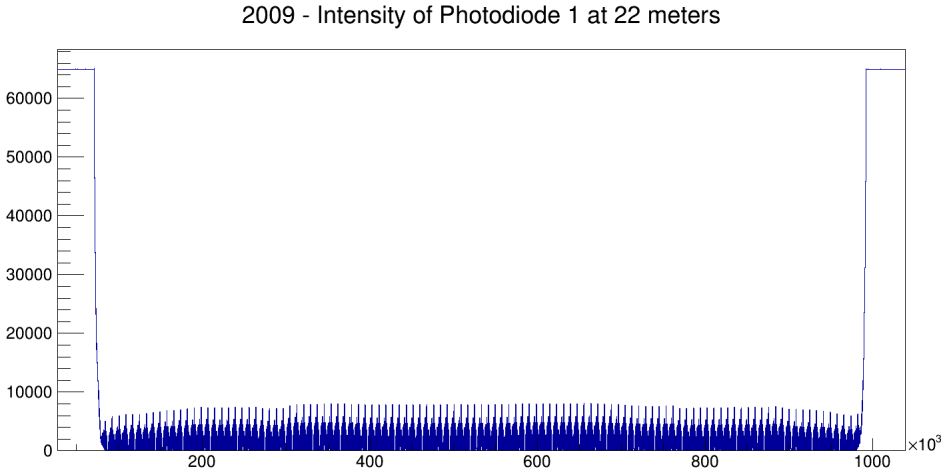

Figure 5.7: KM3NeT-It Site (Capo Passero): All data collected at a distance of 22m from the light source. Intensity (arbitrary units) versus time of measurement (line entry)

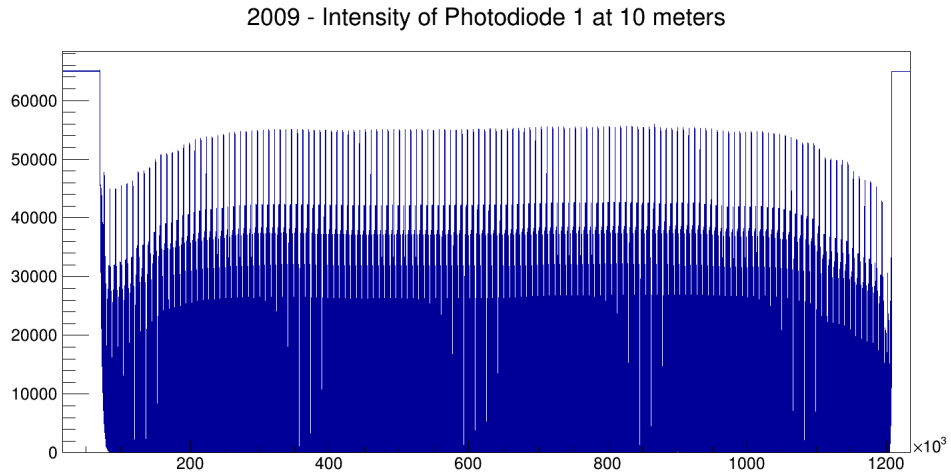

Figure 5.8: KM3NeT-Gr Site (Nestor): All data collected at a distance of 10m from the light source. Intensity (arbitrary units) versus time of measurement (line entry)

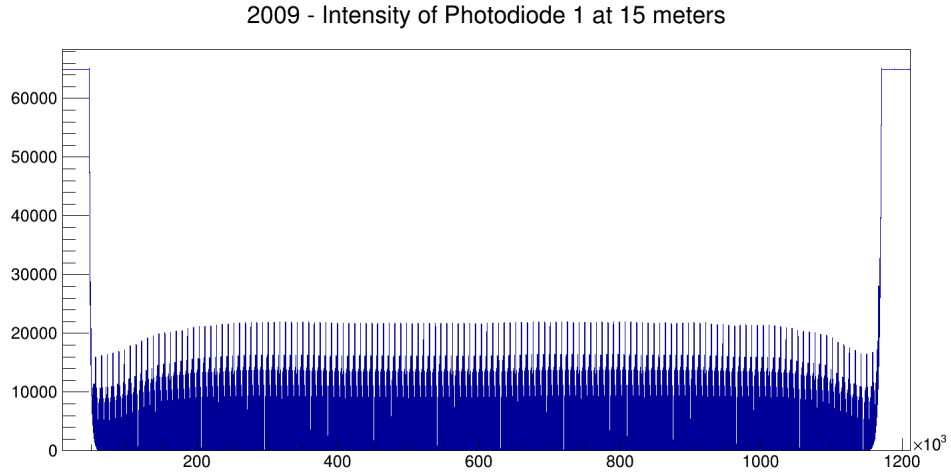

Figure 5.9: KM3NeT-Gr Site (Nestor): All data collected at a distance of 15m from the light source. Intensity (arbitrary units) versus time of measurement (line entry)

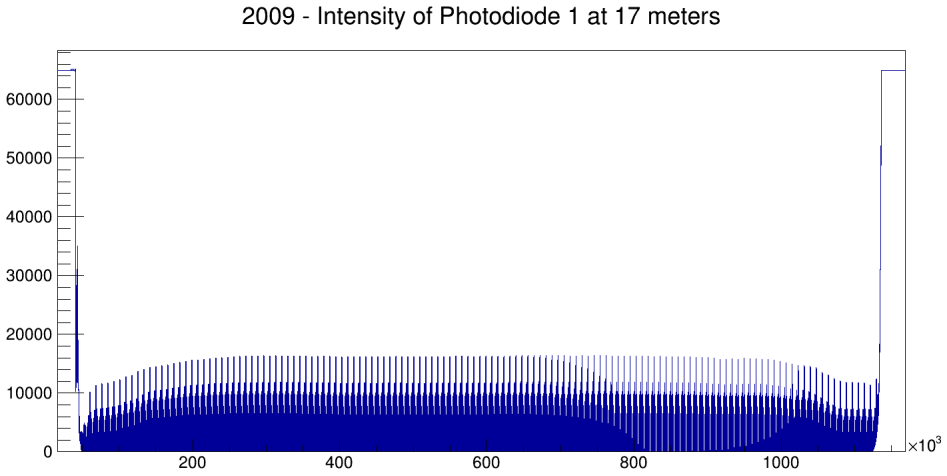

Figure 5.10: KM3NeT-Gr Site (Nestor): All data collected at a distance of 17m from the light source. Intensity (arbitrary units) versus time of measurement (line entry)

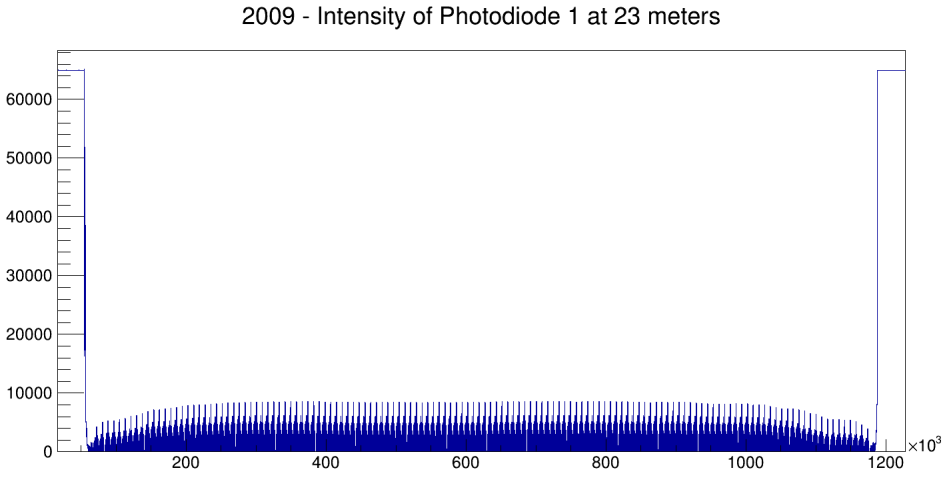

Figure 5.11: KM3NeT-Gr Site (Nestor): All data collected at a distance of 22m from the light source. Intensity (arbitrary units) versus time of measurement (line entry)

As expected, the intensity drops as the distance from the light source is increased. The spikes in intensity on the borders of the histogram is saturation. The PDs are surfaced and as a result, there is abundance of environmental illumination.

The code framework is applied to the original data. The 8 pulses are presented with different color, each color corresponding to a specific wavelength.

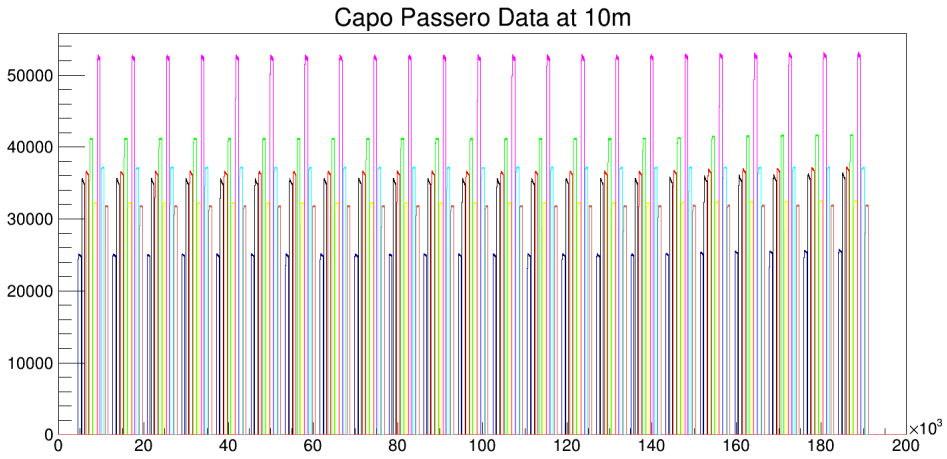

Figure 5.12: Application of the framework on the KM3NeT-It site data, pulses and cycles are visibly separable

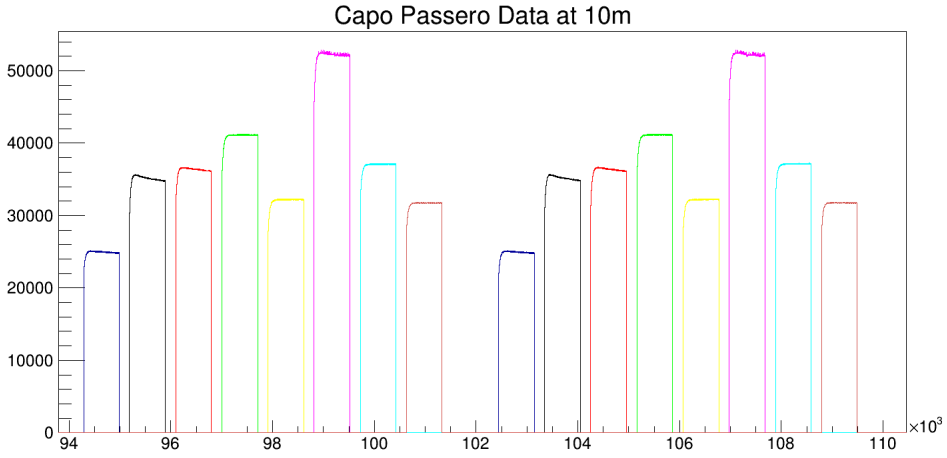

Figure 5.13: Two-cycles sample of processed data for the KM3NeT-It site

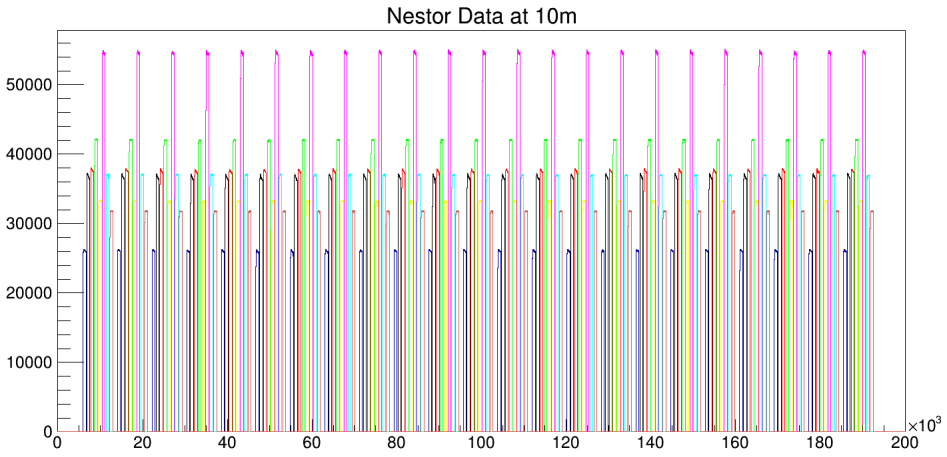

Figure 5.14: Application of the framework on the KM3NeT-Gr site data, pulses and cycles are visibly separable

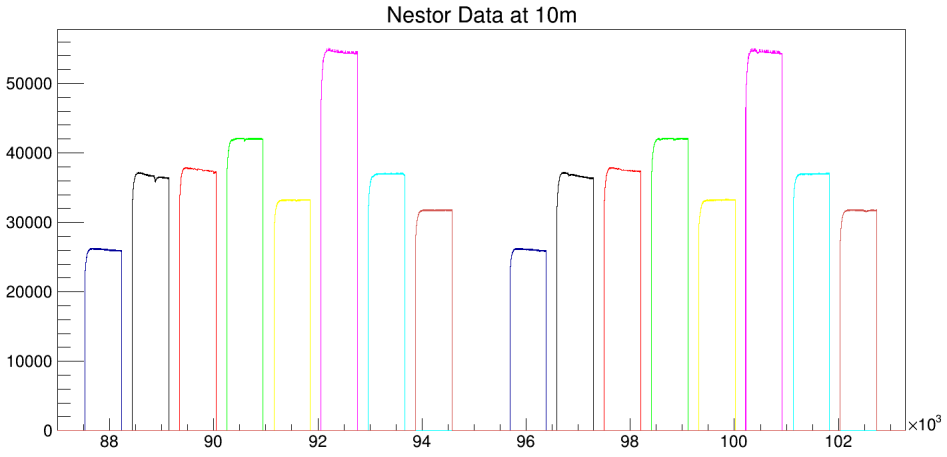

Figure 5.15: Two-cycles sample of processed data for the KM3NeT-Gr site

The original data were analyzed using the new analysis framework for finding pulses, but the old algorithm of fitting to the equation (2.10). Unfortunately, it was not possible to match the intensities with a value of depth, as we have not been able to recover this information. Instead, the mean intensity of all depths for each pulse was calculated and the analysis was pursued in order to confirm the validity of the new analysis procedure. The outcome was compared to the results presented in [28], where the transmission length is measured for the different wavelengths at different depths. Since we have averaged the measurements for different depths, only a qualitative comparison can be made, which confirms the new analysis procedure.

KM3NeT-Gr (Nestor) Mean Intensities				
Wavelength	10 m	15.1 m	17.17 m	22.27 m
Pulse 1: 375.7 nm	25943.0	8919.4	6178.7	2792.9
Pulse 2: 385.7 nm	36582.2	13133.4	9280.2	4373.0
Pulse 3: 400.3 nm	37402.5	13698.8	9856.1	4815.9
Pulse 4: 425.0 nm	41793.0	15933.3	11519.9	5877.1
Pulse 5: 445.4 nm	33015.0	12815.4	9441.4	4855.8
Pulse 6: 462.6 nm	54184.1	21429.9	15976.5	8237.9
Pulse 7: 501.6 nm	36768.7	13416.2	9582.8	4708.0
Pulse 8: 519.5 nm	31572.5	10876.9	7591.3	3452.0

Table 5.1: Intensity (a.u.) results of the new analysis framework applied on the old data, per pulse, per distance for the KM3NeT-Gr site (Nestor)

KM3NeT-It (Capo Passero) Mean Intensities				
Wavelength	10 m	15.1 m	17.17 m	22.27 m
Pulse 1: 375.7 nm	24953.1	8401.3	5671.8	2471.6
Pulse 2: 385.7 nm	35165.5	12278.8	8491.2	3907.7
Pulse 3: 400.3 nm	36313.2	13089.8	9172.4	4416.7
Pulse 4: 425.0 nm	41005.5	15418.7	11021.5	5547.0
Pulse 5: 445.4 nm	32076.0	12300.2	8922.9	4583.7
Pulse 6: 462.6 nm	52087.7	20278.4	14895.3	7714.4
Pulse 7: 501.6 nm	36896.7	13437.6	9489.9	4616.1
Pulse 8: 519.5 nm	31616.0	10801.1	7512.0	3416.2

Table 5.2: Intensity (a.u.) results of the new analysis framework applied on the old data, per pulse, per distance for the KM3NeT-It site (Capo Passero)

Transmission Length after Fitting Intensities to Equation (3.3)				
	Wavelength			
Site	375.7 nm	385.7 nm	400.3 nm	425.0 nm
KM3NeT-Gr	20.32 m	24.6 m	28.05 m	34.96 m
KM3NeT-It	18.25 m	21.4 m	24.86 m	31.52 m

	Wavelength			
Site	445.4 nm	462.6 nm	501.6 nm	519.5 nm
KM3NeT-Gr	40.87 m	47.82 m	27.33 m	20.73 m
KM3NeT-It	36.54 m	41.49 m	26.35 m	20.12 m

Table 5.3: Intensity results of the new analysis framework applied on the old data, per pulse, per distance for the KM3NeT-Gr site (Nestor)

Table 4
Transmission length, L_p, in metres at site N5.2D, October 2008 deployments.

Depth (m)	λ (nm)							
	375.7	385.7	400.3	425.0	445.4	462.6	501.6	519.5
2000	21.5 ± 0.3	25.4 ± 0.3	29.8 ± 0.4	40.3 ± 0.8	42.3 ± 0.8	42.8 ± 0.9	30.2 ± 0.5	21.3 ± 0.2
3000	21.6 ± 0.3	26.0 ± 0.3	30.7 ± 0.5	41.8 ± 0.8	44.7 ± 0.9	45.1 ± 0.9	30.8 ± 0.5	21.6 ± 0.3
4000	20.6 ± 0.2	24.3 ± 0.3	28.5 ± 0.4	38.6 ± 0.7	40.9 ± 0.8	41.7 ± 0.8	29.4 ± 0.4	20.9 ± 0.2
4900	20.3 ± 0.2	24.1 ± 0.3	28.3 ± 0.4	38.0 ± 0.7	40.4 ± 0.8	40.6 ± 0.8	29.3 ± 0.4	20.6 ± 0.2

Table 5
Transmission length, L_p, in metres at site N4.5D, October 2008 and May 2009 deployments.

Depth (m)	Date	λ (nm)							
		375.7	385.7	400.3	425.0	445.4	462.6	501.6	519.5
2000	October 08	21.2 ± 0.2	25.4 ± 0.3	29.3 ± 0.4	40.4 ± 0.8	40.5 ± 0.8	42.2 ± 0.8	29.8 ± 0.4	21.0 ± 0.2
	May 09	20.8 ± 0.5	24.0 ± 0.7	28.4 ± 0.8	34.7 ± 1.2	39.4 ± 1.6	42.0 ± 1.7	27.8 ± 0.8	20.9 ± 0.5
2500	October 08	21.6 ± 0.3	26.1 ± 0.4	30.5 ± 0.5	42.7 ± 0.9	42.5 ± 0.9	44.6 ± 0.9	30.6 ± 0.5	21.4 ± 0.2
	May 09	21.7 ± 0.5	25.4 ± 0.6	30.0 ± 0.9	36.3 ± 1.3	41.9 ± 1.7	45.5 ± 2.0	28.6 ± 0.8	21.4 ± 0.5
3000	May 09	21.9 ± 0.5	25.7 ± 0.7	30.5 ± 1.0	37.8 ± 1.5	43.8 ± 1.9	47.2 ± 2.2	29.3 ± 0.9	21.5 ± 0.6
3400	October 08	21.4 ± 0.2	25.9 ± 0.3	30.1 ± 0.5	43.0 ± 0.9	42.2 ± 0.8	43.8 ± 0.9	30.4 ± 0.5	21.5 ± 0.2
	May 09	21.9 ± 0.5	25.7 ± 0.7	30.4 ± 1.0	38.2 ± 1.4	44.3 ± 1.9	47.8 ± 2.2	29.8 ± 0.9	21.9 ± 0.6
4100	October 08	20.5 ± 0.2	24.7 ± 0.3	28.4 ± 0.4	39.7 ± 0.8	39.8 ± 0.8	41.5 ± 0.8	28.0 ± 0.4	20.9 ± 0.2
	May 09	21.0 ± 0.5	24.8 ± 0.7	29.2 ± 0.9	36.0 ± 1.3	42.3 ± 1.8	46.1 ± 2.0	28.7 ± 0.8	21.3 ± 0.5

Table 6
Transmission length, L_p, in metres at sites CP1 and CP2, May 2009 deployments.

Depth (m)	Site	λ (nm)							
		375.7	385.7	400.3	425.0	445.4	462.6	501.6	519.5
2000	CP1	19.6 ± 0.4	22.9 ± 0.6	27.1 ± 0.7	32.6 ± 1.1	37.8 ± 1.4	39.4 ± 1.6	26.7 ± 0.8	20.8 ± 0.5
	CP2	17.6 ± 0.4	20.4 ± 0.5	23.8 ± 0.6	28.6 ± 0.8	33.1 ± 1.2	35.8 ± 1.3	24.9 ± 0.7	19.4 ± 0.4
2500	CP1	20.1 ± 0.5	23.6 ± 0.6	28.1 ± 0.8	34.5 ± 1.2	40.2 ± 1.6	42.4 ± 1.8	27.9 ± 0.8	21.4 ± 0.5
	CP2	18.2 ± 0.4	21.2 ± 0.5	24.8 ± 0.7	30.4 ± 0.9	34.9 ± 1.3	38.0 ± 1.4	25.8 ± 0.7	19.9 ± 0.4
3100	CP1	19.9 ± 0.4	23.2 ± 0.6	27.8 ± 0.8	34.6 ± 1.2	41.5 ± 1.7	44.1 ± 1.9	28.5 ± 0.8	21.8 ± 0.5
3000	CP2	19.5 ± 0.4	23.0 ± 0.5	27.3 ± 0.8	34.1 ± 1.2	39.6 ± 1.6	43.7 ± 1.8	27.6 ± 0.8	21.1 ± 0.5
3400	CP2	18.6 ± 0.4	21.8 ± 0.5	25.6 ± 0.7	32.4 ± 1.1	38.5 ± 1.5	42.0 ± 1.7	27.1 ± 0.8	20.9 ± 0.5

Figure 5.16: Transmission Lengths of LAMS deployments in 2008 and 2009 [28]

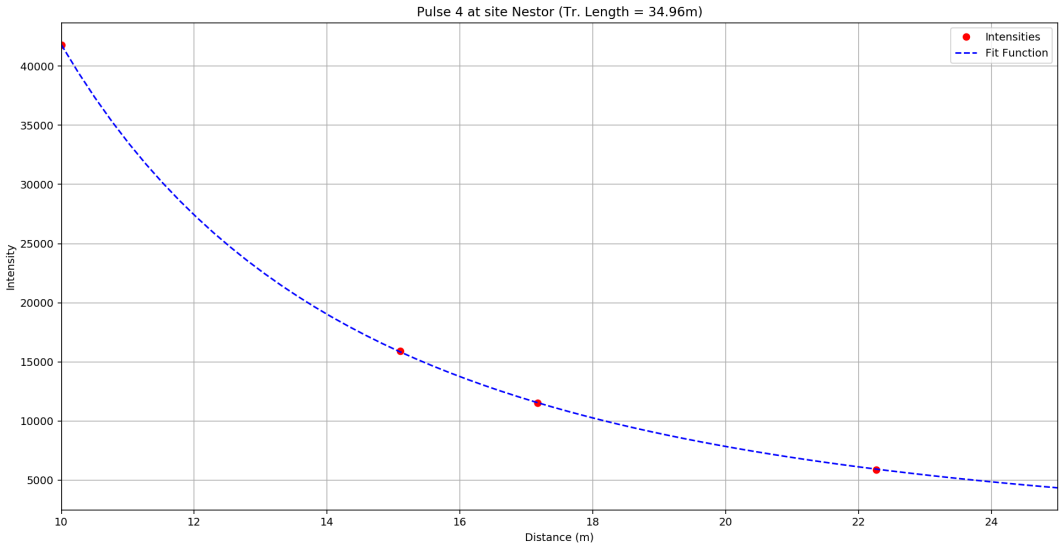

Figure 5.17: Fitting to equation (3.3) for mean intensities (different distances, same wavelength) on the KM3NeT-Gr site (for all depths). Transmission length is 34.96

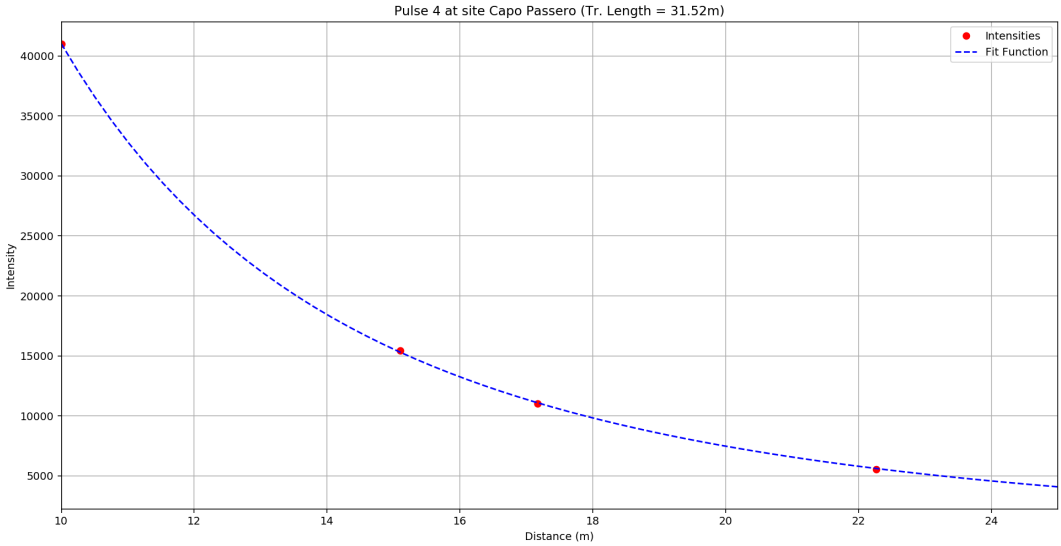

Figure 5.18: Fitting to equation (3.3) for mean intensities (different distances, same wavelength) on the KM3NeT-It site (for all depths). Transmission length is 31.52

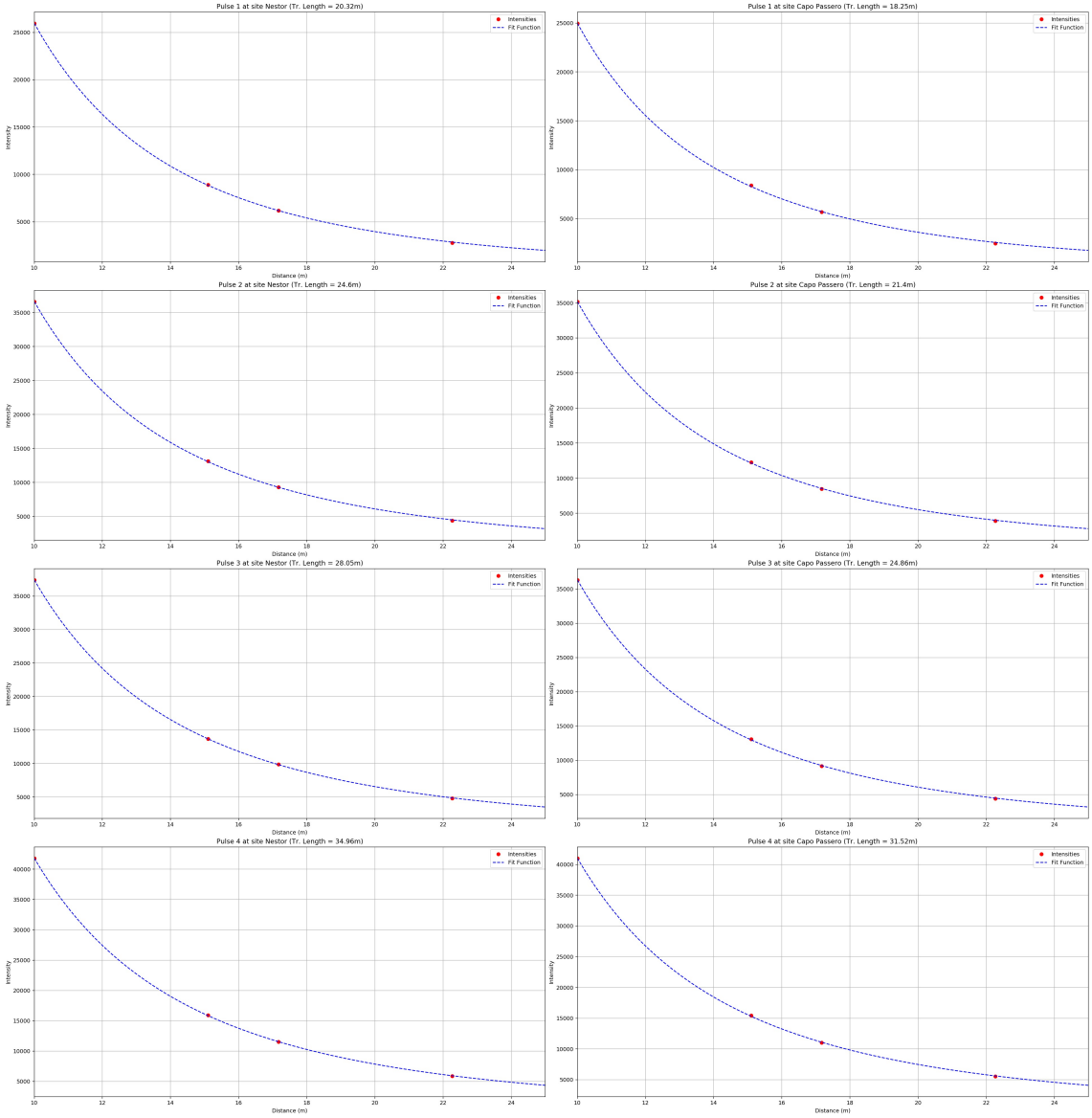

Figure 5.19: Fit graphs of pulses 1 to 4, for sites KM3NeT-Gr and KM3NeT-It

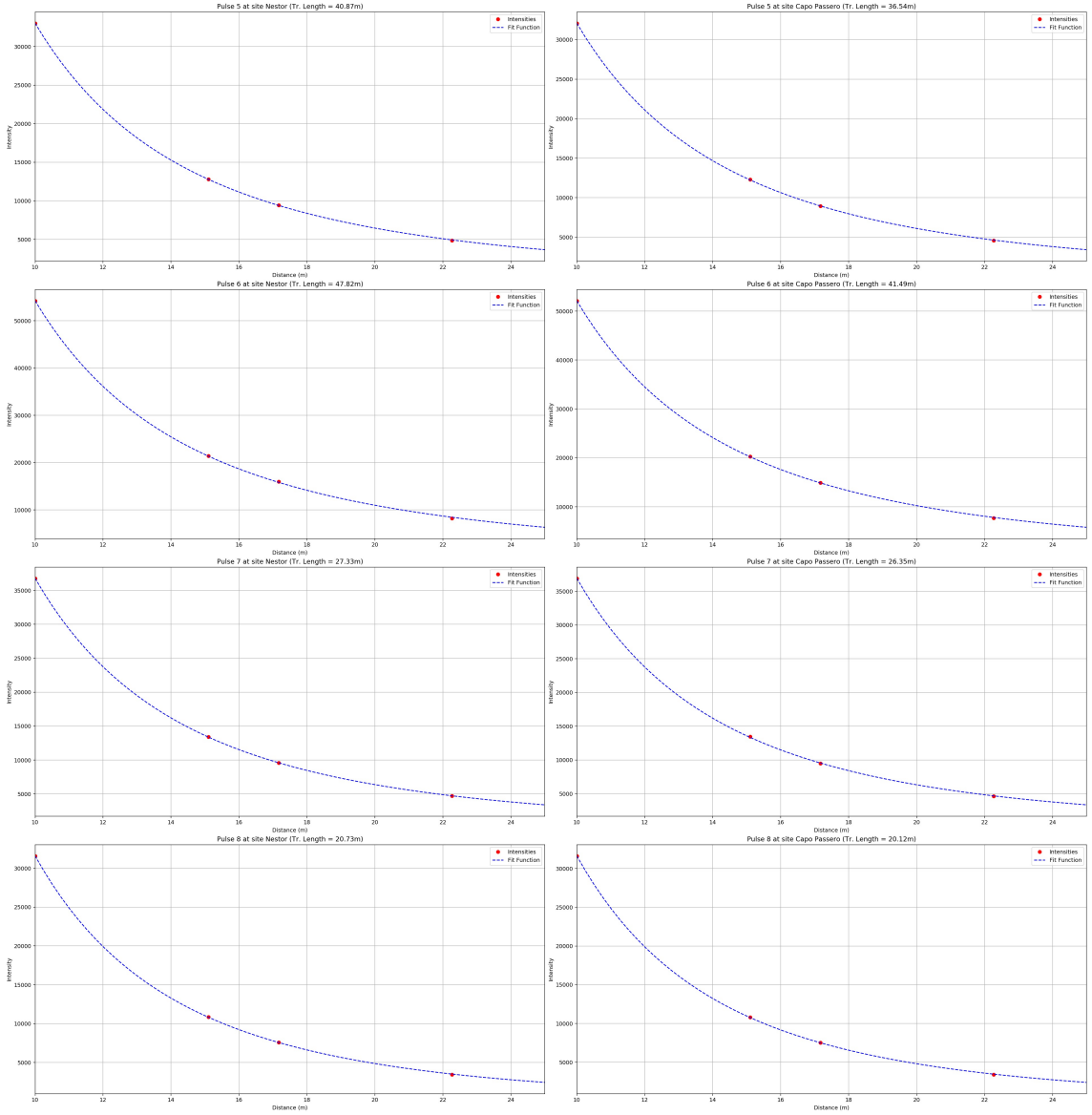

Figure 5.20: Fit graphs of pulses 5 to 8, for sites KM3NeT-Gr and KM3NeT-It

5.4 Tests and Problems

The upgrade of the LAMS equipment to newer and better components required extensive testing. Inevitably, problems emerged and were eventually solved. At this testing phase, my role was to thoroughly analyze the test data in order to spot problems with the newly developed electronics. Some examples follow:

5.4.1 Cycle Rate Drop

One of the problems that occurred at an early stage was a sampling rate drop as a function of time. This inconsistency from the electronics would confuse the algorithms and the data could not be processed correctly. Fake data were constructed as a measure of comparison. The graphs presenting this problem are shown below.

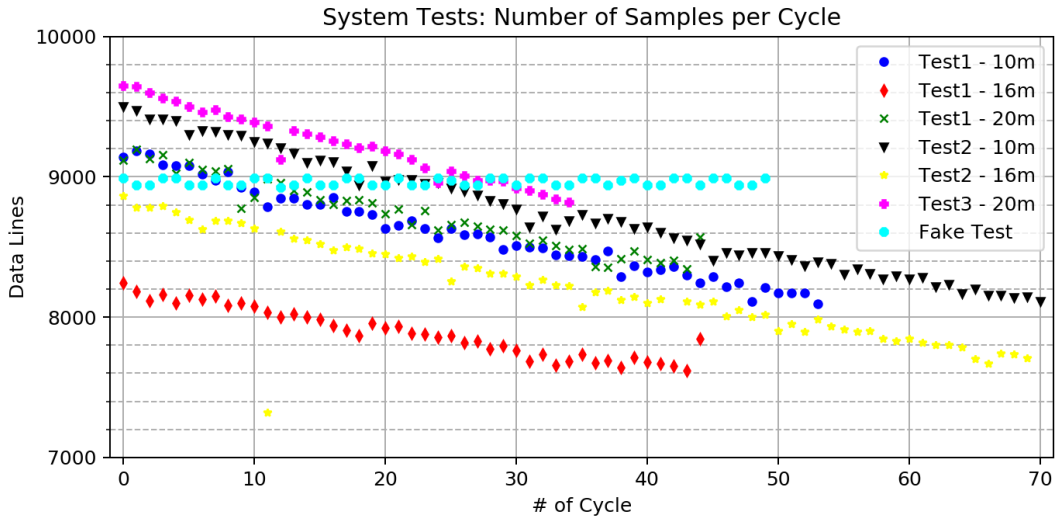

Figure 5.21: The sampling rate (number of line entries) per cycle

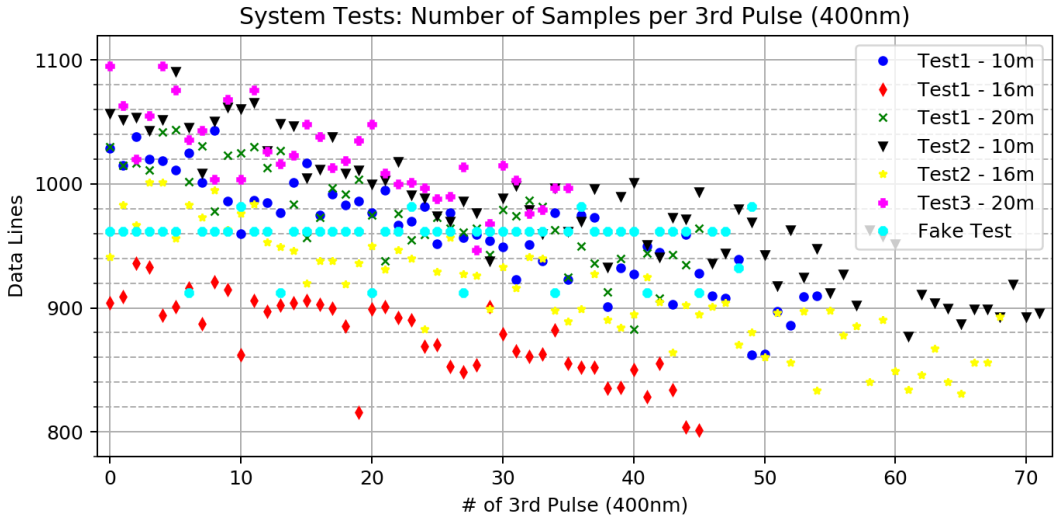

Figure 5.22: The sampling rate (number of line entries) for only one pulse (400nm), per cycle

The problem was further studied and solved as is demonstrated in Figure (4.23). This figure also exposes a new problem where the memory cards would lag and stop recording for fractions of seconds, losing data in the process. This "hiccup" effect was solved promptly.

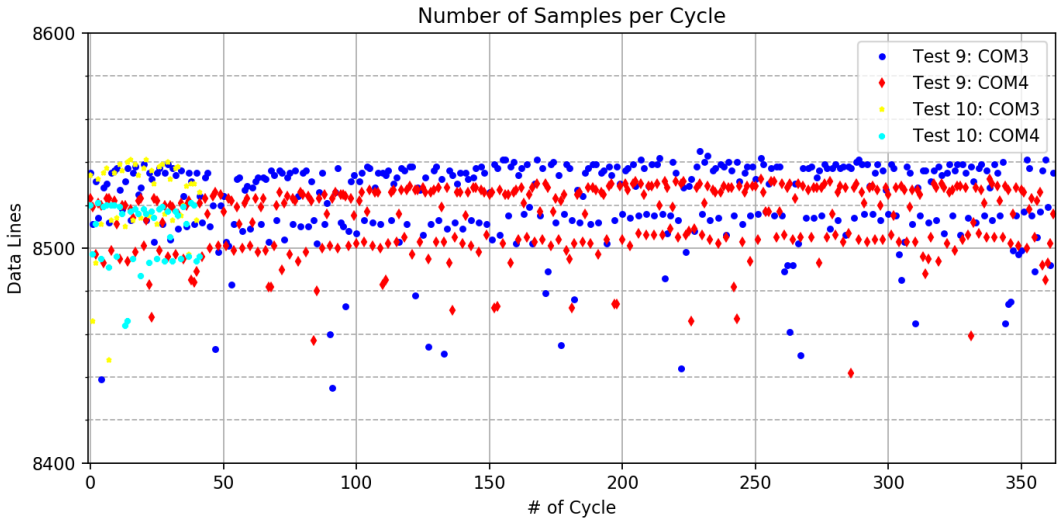

Figure 5.23: The sampling rate remains constant. 350 cycles are equal to 38500 seconds or 10 hours and 42 minutes. Another problem appears, where data is lost due to memory cards lagging

5.4.2 Erratic Behavior of 1 PD

In one of the tests, this erratic behavior on the intensities of a specific PD was detected. The problematic PD and board were examined and the problem was fixed.

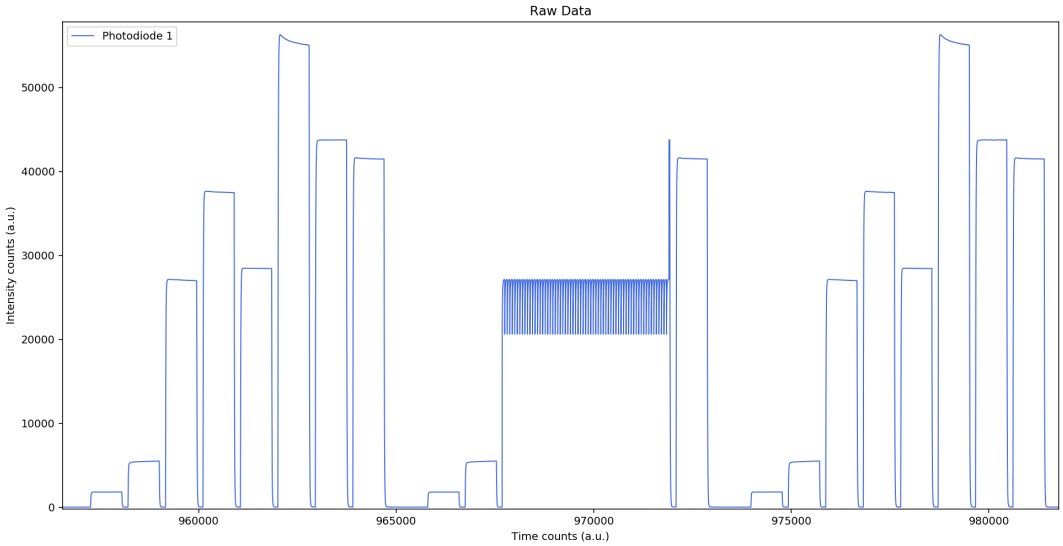

Figure 5.24: Unprocessed data that demonstrate a temporary erratic behavior, caused by an error in the electronics. Note that the erratic shape begins on a pulse and keeps that height

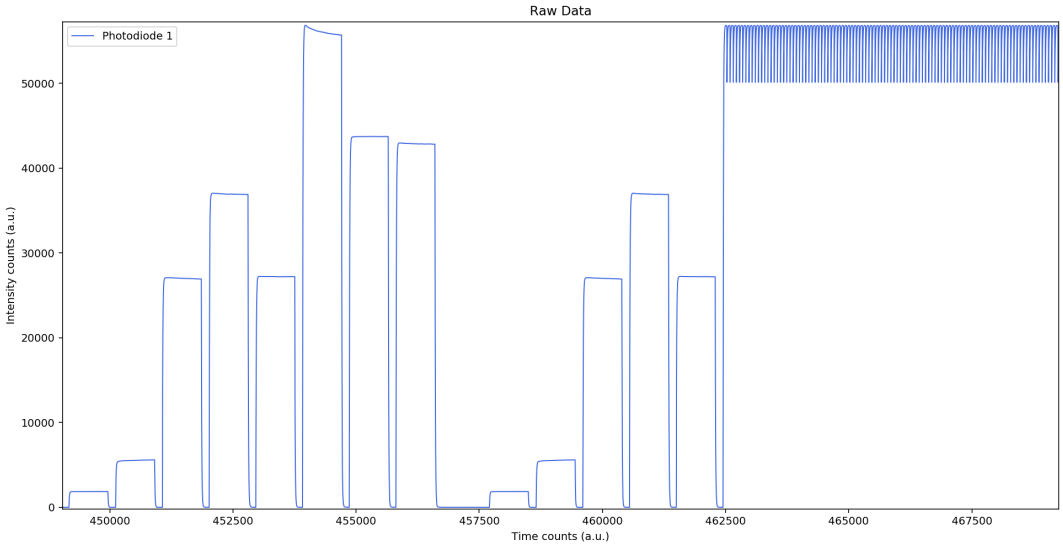

Figure 5.25: A second example of the same behavior in earlier time on the same data. Again, the erratic shape starts on a pulse and retains that height

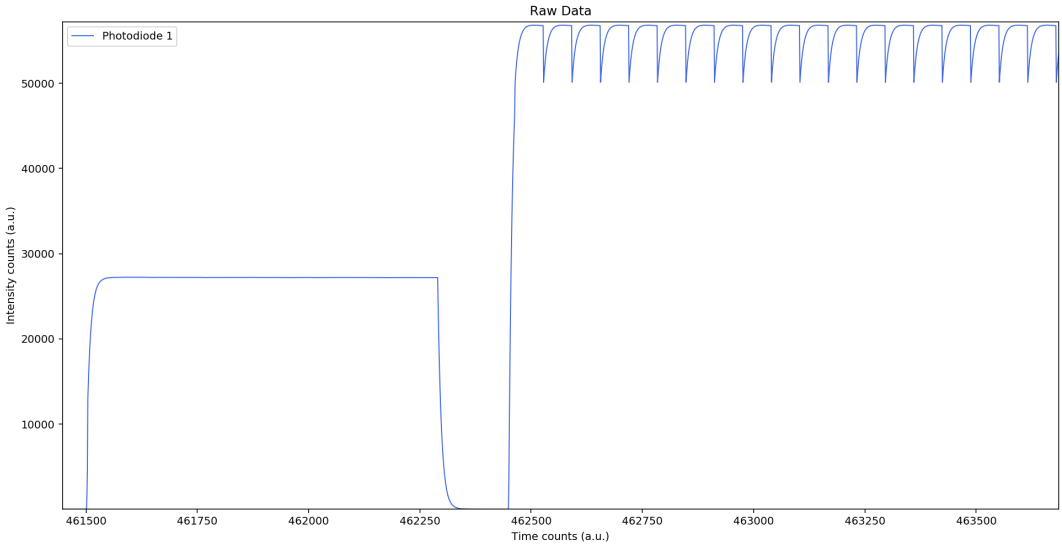

Figure 5.26: The erratic shape zoomed in, indicating a problem in the electronics

5.4.3 Asynchronization of PDs

Another problem was the asynchronization between cases. The boards in each case seemed to not have the same sampling rate, as demonstrated in figure (4.27)

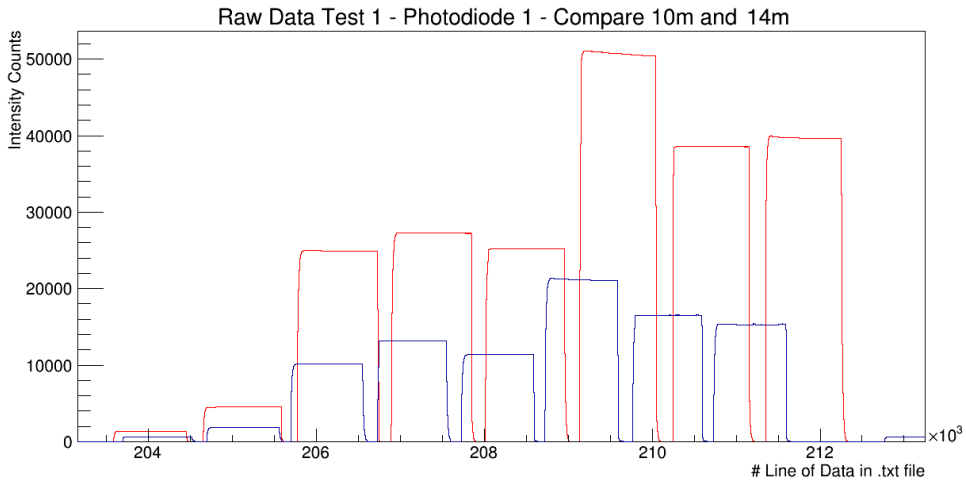

Figure 5.27: The sampling rate is different for distances of 10m and 14m

5.4.4 Shading Effect

The PD-cases are carefully fixed in the inner edges of the LAMS frame. A multitude of cases cannot occupy the same edge, as the case closer to the light source would probably create a shade and partially block the vision of the case behind it. Nonetheless, this shading effect was examined, by placing in succession the 20m case, then the 14m case and finally the 10m case. The first results incorrectly suggest that the 20m case was shaded when the 10m case was fixed on the frame, as can be seen in figures (4.28) and (4.29).

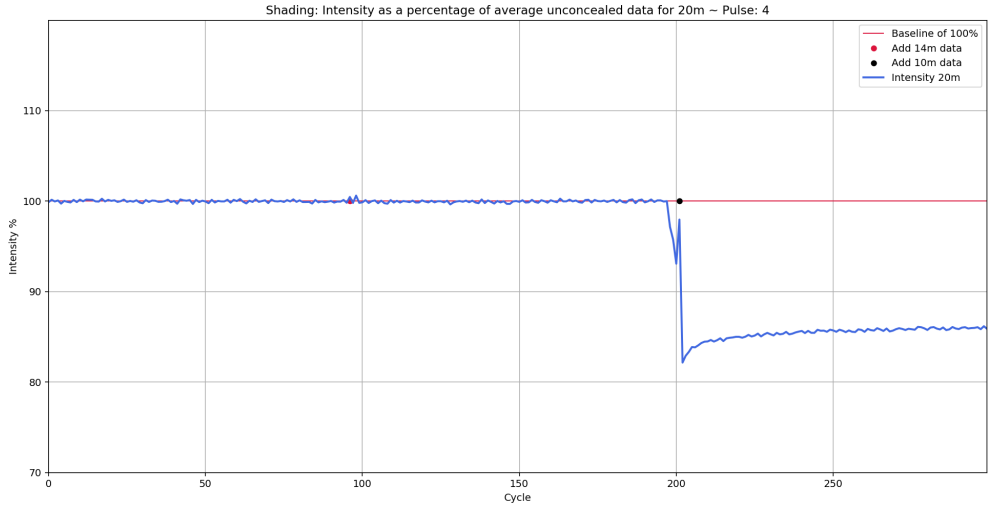

Figure 5.28: The intensity drop in percentage on the 20m PD-1 versus time (measured in cycles = 108 seconds) for pulse 4. The two dots in this plot show the moment when the next case was fixed on the frame. The 100% corresponds to the average intensity before any cases were added to the frame

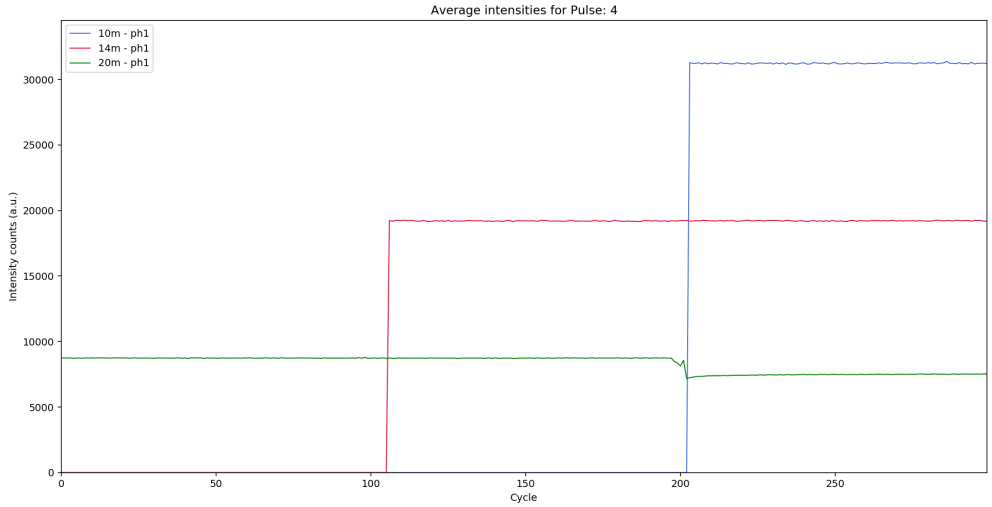

Figure 5.29: All intensities overlaid, with colors corresponding to distance as described in graph's legend

These results were misleading due to the 20m case being accidentally slightly covered, when fixing the 10m case on to the frame. This was discovered by the re-examination of the shading effect during a second test. The results of the second test are shown in figures (4.30), (4.31)

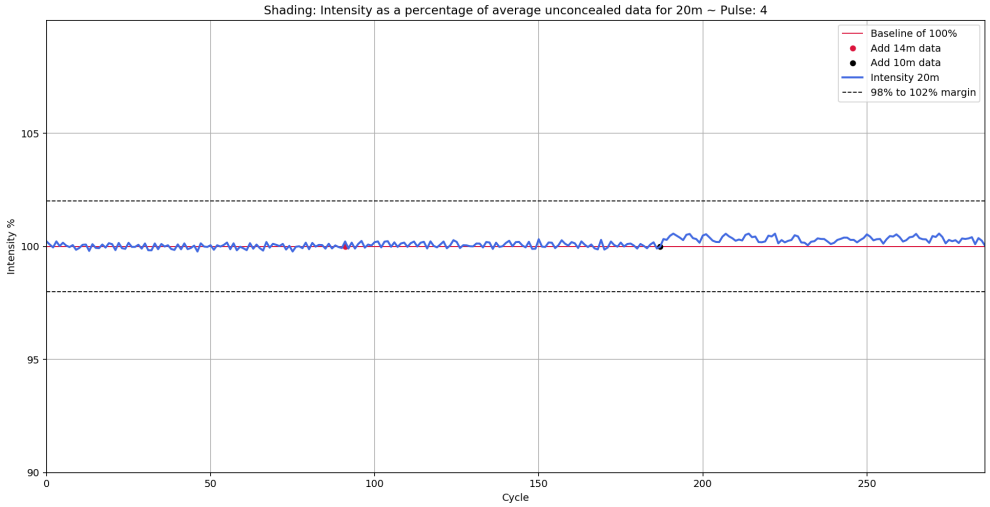

Figure 5.30: The intensity percentage on the 20m PD-1 versus time (measured in cycles) for pulse 4. There is a less than 1% increase in intensity when the 10m case was fixed on the frame. This disproves and dismisses the shading effect that was observed in the previous test

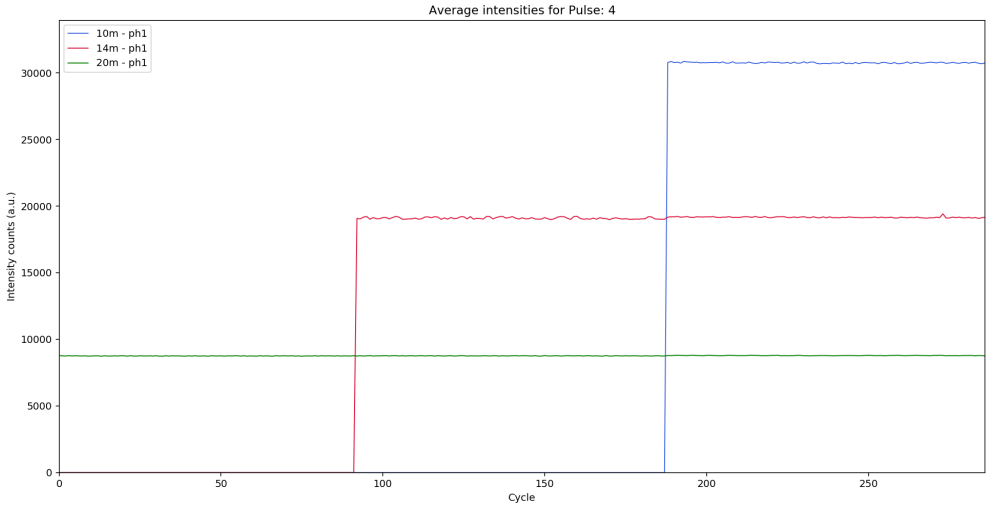

Figure 5.31: All intensities overlaid. No shading effect can be observed after fixing cases on the frame

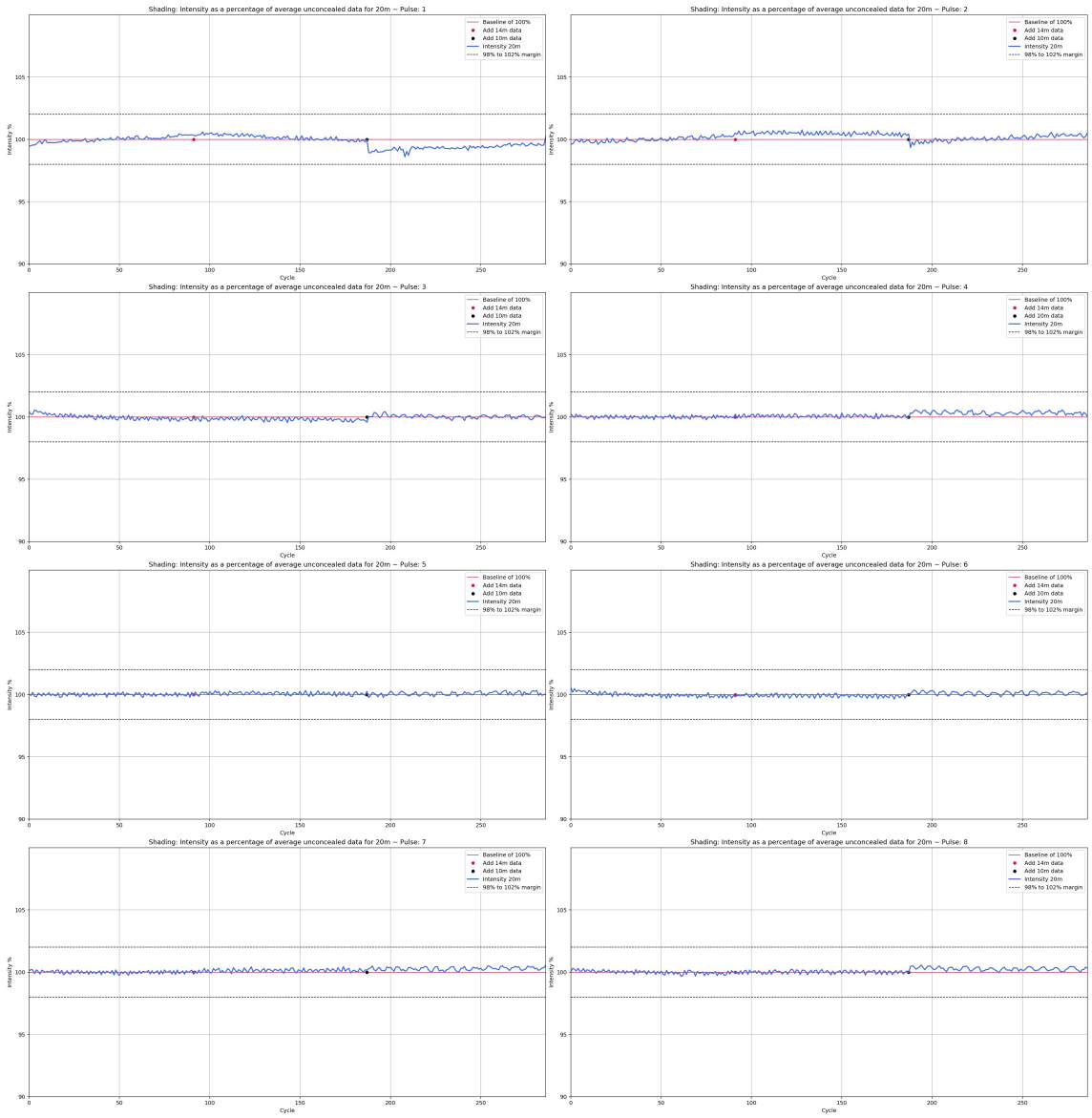

Figure 5.32: Intensity percentages versus time (cycles) for all pulses. Although fluctuations can be observed at points of fixing cases on the frame, the percentage variation is too small to be considered an effect and can be attributed to uncontrollable environmental changes by the personnel placing the cases

Conclusions

For many years, we explored the cosmos by the lens of optical telescopes. Soon was discovered that there was more than visible light to observe and more than light altogether. Neutrino astronomy depends on neutrinos instead of light, to give us new information about the universe that otherwise light could not provide. Neutrino telescopes are the necessary instruments for this and LAMS can assist in the preparation for the new generation telescopes. Determining the optical properties of sea-water is essential information for the water based Cherenkov radiation detectors of KM3NeT.

My task was to prepare an analysis, for both the testing phase and the submersion of LAMS. In the testing phase, I would apply the c++ framework I developed to the data and search for misbehaving of the electronics. Upon finding issues, I would co-operate with my colleagues to determine the causes and re-test the problems until they were solved. Although the testing phase ended successfully, solving all problems that emerged, data collection in sea-water has not occurred and is planed for the future.

Along with the upgrade in the electronics compared to the original equipment, the analysis of the data also required to be upgraded. The software framework that I developed now allows us to not keep record of depth and time by hand. Instead, it can scan the data and automatically recognize the shapes of pulses and separate the data into cycles, as well as flag erroneous data by cause of external events. Along with the data of temperature and pressure that are also recorded, values for depth can be determined and allocated to data cycles.

Our aim is to use the new LAMS device to perform a measurement of the optical properties of deep sea water on the KM3NeT-Gr site (offshore Pylos) in order to validate the functionality of both the upgraded hardware and software. Also, Monte-Carlo simulations of muons and neutrinos for different attenuation lengths and their comparison with real data could provide us with new knowledge.

Συμπεράσματα

Για πολλά χρόνια, εξερευνούσαμε το σύμπαν μέσω των φακών των οπτικών τηλεσκοπίων. Σύντομα ανακαλύφθηκε ότι υπήρχε κάτι περισσότερο να παρατηρηθεί πέρα από το ορατό φως ή ακόμα και από το φως γενικότερα. Με την αστρονομία των νετρίνων, βασιζόμαστε στο νετρίνα αντί στα φωτόνια αστρονομικών πηγών, για να λάβουμε νέες πληροφορίες για το σύμπαν που διαφορετικά το φως δεν θα μπορούσε να μας δώσει. Τα τηλεσκόπια νετρίνων είναι τα απαραίτητα όργανα για αυτό τον σκοπό και το LAMS μπορεί να βοηθήσει στην προετοιμασία των τηλεσκοπίων νέας γενιάς. Ο προσδιορισμός των οπτικών ιδιοτήτων του θαλασσινού νερού είναι απαραίτητη πληροφορία για τους ανιχνευτές ακτινοβολίας Cherenkov με βάση το νερό του KM3NeT.

Το καθήκον μου ήταν να ετοιμάσω μια ανάλυση, τόσο για τη φάση της δοκιμής όσο και για τη βύθιση του LAMS. Στη φάση της δοκιμής, θα εφάρμοζα τον κώδικα c++ που ανέπτυξα στα δεδομένα και θα έψαχνα για κακή συμπεριφορά των ηλεκτρονικών. Με την εύρεση προβλημάτων, θα συνεργαζόμουν με τους συναδέλφους μου για να προσδιορίσω τις αιτίες και να ελέγξω ξανά τα προβλήματα μέχρι να επιλυθούν. Αν και η φάση των δοκιμών ολοκληρώθηκε με επιτυχία, επιλύοντας όλα τα προβλήματα που προέκυψαν, η συλλογή δεδομένων στο θαλασσινό νερό δεν έχει πραγματοποιηθεί και σχεδιάζεται για το μέλλον.

Παράλληλα με την αναβάθμιση στα ηλεκτρονικά σε σχέση με τον αρχικό εξοπλισμό, απαιτούνταν και η αναβάθμιση της ανάλυσης των δεδομένων. Το λογισμικό που ανέπτυξα τώρα πια μας επιτρέπει να μην κρατάμε αρχείο βάθους και χρόνου. Αντίθετα, μπορεί να σαρώσει τα δεδομένα και να αναγνωρίσει αυτόματα τα σχήματα των παλμών και να διαχωρίσει τα δεδομένα σε κύκλους, καθώς και να επισημάνει λανθασμένα δεδομένα λόγω εξωτερικών συμβάντων. Μαζί με τα δεδομένα θερμοκρασίας και πίεσης που επίσης καταγράφονται, μπορούν να προσδιοριστούν και να κατανεμηθούν τιμές για το βάθος σε κύκλους δεδομένων.

Το επόμενο βήμα θα ήταν φυσικά η συλλογή δεδομένων σε θαλασσινό νερό και η ανάλυσή τους, ολοκληρώνοντας αυτή τη μελέτη στην τοποθεσία KM3NeT-Gr (ανοιχτά της ακτής στην Πύλο). Επίσης, οι προσομοιώσεις Monte-Carlo μιονίων και νετρίνων για διαφορετικά μήκη εξασθένησης και η σύγκρισή τους με πραγματικά δεδομένα θα μπορούσαν να μας προσφέρουν νέα γνώση στην φυσική σωματιδίων.

Bibliography

[1] Mark Thomson. *Modern Particle Physics*. Cambridge, United Kingdom: Cambridge University Press, 2013. ISBN: 1107034264.

[2] M. Sajjad Athar and S. K. Singh. *The Physics of Neutrino Interactions*. India: Cambridge University Press, 2020. ISBN: 1108489060.

[3] Vernon Barger, Danny Marfatia, and Kerry Whisnant. *The Physics of Neutrinos*. Princeton and Oxford: Princeton University Press, 2012. ISBN: 0691128537.

[4] Carlo Giunti and Chung W. Kim. *Fundamentals of Neutrino Physics and Astrophysics*. New York: Oxford University Press, 2007. ISBN: 0198508719.

[5] David Griffiths. *Introduction to Elementary Particles 2nd Edition*. United States of America: Wiley-VCH, 2008. ISBN: 9783527406012.

[6] Maurizio Spurio. *Particles and Astrophysics: A Multi-Messenger Approach*. Italy: Springer, 2014. ISBN: 3319080504.

[7] Jorge Ernesto Horvath. *High-Energy Astrophysics: A primer*. Brazil: Springer, 2022. ISBN: 3030921581.

[8] J. L. Hewett et al. "Planning the Future of U.S. Particle Physics (Snowmass 2013): Chapter 2: Intensity Frontier". In: *Arxiv* (2014). DOI: https://doi.org/10.48550/arXiv.1401.6077.

[9] Christian W. Fabjan and Herwig Schopper, eds. *Particle Physics Reference Library*. Vol. 2: Detectors for Particles and Radiation. Cham, Switzerland: Springer Open, 2020. ISBN: 3030353176.

[10] A. Letessier-Selvon. "Establishing the GZK Cutoff with Ultra High Energy Tau neutrinos". In: *ArxiV* (2000).

[11] Barbara Ryden and Bradley M. Peterson. *Foundations of Astrophysics*. United Kingdom: Cambridge University Press, 2020. ISBN: 1108831958.

[12] Ian Morison. *Introduction to Astronomy and Cosmology*. United Kingdom: Wiley, 2008. ISBN: 0470033347.

[13] Houjun Mo, Frank Van Den Bosch, and Simon White. *Galaxy Formation and Evolution*. United Kingdom: Cambridge University Press, 2010. ISBN: 0521857937.

[14] Hagai Netzer. *The Physics and Evolution of Active Galactic Nuclei*. United States of America: Cambridge University Press, 2013. ISBN: 1107021510.

[15] Linda S. Sparke and John S. Gallagher III. *Galaxies in the Universe: An Introduction*. United Kingdom: Cambridge University Press, 2007. ISBN: 0521671868.

[16] *Image taken from wikipedia commons*. URL: https://en.wikipedia.org/.

[17] Alain Mazure and Stephane Basa. *Exploding Superstars: Understanding Supernovae and Gamma-Ray Bursts*. United Kingdom: Praxis, 2009. ISBN: 0387095470.

[18] Michael F. L'Annunziata. *Radioactivity: Introduction and History, From the Quantum to Quarks*. Amsterdam, Netherlands: Elsevier, 2016. ISBN: 0444634894.

[19] Jerome Williams. *Oceanographic Instrumentation*. United States of America: Naval Institute Press, 1973. ISBN: 0870215035.

[20] M. P. M. Reddy. *Descriptive Physical Oceanography*. India: A. A. Balkema, 2001. ISBN: 9054107065.

[21] Lynne D. Talley et al. *Descriptive Physical Oceanography: An Introduction (Sixth Edition)*. United Kingdom: Elsevier, 2011. ISBN: 978-0-7506-4552-2.

[22] Ge Chen, Lin Peng1, and Chunyong Ma. "Climatology and seasonality of upper ocean salinity: a threedimensional view from argo floats". In: (2018). DOI: https://doi.org/10.1007/s00382-017-3742-6.

[23] Curtis Mobley, Emmanuel Boss, and Collin Roesler. *Ocean Optics*. United States: Ocean Biology and Biogeochemistry Program of NASA, 2020.

[24] E.G. Anassontzis et al. "Light transmission measurements with LAMS in the Mediterranean Sea". In: *Nuclear Instruments and Methods in Physics Research Section A: Accelerators, Spectrometers, Detectors and Associated Equipment* (2011). DOI: https://doi.org/10.1016/j.nima.2010.06.353.

[25] URL: https://www.km3net.org/.

[26] *KM3NeT's Google Drive*.

[27] E. Tzamariudaki and S. Koutsoukos. *Final Report on the Water Properties Measurement service*. 2020.

[28] E.G. Anassontzis et al. "Water transparency measurements in the deep Ionian Sea". In: *Astroparticle Physics* (2010). DOI: https://doi.org/10.1016/j.astropartphys.2010.06.008.